UNIVERSITA' VITA-SALUTE SAN RAFFAELE

CORSO DI DOTTORATO DI RICERCA
INTERNAZIONALE IN MEDICINA MOLECOLARE

CURRICULUM IN TERAPIA GENICA E CELLULARE

Gaining insights into hematopoietic stem cell response to ex vivo culture to further advance gene and cell therapies

DoS: Dr. Raffaella Di Micco
Second Supervisor: Dr. Jacob Corn

Tesi di DOTTORATO di RICERCA di Federico Midena
matr. 019194
Ciclo di dottorato XXXVII
SSD: BIO/13

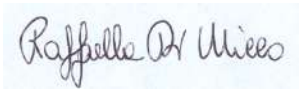
Anno Accademico 2023/2024

UNIVERSITA' VITA-SALUTE SAN RAFFAELE

CORSO DI DOTTORATO DI RICERCA
INTERNAZIONALE IN MEDICINA MOLECOLARE

CURRICULUM IN TERAPIA GENICA E CELLULARE

Gaining insights into hematopoietic stem cell response to ex vivo culture to further advance gene and cell therapies

DoS: Dr. Raffaella Di Micco 
Second Supervisor: Dr. Jacob Corn

Tesi di DOTTORATO di RICERCA di Federico Midena
matr. 019194
Ciclo di dottorato XXXVII
SSD: BIO/13

Anno Accademico 2023/2024

CONSULTAZIONE TESI DI DOTTORATO DI RICERCA

La sottoscritta / *I*	Federico Midena
Matricola / *registration number*	019194
nata a/ *born at*	Motta di Livenza (TV)
Il / *on*	26/12/1996

autore della tesi di Dottorato di ricerca dal titolo / *author of the PhD Thesis titled*

Gaining insights into hematopoietic stem cell response to ex vivo culture to further advance gene and cell therapies

☐ AUTORIZZA la Consultazione della tesi / AUTHORIZES *the public release of the thesis*

☒ NON AUTORIZZA la Consultazione della tesi per 12 mesi /DOES NOT AUTHORIZE *the public release of the thesis for* 12 *months*

a partire dalla data di conseguimento del titolo e precisamente */ from the PhD thesis date, specifically*

Dal / *from* 01/02/2025 Al / *to* 01/02/2025

Poiché /*because*:

□ l'intera ricerca o parti di essa sono potenzialmente soggette a brevettabilità/ *The whole project or part of it might be subject to patentability;*

□ ci sono parti di tesi che sono già state sottoposte a un editore o sono in attesa di pubblicazione/ *Parts of the thesis have been or are being submitted to a publisher or are in press;*

□ la tesi è finanziata da enti esterni che vantano dei diritti su di esse e sulla loro pubblicazione/ *the thesis project is financed by external bodies that have rights over it and on its publication.*

E' fatto divieto di riprodurre, in tutto o in parte, quanto in essa contenuto / *Copyright the contents of the thesis in whole or in part is forbidden*

Data /Date 01/02/2025 Firma/Signature 

DECLARATION

This thesis has been:

- composed by myself and has not been used in any previous application for a degree. Throughout the text, I use both 'I' and 'We' interchangeably.
- has been written according to the editing guidelines approved by the University.

Permission to use images and other material covered by copyright has been sought and obtained. For the following images, Figure 1-10 and Figure 12-15, it was not possible to obtain permission and are therefore included in the thesis under the "fair use" exception (Italian legislative Decree no. 68/2003).

All the results presented here were obtained by myself, except for:

1) Nichoid fabrication was performed in collaboration with Claudio Conci from the group of Professor Manuela Raimondi, Department of Chemistry, Materials and Chemical Engineering "G. Natta", Politecnico di Milano, Milano, Italy.

2) Bioinformatic analyses of gene expression were performed in collaboration with Matteo Barcella, Bioinformatics Core, San Raffaele Telethon Institute for Gene Therapy, Milan, Italy.

3) Z-stacked confocal immunofluorescence microscopy was performed in collaboration with Emanuela Jacchetti from the group of Professor Manuela Raimondi, Department of Chemistry, Materials and Chemical Engineering "G. Natta", Politecnico di Milano, Milano, Italy.

4) Analysis of z-stacked confocal immunofluorescence microscopy was performed in collaboration with Valeria Berno, ALEMBIC, Experimental Imaging Centre, San Raffaele Scientific Institute, Milan, Italy.

5) Deep sequencing of the human graft upon long-range gene editing and base- and prime-editing reagents were provided in collaboration with Stefano Beretta, Martina Fiumara, and Samuele Ferrari from the group of Professor Luigi Naldini, San Raffaele Telethon Institute for Gene Therapy, Milan, Italy.

6) Integration site analyses were performed in collaboration with Fabrizio Benedicenti, Sergio Arevalo Diaz, and Francesco Gazzo from the group of Dr. Eugenio Montini, Vector Integration Core, San Raffaele Telethon Institute for Gene Therapy, Milan, Italy.

7) Wiskott-Aldrich Syndrome patient-derived cells were obtained in collaboration with Francesca Ferrua and Federico Fraschetta from the group of Professor Alessandro Aiuti, Pediatric immunohematology unit, IRCCS San Raffaele, Milan, Italy.

8) Reagents used in experiments with Wiskott-Aldrich Syndrome patient-derived cells were provided in collaboration with Erika Zonari and Milena Perrone from the group of Dr. Marina Radrizzani, Process Development Lab, San Raffaele Telethon Institute for Gene Therapy, Milan, Italy.

All the data reported in the section "A p38 MAPK-ROS axis fuels proliferation stress and DNA damage during CRISPR/Cas9 gene editing in HSPCs" are part of the manuscript *della Volpe, Midena et al.* accepted in principle at *Cell Reports Medicine*, in which I am listed as the co-first author.

All sources of information are acknowledged by means of reference.

Abstract

Hematopoietic stem and progenitor cell gene therapy (HSPC-GT) requires *ex vivo* culture to achieve a sizable fraction of engineered cells. However, despite significant efforts to constantly optimize culture conditions, long-term repopulating hematopoietic stem cells (HSCs) rapidly lose self-renewal potential and differentiate upon *ex vivo* exposure. Combined with different adverse reactions triggered by genetic engineering, such as the activation of the DNA damage response (DDR) and the formation of genotoxic byproducts, these detrimental responses may jeopardize the efficacy and safety of the therapy by delaying hematopoietic reconstitution and affecting the clonal repertoire of repopulating stem cells. Here, we discovered that *ex vivo* culture inadvertently leads to p38 MAPK activation, generating mitogenic reactive oxygen species (ROS) that fuel fast cell cycle progression, causing proliferative stress with accumulation of physical DNA damage and consequent activation of the DDR. Importantly, transient p38 inhibition was sufficient to mitigate the activation of this intricate molecular axis, endowing Cas9/AAV6-edited HSPCs with superior long-term hematopoietic reconstitution and polyclonal output upon transplant.

Alongside p38 MAPK activation, we reasoned that additional detrimental responses may arise from HSPC removal from the hypoxic bone marrow niche and be exacerbated by the absence of 3D stimuli and mechanical support in traditional 2D cultures. Thus, we tested a biocompatible 3D scaffold with cell scale resolution, which increased *ex vivo* cultured HSPC functionality. By performing transcriptomic analyses, we found upregulation of genes belonging to cytoskeleton organization and adhesion, with concomitant downregulation of DNA damage and DDR, replication and cell division, transcription, protein homeostasis, and oxidative respiration, features associated with more primitive and dormant stem cells. Mechanistically, 3D scaffolds prevented HSPC deformation and squashing occurring in traditional 2D culture, conserving nuclei morphology and tubulin polarity. Moreover, 3D scaffolds ameliorated HSPC functionality upon multiple genetic engineering strategies, including Cas9/AAV6, base- and prime-editing, and lentiviral gene addition, increasing the number of engrafting clones and the long-term persistence of edited cells in secondary transplantation experiments. Similar results were obtained when implementing our 3D scaffolds into the clinically approved GT protocol for Wiskott-Aldrich Syndrome using patient-derived samples.

Overall, our results highlight innovative strategies to preserve HSPC functionality during *ex vivo* manipulation for more effective and safer therapeutic applications.

Table of Contents

Acronyms and abbreviations 3
List of figures 7
Introduction 17
The hematopoietic system and hematopoietic stem and progenitor cells (HSPCs) 17
Blood and hematopoiesis *17*
Hematopoietic stem cells (hscs) *19*
The HSC niche in the bone marrow *21*
Mechanobiology of hspcs *23*
Functional assays to investigate human hspcs *25*
HSPC-based clinical applications 27
HSPC transplantation (HSPC-T) vs. HSPC gene therapy (HSPC-GT) *27*
GT with integrating vectors *30*
GT with precise genome editors *31*
Delivery of editing reagents *41*
Current challenges in HSPC-GT 43
Cellular constrains to genetic engineering and safety concerns *43*
Strategies to improve genetic engineering efficiency *45*
HSPC responses to ex vivo culture and optimization of culture conditions *47*
Traditional 2D culture vs. 3D systems *49*
Aim of the work 53
Results 55
A p38 MAPK-ROS axis fuels proliferation stress and DNA damage during CRISPR/Cas9 gene editing in HSPCs 55
P38 MAPK-induced ROS mediate fast cell cycle progression leading to DNA damage and DDR activation *55*
P38 inhibition improves gene-edited HSPC repopulating capacity and clonal output long-term post-transplantation *58*
3D scaffolds enable polyclonal and long-term engraftment of genetically engineered HSPCs 61
Nichoids increase the functionality of hspcs upon ex vivo manipulation *61*
3D culture preserves cellular morphology and polarity, profoundly reshaping the HSPC transcriptional profile *63*

Nichoid pre-culture allows efficient genetic engineering with multiple editing platforms 67
3D culture enables superior long-term engraftment of HDR-edited hspcs 69
Nichoids increase the clonal output of repopulating hspcs upon LV-mediated gene addition..... 71
3D scaffolds ameliorate the functionality of patient-derived hspcs for GT applications 75
Discussion 79
Materials and methods 89
References 99
Appendices 129

Acronyms and abbreviations

53BP1: p53 binding protein 1

7-AAD: 7-aminoactinomycin D

8-oxo-dG: 8-oxo-2’-deoxyguanosine

AAV: Adeno-associated virus

AAV6: Adeno-associated Virus serotype 6

AAVS1: adeno-associated virus integration site 1

ABE: adenine base editor

ADA-SCID: adenosine deaminase deficiency

AdV: Adenovirus

ATM: ataxia telangiectasia mutated

ATR: ataxia telangiectasia and RAD3-related

ATRIP: ATR-interacting protein

BAR: barcode sequence

BARD1: BRCA-associated RING domain protein 1

BE: Base editing

BLM: Bloom Syndrome protein

BM: bone marrow

BRCA1: breast cancer 1

BRCA2: breast cancer 2

Cas: CRISPR-associated protein system

Cas9n: Cas9 nickase

CB: Cord blood

CBE: cytosine base editor

CCR5: chemokine receptor type 5

CDC42: cell division cycle 42

CDK: cyclin-dependent kinase

CDK4/6: cyclin-dependent kinases 4 and 6

CDK4/6i: cyclin-dependent kinases 4 and 6 inhibitor

CFU-C: colony-forming unit cell

CGD: chronic granulomatous disease

CHK1: checkpoint kinase protein 1

CHK2: checkpoint kinase protein 2

CIS: common integration site

CLP: Common Lymphoid progenitor

CMP: Common Myeloid progenitor

CRISPR: Clustered Regularly Interspaced Short Palindromic Repeats
CsH: cyclosporine H
CtIP: CtBP-interacting protein
D-loop: displacement-loop
dCas9: endonuclease dead Cas9
DDR: DNA damage response
DNA-PKcs: DNA-dependent protein kinase catalytic subunit
DNA2: DNA replication helicase/nuclease 2
DSB: double strand break
ECM: extracellular matrix
EdU: 5-ethynil-20-deoxyuridine
EXO1: exonuclease 1
G-CSF: granulocyte-colony stimulating factor
GE: gene editing
GFP: green fluorescent protein
GM-CSF: granulocyte-colony stimulating factor
GMP: good manufacturing practice
GMP: Granulocyte Monocyte Progenitor
gRV: gamma retrovirus
gRNA: guide RNA
GSEA: gene set enrichment analysis
GT: Gene therapy
GvHD: graft-versus-host disease
HDR: homology directed repair
HLA: human leukocyte antigen
HR: homologous recombination
HSC: Hematopoietic stem cell
HSC-T: HSC transplantation
HSPC: Hematopoietic stem and progenitor cell
HSPC-GT: Hematopoietic stem and progenitor cell gene therapy
IDLV: integrase-defective lentiviral vector
IFN I: type I interferons
IL: interleukin
iPSC: induced pluripotent stem cell
IS: Integration site
ITGA3: integrin $\alpha 3$
ITR: inverted terminal repeat

KO: knock out

LIG4: Ligase IV

LMPP: Lymphoid-primed multipotent progenitor

LT-HSC: long-term hematopoietic stem cell

LTC-IC: long-term culture-initiating cell

LV: lentivirus

MAPK: mitogen-activated protein kinase

MDC1: mediator of DNA damage checkpoint 1

MEP: Megakaryocyte Erythrocyte progenitor

MHC: major histocompatibility complex

MK2: MAPKAPK2

MLE: maximum likelihood estimation

MMEJ: microhomology-mediated end joining

MPP: Multipotent progenitor

MRN complex: composed of MRE11, RAD50, and NBS1

MSC: mesenchymal stromal cell

NAC: *N*-acetyl-cystein

NBS1: Nijmegen breakage syndrome 1

NBSGW: NOD.B6.SCID Il2rγ−/−KitW41/W41

NHEJ: non-homologous end joining

NK: natural killer

NOD: non-obese diabetic

NSG: non-obese diabetic (NOD)-severe combined immunodeficiency (SCID)-IL2Rg$^{-/-}$

p-p38: phopsho-p38

p38i: SB203580

PALB2: partner and localizer of BRCA2

PAM: protospacer adjacent motif

PAMP: pathogen-associated molecular pattern

PAXX: paralogue of XCCR4 and XLF

PB: peripheral blood

PE: Prime editing

pegRNA: prime editing guide RNA

PGE2: 16,16-dimethyl prostaglandin E2

PRR: pattern recognition receptor

RNP: ribonucleoprotein

ROS: reactive oxygen species

RPA: replication protein A
RVD: repeated variable di-residue
SCF: Stem cell factor
SCID: Severe combined immune-deficient
SCIDX1: X-linked severe combined immunodeficiency
SDSA: synthesis-dependent strand annealing
sgRNA: single-guide RNA
SMC1: structural maintenance of chromosomes 1
SP: Spleen
SSB: single strand break
ssODN: single-stranded oligodeoxynucleotide
ST-HSC: short-term hematopoietic stem cell
TALEN: Transcription Activator-Like Effector Nuclease
Tru-gRNA: truncated guide RNA
UGI: uracil glycosylase inhibitors
VCN: vector-copy number
WAS: Wiskott-Aldrich Syndrome
XRCC4: x-ray repair cross-complementing protein 4
XLF: XCR4 like factor
yH2AX: phosphorylated form at serine 139 of H2AX
ZFN: Zinc Finger Nuclease
ZFP: Zinc Finger Protein

List of figures

Figure. 1. Human hematopoietic hierarchy models. *The classic hematopoiesis model involves discrete states of cells with uniform potential, in which fate decisions occur through binary steps. In the continuum model, cell states show variable lineage biases with no specific lineage transitions. Finally, the punctuated continuum consists of different cell states of heterogeneous pools of cells, allowing both stepwise lineage-restricting transitions and continuous differentiation events* (adapted from Liggett and Sankaran, 2020)*.*

Figure 2. Human HSC phenotypic markers. *Each HSPC subset is characterized by a unique combination of surface markers, with LT-HSCs enriched in the fraction of Lin-CD34+CD38-CD45RA-CD133+CD90+CD49f+ cells* (adapted from Doulatov *et al.*, 2012)*.*

Figure 3. The hematopoietic stem cell niche. *The complex interplay between HSCs and the BM niche reveals that the combination of many soluble factors, cellular ligands, and biochemical and mechanical stimuli orchestrate HSC quiescence, maintenance, differentiation, and retention* (adapted from Li *et al.*, 2021)*.*

Figure 4. Biomechanical cues in HSCs. *Mechanical inputs, such as the blood flow, are integrated by mechanosensors, generating intrinsic forces that can propagate to bystander cells through cellular junctions or directly to the nucleus. Then, mechanical forces cooperate with biochemical signals to elicit complex cellular responses* (adapted from Li *et al.*, 2021)*.*

Figure 5. Representative images of different colonies in a CFU-C assay. *(**A**) Erythroid colony. (**B**) Myeloid colony. (**C**) Mixed colony* (adapted from *Human Methylcellulose Base Media (HSC002) by R&D Systems, Part of Bio-Techne*)*.*

Figure 6. Ex vivo HSPC-GT. *HSPCs are harvested from the patient, genetically manipulated ex vivo through the preferred engineering platform of choice, and then reinfused upon conditioning to reconstitute the entire hematopoietic system* (adapted from Ferrari *et al.*, 2023)*.*

Figure 7. Zinc-finger nucleases. *ZFNs are dimeric nucleases consisting of zinc-finger protein (ZFP) arrays responsible for sequence specificity and an endonuclease domain of the FokI enzyme. ZFN pairs recognize target sequences that span between 18 and 36 base pairs, generating a DSB with overhangs in the spacer region* (adapted from Kim and Kim, 2014)*.*

Figure 8. Transcription activator-like effector nucleases. *TALENs are dimeric nucleases consisting of TALE modules responsible for sequence specificity through the RVD region (in red) and an endonuclease domain of the FokI enzyme. TALENs*

generate a DSB with overhangs in the spacer region embedded in a 30-40 nucleotide-long specific sequence (adapted from Kim and Kim, 2014).

Figure 9. The CRISPR/Cas9 system. *Cas9 exploits the gRNA to bind its genomic target, allowing efficient DNA cleavage near the PAM sequence, primarily inducing a precise blunt-ended DSB* (adapted from Kim and Kim, 2014).

Figure 10. The two major DSB repair pathways. *Schematic representation of the error-prone NHEJ (left) and the high-fidelity HDR (right) pathways* (adapted from Scully *et al.*, 2019).

Figure 11. General outcomes of nuclease-based gene editing. *Depending on the cell cycle state and the consequent DNA repair mechanism engaged, the nuclease-induced DSB can be repaired by NHEJ to inactivate the target gene or by HDR to correct a faulty gene or allow targeted integration of a therapeutic cassette, usually delivered with an AAV6 vector (created with Biorender).*

Figure 12. Base editors enable single nucleotide conversions. *(A) CBE and (B) ABE deaminates target C and A, generating U and I, respectively, and ultimately allowing C-G to T-A and A-T to G-C conversion* (adapted from Anzalone, Koblan and Liu, 2020).

Figure 13. Prime editing relies on retrotranscription to induce all types of genetic modifications. *PE contains a Cas9n fused with a reverse transcriptase that relies on pegRNA to precisely edit the target locus, introducing the desired modification encoded in the RNA template* (adapted from Anzalone, Koblan and Liu, 2020).

Figure 14. Schematic representation of DDR pathway. *The DDR cascade is a complex cellular response triggered by multiple DNA lesions, which are sensed by DNA damage sensors that promote apical kinases ATM and ATR activation. These two proteins phosphorylate multiple DNA damage mediators and the major downstream kinases CHK2 and CHK1, stimulating DNA repair while inhibiting cell cycle progression* (adapted from Sulli, Di Micco and Di Fagagna, 2012).

Figure 15. Strategies to facilitate ex vivo culture and expansion of HSCs. *The advancement of ameliorating HSC culture conditions focuses on substituting serum albumin with chemically stable compounds, fine-tuning the cytokine cocktail, introducing anti-differentiation small molecules, and, recently, developing more advanced culture systems with synthetic matrixes and scaffolds* (adapted from Meaker and Wilkinson, 2024).

Figure 16. p38-induced ROS mediate fast cell cycle progression leading to DNA damage and DDR activation. *(**A**) Percentage of p-p38+ cells (n=4,6,5). Mann-Whitney test. (**B**) Experimental workflow. Human CB-derived HSPCs were*

*treated with p38i or vehicle (DMSO) in the first two days and collected for downstream analyses on days 3 and 7. (**C,D**) Percentage of cytosolic (**C**) and mitochondrial (**D**) ROS+ cells ((**C**), n=5,5,4,4; (**D**), n=6,7,6,4). Mann-Whitney test. (**E**) Division index measured from CellTrace dye dilution on day 7 (n=6). Wilcoxon test. (**F**) Confluence analysis over time reported as fold change to the first time point (n=3). Mann-Whitney test. (**G**) MFI of 8-oxo-dG on day 7 (n=5). Mann-Whitney test. (**H**) Quantification of SSBs and DSBs by alkaline comet assay; each dot represents a single cell (more than 300 cells were analyzed for each condition). Median ± 95% CI. Mann-Whitney test. (**I,J**) Percentage of (**I**) γH2AX or (**J**) pRPA positive HSPCs ((**I**), n=9,7,3,7,4; (**J**), n=6,6,3,6,3). Mann-Whitney test. (**K**) Western Blot analysis of pATR (left) and pCHK1 (right) on day 7 (n=4). Histone H3 was used as a loading control, and fold change relative to control is reported. One-sample T-test. (**L**) Percentage of phenotypically defined HSPC subsets (n=7). Wilcoxon test. Unless otherwise specified, Mean ± SEM. *p < 0.05; **p < 0.01; ****p < 0.0001.*

Figure 17. p38 inhibition improves gene-edited HSPC repopulating capacity and clonal output long-term post-transplantation. *(**A**) Experimental workflow. Human CB-derived HSPCs were treated with p38i or vehicle (DMSO) in the first two days and and collected on day 3 for Cas9/AAV6 gene editing to insert a GFP reporter within the AAVS1 locus. Edited cells were collected for downstream analyses on days 4 and 7 (24h and 96h post-editing, respectively). After 15 weeks post-injection, CD34+ cells were purified from the BM of the mice and transplanted into secondary recipients. (**B**) Percentage of GFP+ cells (within CD34+ cells) by FACS analysis on day 7 (n=9). (**C**) Percentage of phenotypically defined HSPC subsets (n=8). Wilcoxon test. (**D**) Number of erythroid, myeloid, and mixed colonies generated in CFU-C assay (n=10). Wilcoxon test. (**E,F**) Percentage of human CD45+ (hCD45+) cells measured in the PB (**E**) over time and BM (**F**) at the endpoint of transplanted mice (n=16,18). Mann-Whitney test (calculated at the last time point for PB). (**G,H**) Percentage of GFP+ cells (within hCD45+ cells) in the PB (**G**) over time and BM (**H**) from mice in (**E,F**) (n=16,18). Mann-Whitney test (calculated at the last time point for PB). (**I,J**) Number of unique indels (**I**) and BARs (**J**) in the BM of mice from (**F**) at the endpoint ((**I**), n=8,10; (**J**), n=19,24). Mann-Whitney test (**K**) Percentage of hCD45+ cells measured in the PB over time of transplanted secondary recipients (n=9,11). Mann-Whitney test (calculated at the last time). (**L**) Percentage of GFP+ cells (within hCD45+ cells) in the PB over time from mice in (**K**) (n=9,11). Mann-Whitney test. Mean ± SEM. *p < 0.05; **p < 0.01.*

Figure 18. Nichoids increase the functionality of HSPCs upon ex vivo manipulation. *(**A**) Representative image (top) and scanning electron microscopy*

*(bottom) of the nichoid culture substrate. (**B**) Experimental workflow. Human CB-derived HSPCs were seeded on 2D or 3D immediately after thawing and collected for downstream analyses on days 3 and 7. (**C**) Percentage of phenotypically defined HSPC subsets (n=9,9,10,10). (**D**) Number of erythroid, myeloid, and mixed colonies generated in CFU-C assay (n=5). Mann-Whitney test. (**E,F**) Number of lineages (**E**) and cells (**F**) per colony generated by HSC-enriched single cells (more than 250 colonies analyzed for each condition). Median ± 95% CI. Mann-Whitney test. (**G-I**) Percentage of human CD45+ (hCD45+) cells measured in the PB (**G**) over time, and BM (**H**) and SP (**I**) at the endpoint of transplanted mice (n=5). Mann-Whitney test (calculated at the last time point for PB). (**J**) Number of erythroid, myeloid, and mixed colonies generated by BM-derived CD34+ cells purified from mice in (**H**) (n=5). Mann-Whitney test. (**K**) Relative number of HSCs required to generate comparable engraftment calculated by MLE from (**H**) (n=5). Mann-Whitney test. Unless otherwise specified, Mean ± SEM. *p < 0.05; **p < 0.01.*

Figure 19. 3D culture preserves cellular morphology and polarity, profoundly reshaping the HSPC transcriptional profile. *(**A**) Differentially modulated categories from GSEA (FDR < 0.05) of 3D- vs. 2D-cultured HSPCs. Color gradient reflects the normalized enrichment score (NES). (**B**) Average gene expression (Zscore). Differentially expressed genes (FDR < 0.05) are represented with larger symbols. (**C**) Representative plot (left) and MFI (Median Fluorescence Intensity) (right) of CellTrace dye dilution on day 7 (n=6). Wilcoxon test. (**D**) MFI of ROS (by CellROX staining) on day 7 (n=5). Mann-Whitney test. (**E**) MFI of 8-oxo-dG on day 7 (n=6). Wilcoxon test. (**F**) Quantification of SSBs and DSBs by alkaline comet assay; each dot represents a single cell (more than 200 cells were analyzed for each condition). Median ± 95% CI. Mann-Whitney test. (**G**) Percentage of phospho-p38 (p-p38)-positive cells on day 7 (n=5). Mann-Whitney test. (**H**) Representative 3D renderings of HSPCs on day 7 of 2D or 3D culture. (**I,J**) Quantification of (**I**) volume and (**J**) squashing morphological parameters on day 7; each dot represents a single cell or nucleus (more than 250 cells were analyzed for each condition). Median ± 95% CI. Mann-Whitney test. (**K**) Representative immunofluorescence staining of tubulin spatial localization on day 7. (**L**) Representative images (left) and quantification (right) of tubulin score on day 7 (more than 100 cells were analyzed for each condition). Median Value. Mann-Whitney test. Unless otherwise specified, Mean ± SEM. *p < 0.05; **p < 0.01; ****p < 0.0001.*

Figure 20. Nichoid pre-culture allows efficient genetic engineering with multiple editing platforms. *(**A**) Experimental workflow. Human CB- or mPB-derived HSPCs were seeded on 2D or 3D immediately after thawing and collected on*

*day 3 for nucleofection. Specifically, CB-derived cells were edited with Cas9/AAV6 to insert a GFP reporter within the AAVS1 locus, while mPB-derived cells were edited with BE or PE to disrupt the B2M gene. HSPCs from both the 2D and 3D conditions were seeded in 2D after nucleofection and collected for downstream analyses on days 4 and 7. Transplantation was performed only for the Cas9/AAV6 treatment. (**B**) Percentage of CD34+ edited cells by FACS analysis on day 7 (n=6). (**C**) Number of erythroid, myeloid, and mixed colonies generated in CFU-C assay from edited HSPCs seeded on day 4 (n=6). Wilcoxon test. (**D,E**) Percentage of hCD45+ cells measured in the PB (**D**) over time and BM (**E**) at the endpoint of transplanted mice (n=11). Mann-Whitney test (calculated at the last time point for PB). (**F**) Percentage of GFP+ cells (within hCD45+ cells) in the PB over time from mice in (**D**) (n=11). (**G**) Number of erythroid, myeloid, and mixed colonies generated by BM-derived CD34+ cells purified from mice in (**E**) (n=11). Mann-Whitney test. (**H**) Relative number of HSCs required to generate comparable engraftment calculated by MLE from (**E**) (n=11). Mann-Whitney test. Mean ± SEM. *p < 0.05; **p < 0.01.*

Figure 21. 3D culture enables superior long-term engraftment of HDR-edited HSPCs. *(**A**) Experimental workflow. Human CB-derived HSPCs were seeded on 2D or 3D immediately after thawing and collected on day 3 for Cas9/AAV6 gene editing in the presence of GSE56 and Ad5-E4orf6/7 editing enhancers to insert a GFP reporter within the AAVS1 locus. HSPCs from both the 2D and 3D conditions were seeded in 2D after nucleofection and collected for downstream analyses on days 4 and 7. After 15 weeks post-injection, CD34+ cells were purified from the BM of the mice and transplanted into secondary recipients. (**B,C**) Percentage of hCD45+ cells measured in the PB (**B**) over time and BM (**C**) at the endpoint of transplanted mice (n=5). Mann-Whitney test (calculated at the last time point for PB). (**D**) Percentage of GFP+ cells (within hCD45+ cells) in the PB over time from mice in (**B**) (n=5). (**E**) Number of erythroid, myeloid, and mixed colonies generated by BM-derived CD34+ cells purified from mice in (**C**) (n=5). Mann-Whitney test. (**F**) Relative number of HSCs required to generate comparable engraftment calculated by MLE from (**C**) (n=5). Mann-Whitney test. (**G,H**) Percentage of hCD45+ cells measured in the PB (**G**) over time and BM (**H**) at the endpoint of transplanted secondary recipients (n=8,6). Mann-Whitney test (calculated at the last time point for PB). (**I,J**) Percentage of GFP+ cells (within hCD45+ cells) in the PB (**I**) over time and BM (**J**) from mice in (**G,H**) (n=8,6). Mann-Whitney test (calculated at the last time point for PB). (**K**) Relative number of HSCs required to generate comparable engraftment calculated by MLE from (h) (n=8,6). Mann-Whitney test. Mean ± SEM. *p < 0.05; **p < 0.01.*

Figure 22. Nichoids increase the clonal output of repopulating HSPCs upon LV-mediated gene addition. *(**A**) Experimental workflow. Human mPB-derived HSPCs were seeded on 2D or 3D immediately after thawing and transduced on day 1 with a GFP-expressing LV vector in the presence of PGE2 alone or in combination with CsH. Specifically, transduction was performed at MOI 100 for PGE2 alone and MOI 30 with CsH. After 14h post-transduction (day 2), HSPCs from both the 2D and 3D conditions were seeded in 2D and collected for downstream analyses on days 2 and 10. Transplantation was performed only for the CsH condition. (**B**) Percentage of GFP+ cells (within CD34+ cells) by FACS analysis on day 10 (n=6). Mann-Whitney test. (**C**) Number of erythroid, myeloid, and mixed colonies generated in CFU-C assay from transduced HSPCs seeded on day 2 (n=6). Wilcoxon test. (**D,E**) Percentage of hCD45+ cells measured in the PB (**D**) over time and BM (**E**) at the endpoint of transplanted mice (n=7). Mann-Whitney test (calculated at the last time point for PB). (**F**) Percentage of GFP+ cells (within hCD45+ cells) in the PB over time from mice in (**D**) (n=7). (**G**) Number of erythroid, myeloid, and mixed colonies generated by BM-derived CD34+ cells purified from mice in (**E**) (n=7). Mann-Whitney test. (**H**) Relative number of HSCs required to generate comparable engraftment calculated by MLE from (**E**) (n=7). Mann-Whitney test. (**I**) Representative plots of tracked ISs and their relative abundance over time from mice of the 2D (top, mouse A4) and 3D (bottom, mouse B12) conditions. Each colored bar univocally identifies an IS with ≥1% representation in at least one time point, with its abundance proportional to the height of the bar; a colored ribbon connects two neighboring time points for each recaptured clone. The total number of unique ISs is reported on top of each bar. (**J,K**) Number of estimated clones (**J**) and clonal population diversity measured by Shannon index normalized on VCN (**K**) from IS analyses. Mann-Whitney test. (**L**) Representative plots of CIS from mice of the 2D (left, mouse A4) and 3D (right, mouse B12) conditions. Each dot represents a gene, which is labeled with the corresponding color if observed as significant. The dashed line is the alpha value 0.05. Grubbs test. Mean ± SEM. *p < 0.05; **p < 0.01; ***p < 0.001.*

Figure 23. 3D scaffolds ameliorate the functionality of patient-derived HSPCs for GT applications. *(**A**) Experimental workflow. mPB-derived HSPCs from WAS patients were seeded on 2D (upon coating with retronectin) or 3D immediately after thawing and transduced with two hits of WASP-expressing LV on day 1 and 2 at MOI 100. After 14h from the second round of transduction (day 3), HSPCs from both the 2D and 3D conditions were seeded in 2D and collected for downstream analyses on days 3 and 10. Three independent technical replicates were performed for each donor (different symbols identify the two patients). (**B**) VCN of transduced*

*HSPC on day 10 (n=6). (**C**) Number of erythroid, myeloid, and mixed colonies generated in CFU-C assay from transduced HSPCs seeded on day 3 (n=6). Mann-Whitney test. (**D,E**) Percentage of hCD45+ cells measured in the PB (d) over time and BM (e) at the endpoint of transplanted mice (n=5). Mann-Whitney test. (**F**) Relative number of HSCs required to generate comparable engraftment calculated by MLE from (**E**) (n=5). Mann-Whitney test. Mean ± SEM. *p < 0.05; **p < 0.01.*

Appendix 1. Mitogenic ROS promotes HSPC proliferation leading to DNA damage. *(**A**) Western Blot analysis of the p38 target pMK2 (n=3). MK2 was used as loading control and fold changes relative to DMSO are reported. One-sample T-test. (**B**) Apoptosis analysis performed within CD34+ cells (n=4). (**C**) MFI of CellROX (n=5). Mann-Whitney test. (**D**) Proliferation rate of HSPC over time (n=6). Wilcoxon test. (**E**) Percentage of p-p38+ cells on day 7 (n=5). (**F**) MFI of CellROX (n=3). Kruskal-Wallis test. (**G**) Proliferation rate of HSPC over time (n=5). Mann-Whitney test (each treatment vs. vehicle). (**H**) Percentage of p-p38+ cells on day 7 (n=3). (**I**) Quantification of SSBs and DSBs by alkaline comet assay on day 7; each dot represents a single cell (more than 200 cells were analyzed for each condition). Median ± 95% CI. Mann-Whitney test. (**J**) Division index measured from CellTrace dye dilution on day 7 (n=6). Wilcoxon test. (**K**) Representative immunofluorescence staining of DAPI (blue), yH2AX (green), and pRPA (red). Yellow boxes indicate zoomed-in images. Unless otherwise specified, Mean ± SEM. *p < 0.05; **p < 0.01; ****p < 0.0001.*

Appendix 2. p38i increases the long-term engraftment of HDR-edited HSPCs. *(**A**) Apoptosis analysis performed within CD34+ cells on day 4 (n=6). (**B**) Percentage of GFP+ cells within HSPC subsets on day 7 (n=9). (**C**) Percentage of hCD45+ cells measured in the SP at the endpoint of transplanted mice (n=16,18). Mann-Whitney test. (**D-F**) Percentage of human graft composition in the PB (**D**), BM (**E**), and SP (**F**) at the endpoint of transplanted mice (n=16,18). (**G**) Percentage of GFP+ cells (within hCD45+ cells) in the SP at the endpoint of mice in (**C**) (n=16,18). (**H,I**) Percentage of hCD45+ cells measured in the BM (**H**) and SP (**I**) at the endpoint of transplanted secondary recipients (n=9,11). (**J-L**) Percentage of human graft composition in the PB (**J**), BM (**K**), and SP (**L**) at the endpoint of transplanted secondary recipients (n=9,11). Mann-Whitney test. (**M,N**) Percentage of GFP+ cells (within hCD45+ cells) measured in the BM (**M**) and SP (**N**) at the endpoint of mice in (**H,I**) (n=9,11). Mann-Whitney test. Mean ± SEM. *p < 0.05; **p < 0.01.*

Appendix 3. Nichoids increase the functionality of ex vivo cultured HSPCs. *(**A**) Representative gating strategy for apoptosis analysis. Cells are distinguished as alive (7-AAD-Annexin V-), early apoptotic (7-AAD-Annexin V+), late apoptotic (7-*

*AAD+Annexin V+), and necrotic (7-AAD+Annexin V-). (**B**) Apoptosis analysis performed within CD34+ cells treated or not with a citrate solution (n=5). (**C**) Number of erythroid, myeloid, and mixed colonies generated in CFU-C assay from HSPCs treated or not with a citrate solution seeded on day 3 (n=5). (**D**) Apoptosis analysis performed within CD34+ cells (n=6,6,5,5). (**E**) Representative gating strategy for phenotypically defined HSPC subsets analysis. CD34+ cells were identified within alive cells from (a). HSPC subpopulations were discriminated as CD34+CD133-CD90-, CD34+CD133+CD90-, and primitive fraction CD34+CD133+CD90+. (**F**) Number of erythroid, myeloid, and mixed colonies generated in CFU-C assay from HSPCs seeded on day 3 upon culture in different settings (n=5). Mann-Whitney test. (**G**) Number of erythroid, myeloid, and mixed colonies generated in CFU-C assay from HSPCs seeded on 2D or 3D immediately after thawing or upon one or two days after initial 2D culture (n=6). Wilcoxon test. (**H**) Representative gating strategy for HSC-enriched single-cell differentiation assay. Colonies were considered in the analysis only if >30 cells were present in the following gates: Erythroid, Ery (CD45-GlyA+); Myeloid, My (CD45+CD11b+); Natural Killer, NK (CD45+CD56+CD11b-); Megakaryocyte, Meg (CD45+CD41+GlyA-). (**I,J**) Percentage of different lineages within uni-lineage (i) or bi/multi-lineage (j) colonies generated in single-cell differentiation assay. (**K**) Representative gating strategy for PB, BM, and SP analyses. hCD45+ cells were identified within alive cells (7-AAD-). Within the human graft, cells were discriminated as B cells (CD45+CD19+), myeloid cells (CD45+CD19-CD13+), T cells (CD45+CD19-CD13-CD3+), HSPCs (CD45+CD19-CD13-CD3-CD34+) or other (CD45+CD19-CD13-CD3-CD34-). (**L-N**) Percentage of human graft composition in the PB (**L**), BM (**M**), and SP (**N**) at the endpoint of transplanted mice (n=5). Mann-Whitney test. Mean ± SEM. *p < 0.05; **p < 0.01.*

Appendix 4. 3D culture remodels HSPC transcriptional profile, reducing cell proliferation and DNA damage accumulation. *(**A**) Differentially expressed genes (FDR < 0.05) in 3D- vs. 2D-cultured HSPCs. (**B**) Representative plot (left) and MFI (right) of CellTrace dye dilution on day 7 (n=6) in the HSC-enriched subset. Mean ± SEM. Wilcoxon test. (**C**) Representative immunofluorescence staining (left) of DAPI (blue), pRPA (red), and γH2AX (green) and number of DDR foci (right) per cell (more than 800 cells were analyzed for each condition). Median. Mann-Whitney test. *p < 0.05; **p < 0.01; ****p < 0.0001.*

Appendix 5. Nichoids allow efficient GE by Cas9/AAV6, BE, and PE. *(**A**) Apoptosis analysis performed within CD34+ cells on day 4 (n=6). (**B**) Percentage of phenotypically defined HSPC subsets on day 4 (n=6). (**C**) Representative gating*

*strategy for editing efficiency analysis. GFP+ or B2M- cells were identified within CD34+ cells (gated within alive cells). (**D**) Percentage of edited cells within HSPC subsets on day 7 (n=6). (**E**) Proliferation rate of HSPC upon GE (GE=day 3, 24h=day 4, 96h=day 7). (n=6). Wilcoxon test. (**F**) Representative plot (left) and percentage of HSPCs in indicated cell cycle phases (right) on day 3 (before GE). (**G**) Percentage of hCD45+ cells measured in the SP at the endpoint of transplanted mice (n=11). Mann-Whitney test. (**H,I**) Percentage of GFP+ cells (within hCD45+ cells) in the BM (**H**) and SP (**I**) at the endpoint of transplanted mice (n=11). (**J-L**) Percentage of human graft composition in the PB (**J**), BM (**K**), and SP (**L**) at the endpoint of transplanted mice (n=11). Mean ± SEM. *p < 0.05.*

Appendix 6. 3D culture improves HDR-edited HSPC repopulating capacity in long-term experiments. *(**A**) Apoptosis analysis performed within CD34+ cells on day 4 (n=4). (**B**) Percentage of phenotypically defined HSPC subsets on day 4 (n=4). (**C,D**) Percentage of GFP+ cells within CD34+ cells (c) and HSPC subsets (d) on day 7 (n=4). (**E**) Number of erythroid, myeloid, and mixed colonies generated in CFU-C assay from edited HSPCs seeded on day 4 (n=4). Mann-Whitney test. (**F**) Percentage of hCD45+ cells measured in the SP at the endpoint of transplanted mice (n=5). Mann-Whitney test. (**G,H**) Percentage of GFP+ cells (within hCD45+ cells) in the BM (g) and SP (h) at the endpoint of transplanted mice (n=5). (**I-K**) Percentage of human graft composition in the PB (i), BM (j), and SP (k) at the endpoint of transplanted mice (n=5). (**L,M**) Percentage of hCD45+ cells (**L**) and GFP+ cells (within hCD45+ cells) (**M**) measured in the SP at the endpoint of transplanted secondary recipients (n=8,6). Mann-Whitney test. (**N-P**) Percentage of human graft composition in the PB (**N**), BM (**O**), and SP (**P**) at the endpoint of transplanted secondary recipients (n=8,6). Mean ± SEM. *p < 0.05; **p < 0.01; ***p < 0.001.*

Appendix 7. 3D culture enables efficient LV-mediated gene addition. *(**A**) Apoptosis analysis performed within CD34+ cells on day 2 (n=3). (**B**) Percentage of GFP+ cells within HSPC subsets on day 10 (n=6). Mann-Whitney test. (**C**) VCN of transduced HSPC on day 10 (n=6). Mann-Whitney test. (**D**) Percentage of hCD45+ cells measured in the SP at the endpoint of transplanted mice (n=7). Mann-Whitney test. (**E,F**) Percentage of GFP+ cells (within hCD45+ cells) in the BM (**E**) and SP (**F**) at the endpoint of transplanted mice (n=7). (**G-I**) Percentage of human graft composition in the PB (**G**), BM (**H**), and SP (**I**) at the endpoint of transplanted mice (n=7). Mann-Whitney test. Mean ± SEM. *p < 0.05; **p < 0.01; ***p < 0.001.*

Appendix 8. IS analyses in the human graft of LV-transduced HSPCs. *(**A**) Number of unique integrations from IS analyses. Mean ± SEM. Mann-Whitney test. (**B**) Tracking and relative abundance of ISs reported over time in transplanted mice*

*(A=2D, B=3D). Each colored bar univocally identifies an IS with ≥1% representation in at least one time point, with its abundance proportional to the height of the bar; a colored ribbon connects two neighboring time points for each recaptured clone. The total number of unique ISs is reported on top of each bar. *p < 0.05; **p < 0.01.*

Appendix 9. Integration profile from IS analyses. *(**A**) IS gene frequency and CIS analysis in transplanted mice (A=2D, B=3D). Each dot represents a gene, which is labeled with the corresponding color if observed as significant. The dashed line is the alpha value 0.05. Grubbs test.*

Appendix 10. Nichoids for gene addition in WAS patient-derived HSPCs. *(**A**) Apoptosis analysis performed within CD34+ cells on day 3 (n=6). (**B**) Percentage of phenotypically defined HSPC subsets on day 3 (n=6). (**C**) Percentage of hCD45+ cells measured in the SP at the endpoint of transplanted mice (n=5). Different symbols identify the two patients. Mann-Whitney test. (**D-F**) Percentage of human graft composition in the PB (**D**), BM (**E**), and SP (**F**) at the endpoint of transplanted mice (n=7). Mann-Whitney test. Mean ± SEM. **p < 0.01.*

Introduction

The hematopoietic system and hematopoietic stem and progenitor cells (HSPCs)

Blood and hematopoiesis

Blood connective tissue consists of a protein-rich fluid mixed with a corpuscular fraction of heterogeneous cells, responsible for multiple vital functions, including oxygen transport, coagulation and wound healing, tissue homeostasis and remodeling, and immune surveillance. Plasma represents the liquid component of the blood and contains primarily water, electrolytes, blood proteins like albumin and globulin, vitamins, coagulants, immunoglobulins, hormones, and other enzymes (Mathew, Sankar and Varacallo, 2023). Conversely, the cellular fraction is classically divided into the myeloid and lymphoid branches: the former is responsible for oxygen transport, homeostasis, and innate immunity, while the latter serves primarily as adaptive immunity. The major myeloid cell types include erythrocytes, megakaryocytes (MKs), monocytes, neutrophils, eosinophils, basophils, and dendritic cells (DCs), while the lymphoid lineage is characterized by B and T lymphocytes (B and T cells), and natural killer cells (NKs) (Liggett and Sankaran, 2020). Hematopoietic cell's life span varies from a few days to multiple years, requiring their continuous replenishment. Indeed, most circulating blood cells are postmitotic and result from a series of differentiation intermediates of hematopoietic stem and progenitor cells (HSPCs), which are responsible for lifelong blood cell production, generating an astonishing 500 billion cells each day (Fliedner *et al.*, 2002). This complex process of blood production is called hematopoiesis. Hematopoiesis begins in the embryo with the generation of the hemogenic endothelium (Ivanovs *et al.*, 2014), moves to the fetal liver (Yokomizo *et al.*, 2022), and continues in the bone marrow (BM) through adult life, which is located in the medullary cavity of long and flat bones, where hematopoietic stem cells (HSCs) reside (Dzierzak and Speck, 2008).

Hematopoiesis is organized as a hierarchical cellular system, with a restricted pool of HSCs that produce a sequence of increasingly more lineage-restricted progenitors and mature cells, thus enabling the maintenance of blood homeostasis while also rapidly respond to non-physiological demands (Notta *et al.*, 2011). According to the classical model, HSC fate decision occurs through binary steps, with discrete cell states of uniform potential committed only to a specific lineage (Orkin and Zon,

2008). In general, the immediate progeny of HSCs consists of multipotent progenitor cells (MPPs), which retain full lineage differentiation capacity but show only transient multilineage reconstitution due to limited self-renewal. In turn, MPPs give rise to lymphoid-primed multipotent progenitors (LMPPs) and common myeloid progenitors (CMPs), which will then generate common lymphoid progenitors (CLPs), granulocyte/macrophage progenitors (GMPs), and megakaryocyte/erythroid progenitors (MEPs). Finally, these oligopotent progenitors will continue to differentiate towards more lineage-restricted progenitors and eventually mature into terminal mature blood cells (Weissman and Shizuru, 2008). However, our unique understanding of the hematopoietic system has evolved over the years, and this model has been constantly updated. For instance, recent in-depth studies on lineage tracing showed that rather than a classical stepwise roadmap, hematopoiesis is more a continuous process (Laurenti and Göttgens, 2018), as supported by the evidence that megakaryocytes can directly differentiate from HSCs, skipping the MPPs and MEPs intermediate stages (Notta *et al.*, 2016). From this and other studies, hematopoiesis is now defined as a punctuated continuum organized in different cell states of heterogeneous cell pools, each primed to differentiate towards different hematopoietic lineages, where stepwise lineage-restricting transitions coexist alongside continuous differentiation events (Figure 1) (Liggett and Sankaran, 2020).

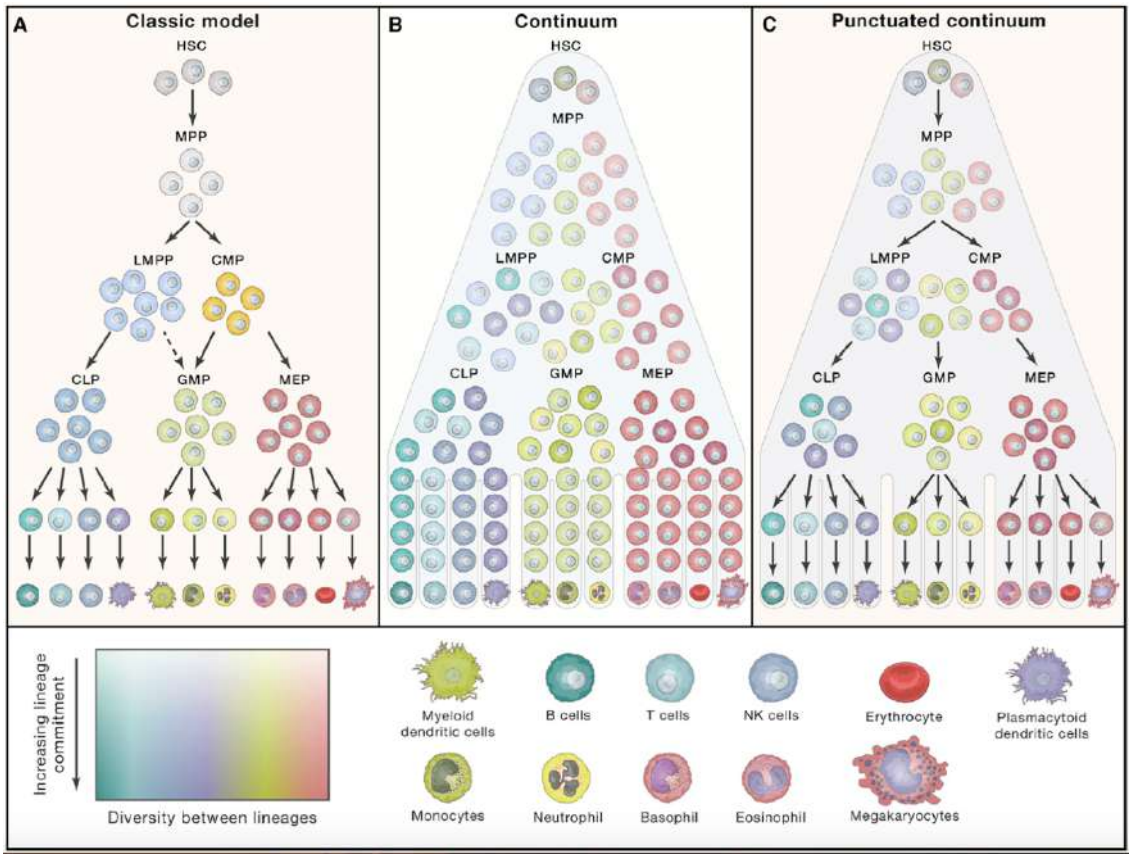


Figure. 2. Human hematopoietic hierarchy models. *The classic hematopoiesis model involves discrete states of cells with uniform potential, in which fate decisions occur through binary steps. In the continuum model, cell states show variable lineage biases with no specific lineage transitions. Finally, the punctuated continuum consists of different cell states of heterogeneous pools of cells, allowing both stepwise lineage-restricting transitions and continuous differentiation events* (adapted from Liggett and Sankaran, 2020).

Hematopoietic stem cells (HSCs)

HSCs are defined by three main functional properties (Dalerba, Cho and Clarke, 2007): i) self-renewal - the potential to generate identical daughter cells with the same proliferation, expansion, and differentiation capacity (maintenance of the stem cell pool); ii) multipotency - the potential to originate differentiated cells across multiple lineages, which progressively acquire specialization losing stemness-capacity; and iii) homeostatic control - the propensity to respond to different environmental stimuli and genetic constraints to balance self-renewal and differentiation. Although these features were originally described several decades ago, the recent development of advanced single-cell omics revealed that previously defined HSCs are a surprisingly heterogeneous population, characterized by different molecular signatures and functional properties (Copley, Beer and Eaves, 2012; Crisan and Dzierzak, 2016). Thus, HSCs are now classified as long-term (LT) and short-term (ST)-HSCs. Indeed, LT-HSCs are able to permanently reconstitute lethally irradiated

recipients upon transplantation (Brunet de la Grange *et al.*, 2013; Publicover *et al.*, 2013). On the contrary, ST-HSCs are capable of rapidly restoring the hematopoietic system, but only in the short-term, 8–12 weeks post-transplantation (Laurenti and Göttgens, 2018).

HSCs are highly quiescent, and their division is estimated to occur a total of 5 to 60 times through the entire lifespan (Bernitz *et al.*, 2016; Boyle, Lansdorp and Edelstein-Keshet, 2023). From a metabolic perspective, they are characterized by low rate of staining with metabolic fluorochromes, high mitochondrial mass and membrane potential but low oxidative phosphorylation, low protein translation, and high cholesterol biosynthesis (Cabezas-Wallscheid *et al.*, 2014; de Almeida *et al.*, 2017; Bonora *et al.*, 2018, 2024; Lauridsen *et al.*, 2018; Morganti *et al.*, 2019; Takihara *et al.*, 2019; García-Prat *et al.*, 2021). In addition, the urgency of purifying this rare subset from the bulk of HSPCs led to an extremely curated characterization of HSC surface markers. In particular, human HSCs enrich within a population uniquely defined as Lineage- (Lin-), CD34+ (glycoprotein promoting L-selectin mediated cell-to-cell adhesion, expressed across HSPCs), CD38- CD45RA- (expressed mainly by progenitors and acquired during differentiation), and CD133+ CD90+ CD49f+ (surface markers that in sequence enrich for multilineage repopulating potential) (Notta *et al.*, 2011) (Figure 2). However, despite the continuous identification of novel surface markers, HSC heterogeneity can only be fully eviscerated through single-cell omic approaches, which allowed the identification of some LT-HSC-specific markers, such as *HLF* (Lehnertz *et al.*, 2021).

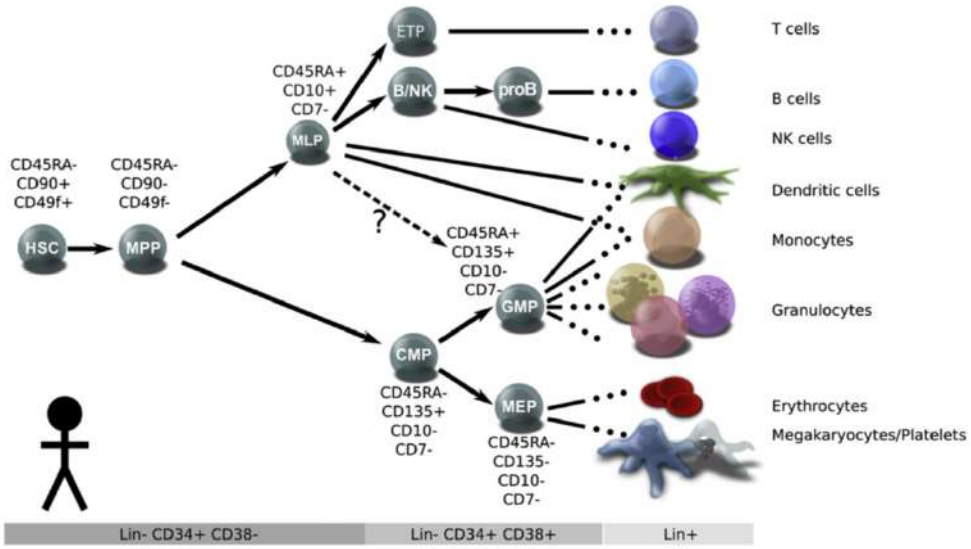


Figure 2. Human HSC phenotypic markers. *Each HSPC subset is characterized by a unique combination of surface markers, with LT-HSCs enriched in the fraction of Lin-CD34+CD38-CD45RA-CD133+CD90+CD49f+ cells* (adapted from Doulatov *et al.*, 2012).

The HSC niche in the bone marrow

HSC profile is guaranteed by a unique combination of a tightly regulated epigenetic state, transcriptional program, and cell cycle progression. While these intrinsic factors determine multiple aspects of stem cell fate, HSC stemness also depends on a multifaceted combination of extrinsic factors derived from their microenvironment, called the HSC niche. The concept of niche was first introduced in the late '70s (Schofield, 1978) and refers to the entirety of soluble factors, cellular ligands, and biochemical stimuli that interact with stem cells. Throughout the adult life, HSCs are found primarily in the medullary cavity of long and flat bones, the BM, and this controlled local microenvironment contributes to preserving HSC functionality and regulating their metabolism, dormancy or proliferation, and differentiation (Scadden, 2006; Morrison and Scadden, 2014). Indeed, the complex net of interactions between stem cells and their local microenvironment is necessary for homeostatic maintenance and regeneration upon alterations or injuries (Mendelson and Frenette, 2014). Accordingly, the stem cell niche can: i) maintain stem cell quiescence, providing proliferation-inhibiting stimuli; ii) provide cell cycle entry or differentiation-inducing signals to give rise to high numbers of progenitors that may expand into committed cell lineages, and iii) ensure a continuous reserve of stem cells through a tight control on stem cell self-renewal divisions.

The hematopoietic niche is composed of several cell types, including mesenchymal stromal cells (MSCs), osteoblasts, perivascular cells, adipocytes, and glial cells.

Importantly, these cells can directly interact with HSCs through cell-to-cell interactions as well as through the release of soluble factors and extracellular matrix (ECM) components. Indeed, several factors are involved in regulating HSC activity, such as osteopontin, Notch ligands, CXCL12, SCF, pleiotrophin, CXCL4, TGF-β, and FGF1 (Nilsson *et al.*, 2005; Sugiyama *et al.*, 2006; Butler *et al.*, 2010; Ding *et al.*, 2012; Greenbaum *et al.*, 2013; Bruns *et al.*, 2014; Zhao *et al.*, 2014). Moreover, biochemical and mechanical characteristics of the BM influence HSC behavior (Congrains *et al.*, 2021). For instance, quiescent HSCs localize preferentially in the endosteal region, which is composed primarily of fibronectin and possesses high stiffness (40-50 kPa) and low oxygen tension. Conversely, activated HSCs generally reside in the perivascular area, enriched with laminin (3 kPa), and thus lower stiffness, and higher oxygen concentration (Li *et al.*, 2021). In addition, HSCs are subject to a variety of hemodynamic forces that regulate their activity. For example, the onset of the blood flow regulates HSC formation by shear stress and cyclic stretch through the activation of the YAP pathway (Lundin *et al.*, 2020) (Figure 3).

The hematopoietic niche is not a static system, and it can be tuned depending on pathological or physiological conditions. Indeed, aging is associated with extensive niche remodeling, and an altered BM niche may contribute to malignant transformation (Raaijmakers *et al.*, 2010; Nakamura-Ishizu, Takizawa and Suda, 2014). On the same line, leukemic stem cells *per se* can reorganize the niche to create a cancer-supportive environment (Boyd *et al.*, 2014). Finally, genetic disorders like thalassemia and sickle cell disease are characterized by an altered bone marrow microenvironment, which contributes to HSPC dysfunction (Gnani *et al.*, 2019; Aprile *et al.*, 2020).

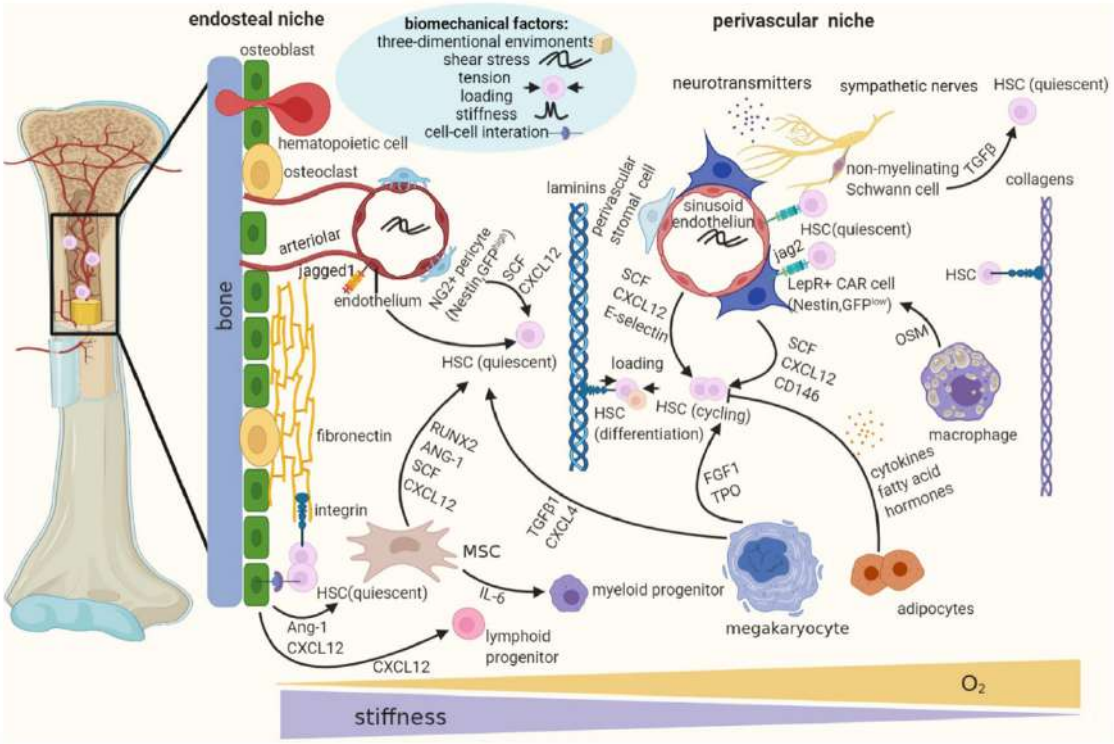


Figure 3. The hematopoietic stem cell niche. *The complex interplay between HSCs and the BM niche reveals that the combination of many soluble factors, cellular ligands, and biochemical and mechanical stimuli orchestrate HSC quiescence, maintenance, differentiation, and retention* (adapted from Li *et al.*, 2021).

Mechanobiology of HSPCs

Different mechanical stimuli shape the behavior and function of HSPCs at every stage, including development, homeostasis, and response to various insults. Mechanobiology comprehends the sensing of mechanical stimuli through various mechanosensors and consequent signal transduction to modulate downstream cellular responses. In detail, mechanical cues include ECM stiffness and elasticity, tensile forces, shear stress and hydrostatic pressure, and fluid viscosity. These stimuli are then sensed by mechanically gated ion channels, adhesion molecules, and primary cilia or directly from the cytoskeleton, generating internal mechanical forces that can potentially propagate to bystander cells (Ferrai and Schulte, 2024). Eventually, intrinsic forces will activate downstream signaling hubs or converge directly to the nucleus, influencing chromatin structure, epigenetic profile, and transcriptional programs. For instance, YAP/TAZ, JAK/STAT, and Wnt/β-catenin are among the most characterized mechanoregulated cascades. Importantly, because mechanical cues can cooperate with biochemical signals, the integration of multiple signaling pathways is thus intimately interconnected and not mutually exclusive, and the resulting complex regulation cannot be fully recapitulated by manipulating a

single signaling axis (Figure 4). The critical role of mechanotransduction is indeed highlighted by its alteration in numerous pathological conditions, such as fibrosis, tumorigenesis, and tumor resistance (Di *et al.*, 2023).

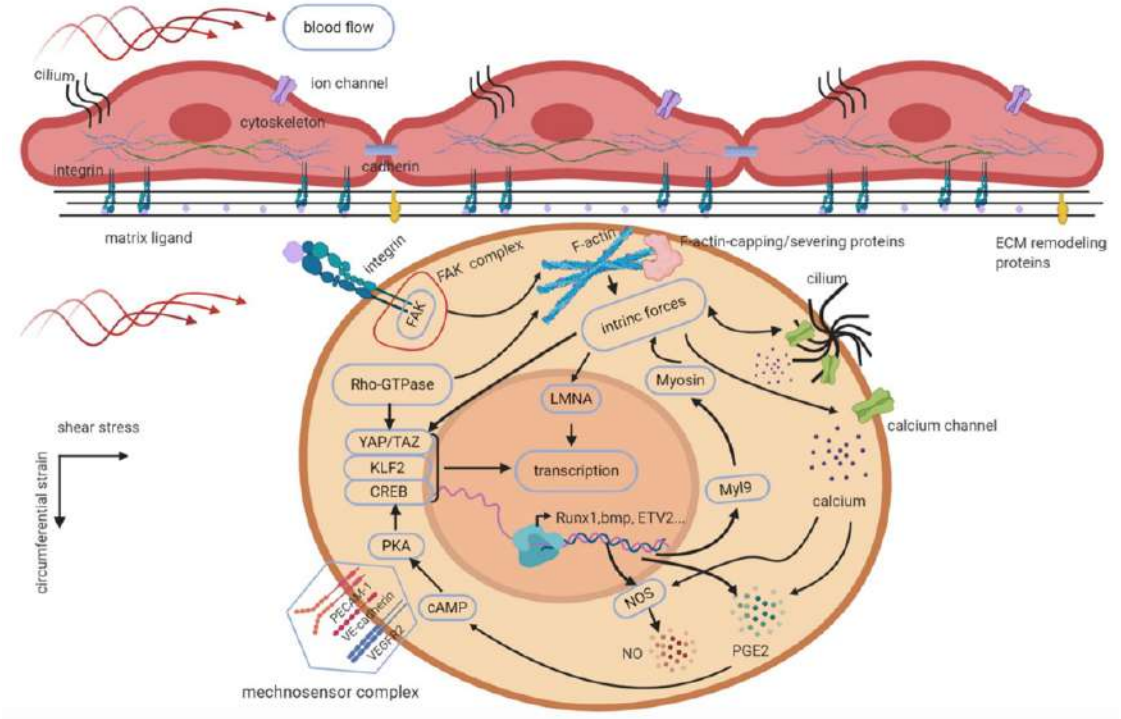


Figure 4. Biomechanical cues in HSCs. *Mechanical inputs, such as the blood flow, are integrated by mechanosensors, generating intrinsic forces that can propagate to bystander cells through cellular junctions or directly to the nucleus. Then, mechanical forces cooperate with biochemical signals to elicit complex cellular responses* (adapted from Li *et al.*, 2021).

Although the HSC mechanobiology field is still relatively in its infancy, our understanding of these intriguing regulation processes is now rapidly increasing. For instance, at the cell-cell junction between HSCs and endothelial cells, there is a mechanosensor complex made by platelet endothelial cell adhesion molecule-1 (PECAM-1), vascular endothelial (VE) cadherin, and vascular endothelial growth factor receptor-2 (VEGFR2), which is primarily deputed to shear stress sensing (Hoffman and Yap, 2015). Additionally, β7 integrins on HSC promote homing and long-term engraftment through the interaction with its endothelial ligand mucosal addressin cell adhesion molecule (MadCAM-1) (Murakami *et al.*, 2016), while α5 integrins regulate the maintenance of HSC quiescence (Khurana *et al.*, 2016). Moreover, sensing of matrix stiffness affects HSC morphology and lineage specification through integrin-dependent myosin II engagement (Choi and Harley, 2017). Interestingly, preliminary results suggest that the mechano-gated ion channel Piezo1 is involved in HSC specification during development (Scapin *et al.*, 2018).

Finally, HSCs possess primary cilia, which regulate stem cell specification during development through Notch signaling (Z. Liu *et al.*, 2019).

While actin microfilaments, intermediate filaments, and microtubules represent the main cytoskeletal components, the recent identification of septins paved the way for new mechanobiology studies. Indeed, Septin1 is normally dephosphorylated by Ptpn21, a protein tyrosine phosphatase highly expressed in HSCs, maintaining high levels of intracellular rigidity, and preventing stem cell egress from the BM niche (Ni *et al.*, 2019). In addition, cellular rigidity is also dependent on laminA/C, which in turn regulates chromatin architecture and nuclear polarity, influencing HSC behavior during aging (Grigoryan *et al.*, 2018). Finally, various GTPases of the Rho family are essential regulators of HSC migration, proliferation, and self-renewal (Sadok and Marshall, 2014). Among those proteins, high cell division cycle 42 (cdc42) activity correlates with loss of cell polarity and epigenetic alterations during aging of the hematopoietic system, and its inhibition promotes functional rejuvenation of aged HSCs (Florian *et al.*, 2012).

Functional assays to investigate human HSPCs

Despite HSPCs being extensively studied for several decades, the number of assays to assess their functionality remains limited to date. The fastest and easiest *in vitro* functional assay is the colony-forming unit cell (CFU-C) assay (Dexter, Moore and Sheridan, 1977), which was developed from the observation that rare cells in the human BM were able to generate colonies in agar if plated on a feeder layer from human peripheral blood (PB) (Pike and Robinson, 1970). This assay exploits semi-solid media (soft agar, methylcellulose, and plasma gel) to reduce cell movement, allowing individual cells to develop into cell clones upon two weeks of cytokine stimulation. In these settings, a single HSPC can develop into single colonies, recognizable by morphological criteria based on the lineage in which cells differentiate (Figure 5).

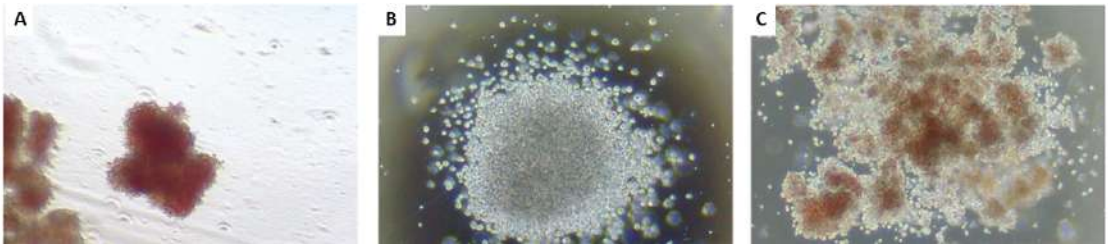


Figure 5. Representative images of different colonies in a CFU-C assay. *(**A**) Erythroid colony. (**B**) Myeloid colony. (**C**) Mixed colony* (adapted from *Human Methylcellulose Base Media (HSC002) by R&D Systems, Part of Bio-Techne*).

Secondary clonogenic assays were developed to study long-term culture-initiating cells (LTC-ICs) that do not immediately differentiate in semisolid media. LTC-ICs generate colonies detectable after a minimum of 5-8 weeks incubation (Barnett *et al.*, 1991), and this procedure thus enables to address the long-term *in vitro* functionality of HSPC. Despite various improvements, the CFU-C assay presents some limitations, including difficulties in discriminating between different colony types and wide inter-individual variations due to its qualitative and relatively subjective nature.

Recently, Laurenti and colleagues developed a single-cell *in vitro* differentiation assay to assess the differentiation of individual HSCs along different lineages. In detail, they index-sorted single HSCs and plated them in a cytokine-rich media that enables differentiation along the myeloid, erythroid, megakaryocyte, and NK lineages. After two- to three weeks of culture, single wells are analyzed by flow cytometry to characterize HSC heterogeneity based on the colony types produced (Belluschi *et al.*, 2018).

Nevertheless, studies on human HSPC functionality require validation into *in vivo* settings, and the mouse has become the most widely used model system for studying hematopoiesis. The procedure of transplanting human HSPCs into mice is called xenotransplantation, as the blood tissue is transplanted from one species to another. The first xenograft models were reported in 1988 by three independent groups who transplanted human hematopoietic cells into Severe Combined Immune-Deficient (SCID) mice lacking B and T cells due to a genetic autosomal recessive mutation of the $Prkdc^{scid}$ allele (McCune *et al.*, 1988; Mosier *et al.*, 1988; Namikawa *et al.*, 1988). These mice were conditioned through sublethal irradiation (to make room for transplanted cells within the receiving bone marrow) and used as recipients for human peripheral blood, human fetal tissues, and human BM hematopoietic progenitor cells. SCID mice supported human B and T cells production. However, no myeloid engraftment was observed, likely due to poor cross-reactivity of the murie and human myeloid growth factors. Thus, human interleukin-6 (IL-6), granulocyte-colony stimulating factor (G-CSF), and stem cell factor (SCF) cytokines were administered into irradiated SCID mice to sustain the production of human myeloid cells (Kamel-Reid and Dick, 1988; Lapidot *et al.*, 1992). Despite the achievement of generating both lymphoid and myeloid progeny, SCID recipients showed only low and transient engraftment due to the activity of the host innate immuity. Thus, to generate improved humanized mouse models, the SCID mutation was backcrossed onto Non-Obese Diabetic (NOD) mice, characterized by impaired innate immune compartment (Shultz *et al.*, 1995). Despite the improvement in human engraftment,

NOD-SCID showed only modes human T and B cell development, together with a high frequency of thymic lymphoid leukemia, and residual NK-dependent killing of the human graft.

Therefore, NOD-SCID mice were further engineered with complete truncation (NOG) or partial knock out (KO) of the IL-2 receptor γ-chain (NSG) (Ito *et al.*, 2002; Shultz *et al.*, 2005). This mutation affects several interleukin signaling (IL-2, IL-4, IL-7, IL-9, IL-15, and IL-21), resulting in complete loss of B, T, and NK cells, leading to higher human engraftment and maintenance of human hematopoietic cells. Although human chimerism was detectable up to 12 months, human engraftment was progressively lost after the sixth month post-transplant, likely resulting from the incomplete cross-reactivity of murine cytokines and human receptors. Thus, new mouse strains are now being engineered to express of human thrombopoietin (TPO), IL-3, and granulocyte-colony stimulating factor (GM-CSF) (Rongvaux *et al.*, 2011; Willinger *et al.*, 2011). However, lymphoid maturation is still incomplete in these xenograft models, generating not fully functional T and B cells. Interestingly, human HSPC engraftment is also subject to steroid hormones and sex-specific stimuli, with female NSG mice that allow single human HSCs detection with a six-fold increase compared to male recipients (Notta, Doulatov and Dick, 2010), suggesting that different still-undefined factors can regulate the human engraftment on xenograft models.

All the models described above require myeloablative conditioning, such as irradiation, to make space in the bone marrow niche and allow efficient engraftment of donor cells. However, irradiation represents a stressful procedure and can lead to detrimental effects, such as severe inflammation and premature death. Thus, a new strain of mice named NOD.B6.SCID Il2rγ−/−KitW41/W41 (NBSGW) was generated to allow the transplantation of human HSC without the need for irradiation thanks to a mutation in c-kit (McIntosh *et al.*, 2015), which is a tyrosine kinase receptor expressed on hematopoietic cells that binds to SCF. In its absence, the lack of binding with its cognate ligand causes murine HSC dysfunction and loss, making room for human cells to engraft in the BM.

HSPC-based clinical applications

HSPC transplantation (HSPC-T) vs. HSPC gene therapy (HSPC-GT)

The extensive regenerative potential of HSPCs and the increasing knowledge of hematopoiesis have been gradually translated into clinical practice, enabling life-

saving interventions for a plethora of blood disorders. HSPC transplantation (HSC-T) represented the first regenerative medicine approach applied to patients, and it is now the most widely used cell transplantation procedure (Appelbaum, 2007; Gratwohl *et al.*, 2015). In general, HSPC-T delivers healthy donor stem cells to replace the dysfunctional hematopoietic system of patients affected by genetic disorders, such as immunodeficiencies and hemoglobinopathies, or hematological malignancies, upon proper recipient conditioning, mainly based on immunosuppressants and chemotherapeutics, to ensure sufficient space in the BM to accept the graft (Copelan, 2006).

HSPCs are collected and purified from various sources, including umbilical cord blood (CB), apheresis from the iliac crest of the BM, or leukapheresis of the PB after mobilization (mPB). Each source has unique characteristics that influence the transplantation process. For instance, CB has a higher immunological tolerance, but the limited cell dose is challenging, particularly for adult patients. Conversely, BM apheresis is a complex and painful procedure, although BM-derived HSPC transplant achieved impressive clinical benefits. Nowadays, mPB is the preferred choice for clinical applications, as HSPCs are collected through a minimally invasive procedure while also allowing faster hematological recovery. Mobilization is achieved through the combined use of drugs that interfere with the interactions responsible for anchoring HSPCs to the niche, with the final effect of releasing CD34+ cells into the bloodstream. For example, G-CSF degrades the adhesion molecules VCAM-1, c-kit, CXCR4, and SDF-1, while Plerixafor is a CXCR4 antagonist (Gertz *et al.*, 2010; Ferrari, Thrasher and Aiuti, 2021).

HSPC-T can be classified according to the donor of HSPCs. Indeed, in syngenic transplantation, HSPCs are donated from an identical twin, while the allogeneic setting refers to an unrelated person and, thus, is the most exploited clinical approach for obvious reasons. However, allogenic transplant requires matching of the major histocompatibility complex (MHC) class I and class II between the donor and the recipient, which is dependent on a specific combination of human leukocyte antigens (HLAs) (Dausset, 1958). Unfortunately, finding HLA-matched donors is extremely difficult, and a partially-matched transplant may result in graft rejection, limiting the efficacy of this therapy and the number of treatable patients. On the contrary, graft-versus-host disease (GvHD) represents a frequent and severe complication of HSPC-T, where donor lymphocytes induce a potent immune response against the host tissue (Krstevska *et al.*, 2011).

Autologous transplantation (from the same donor) of genetically modified HSPCs represents the best therapeutic intervention for patients with multiple

immunohematological disorders missing HLA-matched donors. Gene therapy (GT) aims to genetically engineer patient cells to replace a defective gene or to insert an exogenous therapeutic cassette guaranteeing prolonged clinical benefits to patients (Naldini, 2015). GT approaches rely on two strategies: *in vivo* and *ex vivo* GT. *In vivo* GT is necessary to target cells that cannot be harvested from the patient, such as retinal and myoblast cells, and the engineering tools or transgenes are administered either directly to the organ of interest or systemically (Le Guiner *et al.*, 2017; Russell *et al.*, 2017). Instead, *ex vivo* GT is best suitable for applications in which defective cells can be isolated from the patient and ultimately re-infused into the same subject upon genetic engineering (O'Connor and Crystal, 2006).

HSPC *ex vivo* GT represents a promising one-time solution for the treatment of multiple immune-hematologic and genetic diseases, as well as enabling potential cross-correction of some non-hematological disorders (Naldini, 2015; Morgan *et al.*, 2017; Ferrari, Thrasher and Aiuti, 2021; Ferrari *et al.*, 2023). Indeed, HSPCs are harvested and purified from patients, genetically manipulated *ex vivo*, and finally infused back after conditioning. Thus, gene-modified HSCs are capable to engraft in the bone marrow and differentiate into all hematopoietic lineages, providing life-long persistence of corrected cells (Jaenisch and Young, 2008; Laird, von Andrian and Wagers, 2008; Morrison and Spradling, 2008; Murry and Keller, 2008; Orkin and Zon, 2008; Zhao, Deng and Gage, 2008). Genetic engineering of HSPCs was first achieved through semi-randomly integrating viral vectors, such as gamma-retroviruses (gRVs) and pseudotyped lentiviral vectors (LVs) (Cavazzana-Calvo *et al.*, 2000; Aiuti *et al.*, 2002, 2013; Biffi *et al.*, 2013), while nowadays we can induce targeted genetic modifications with up to single-nucleotide resolution thanks to the constant improvements of gene editing (GE) platforms, such as programmable nucleases like CRISPR/Cas9, and base- or prime-editors (Schiroli *et al.*, 2017; Charlesworth *et al.*, 2018; Zeng *et al.*, 2020; Everette *et al.*, 2023) (Figure 6). This strategy overcomes allogenic transplant limitations, such as the low availability of HLA-matched donors, graft rejection, GvHD, and post-transplant immunosuppressive regimen (Morgan *et al.*, 2017).

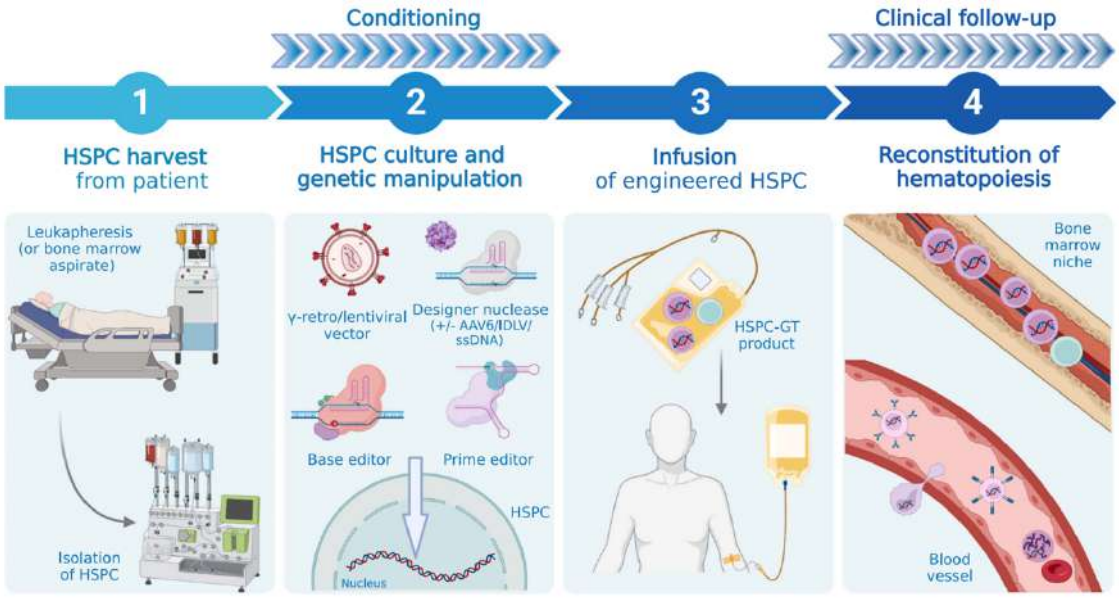


Figure 6. Ex vivo HSPC-GT. *HSPCs are harvested from the patient, genetically manipulated ex vivo through the preferred engineering platform of choice, and then reinfused upon conditioning to reconstitute the entire hematopoietic system* (adapted from Ferrari *et al.*, 2023).

GT with integrating vectors

Modified viral vectors, lacking their replicative and pathogenic capacity, represent the most suitable engineered platforms to deliver GT products in primary cells (Kay, 2011; Mingozzi and High, 2011). Depending on the capacity to integrate the transgene into the genome of the transduced cells, viral vectors can be classified as integrating or non-integrating vectors (Verma and Weitzman, 2005). Gene insertion in HSPCs exploits integrating gamma-retroviruses (gRVs) and pseudotyped lentiviral vectors (LVs) to permanently insert the desired transgene semi-randomly into the genome of patient-derived cells, often consisting of a healthy copy of a faulty gene or a therapeutically relevant cassette (Cavazzana-Calvo *et al.*, 2000; Aiuti *et al.*, 2002; Maier, Von Kalle and Laufs, 2010; Mátrai *et al.*, 2011). gRVs and LVs classify in the *Retroviridae* family, characterized by a relatively short (7-10 kilobases) diploid single-stranded RNA genome enclosed in a protein cone-shaped core embedded in a bilipid membrane. Different glycoproteins exposed on the lipid bilayer determine the viral pseudotype, which is exploited for receptor-mediated entry of the virus. Upon endocytosis, the capsid is uncoated, freeing the viral RNA genome that determines the synthesis of multiple proteins responsible for retro-transcription and final integration of the viral genome (Bushman *et al.*, 2005).

The first HSPC-GT clinical trials involved gRV-mediated gene addition to treat primary immunodeficiency patients (Cavazzana-Calvo *et al.*, 2000; Aiuti *et al.*, 2002; Hacein-Bey-Abina *et al.*, 2002). Although gene transfer efficiency was low, these

groundbreaking studies proved that substantial therapeutic efficacy could be achieved even in the presence of few engineered HSCs, leading to the first market-approved HSPC-GT product (Aiuti, Roncarolo and Naldini, 2017). Unfortunately, the initial enthusiasm in the field was shattered by the insurgence of leukemia in patients treated with HSPC-GT for X-linked severe combined immunodeficiency (SCID-X1) due to T cell clonal expansion caused by the insertion of the gRV in the proximity of a proto-oncogene (Hacein-Bey-Abina *et al.*, 2003). For this reason, gRVs were then surpassed by the advent of safer LVs engineered from the Human Immunodeficiency Virus 1 (HIV-1) (Naldini *et al.*, 1996). LV have a reduced risk of insertional mutagenesis and aberrant transcriptional activation since they preferentially integrate into gene bodies over promoters (Biffi *et al.*, 2011). Moreover, they have been further optimized by inactivating the viral promoter located in the LTR (long terminal repeats), thus minimizing the transactivation of cellular genes (Zufferey *et al.*, 1998). In the last decades, GT clinical trials have cured hundreds of patients affected by several genetic diseases, such as adenosine deaminase deficiency (ADA-SCID), SCID-X1, chronic granulomatous disease (CGD), Wiskott-Aldrich Syndrome (WAS), β-thalassemia, Fanconi anemia and hematological malignancies (Cavazzana-Calvo *et al.*, 2000; Aiuti *et al.*, 2002; Thompson *et al.*, 2018; Ferrua *et al.*, 2019; Marktel *et al.*, 2019; Río *et al.*, 2019; Kohn *et al.*, 2020). Notably, among the market-approved HSPC-GT products, there are Strimvelis (for ADA-SCID), Zynteglo (for β-thalassemia), Skysona (cerebral adrenoleukodystrophy), and Libmeldy (for metachromatic leukodystrophy).

Despite the constant advancements in vector design and the numerous successful clinical trials, integrating vectors-mediated GT safety remains constrained by the potential semi-random insertion of the transgene into tumor suppressors and proto-oncogenes (Cavazza, Moiani and Mavilio, 2013). From an efficacy standpoint, independently from the use of endogenous promotes, transgene expression is typically non-physiological given the lack of additional genomic regulatory elements, and the outcomes of this approach vary depending on transduction efficiency, the pathophysiology of the disease (such as defects in the BM niche), and individual patient characteristics (Hacein-Bey-Abina *et al.*, 2003; Woods *et al.*, 2006). Consequently, precise genome editor technologies offer the potential to expand the clinical applications of HSPC-GT beyond traditional gene addition.

GT with precise genome editors

Over the last two decades, the GT field has grown exponentially thanks to the optimization of new cutting-edge technologies, allowing precise and site-specific

modification of virtually any genomic target locus. Indeed, we can now manipulate genomic DNA to induce deletions, insertions of exogenous templates, nucleotide changes with up to single-base resolution, and even epigenetic modifications (Doudna, 2020).

The advent of programmable nucleases marked the milestone that enabled genetic engineering beyond gene addition, opening the frontiers of precise gene editing (GE). These engineered enzymes contain an endonuclease domain and a DNA binding component that determines nuclease specificity. The first programmable nucleases for GE applications were engineered from Zinc Finger Nucleases (ZFNs), immediately followed by Transcription Activator-Like Effector Nucleases (TALENs), and now almost completely surpassed by the Clustered Regularly Interspaced Short Palindromic Repeats (CRISPR) / CRISPR-associated protein (Cas) system.

ZFNs are structured in a modular fashion, typically containing a sequence three/six Zinc Finger Proteins (ZFPs), each composed of a 30 amino acid sequence that recognizes and binds specific DNA triplets, and the FokI nuclease, originally described in *Flavobacterium okeanokoites* (Kim, Cha and Chandrasegaran, 1996). By combining multiple ZFP modules with different DNA binding properties, ZFNs allow the targeting of unique genomic loci. FokI requires dimerization to effectively cleave the target DNA sequence and induce a precise double-strand break (DSB) (Bitinaite *et al.*, 1998; Vanamee, Santagata and Aggarwal, 2001). Thus, two ZFN monomers assemble into an active nuclease. These monomers bind the two target sequences on opposite DNA strands spaced by a 5-7 base pair region, where DSB induction occurs, generating complementary overhanging ends (Figure 7) (Durai *et al.*, 2005; Isalan, 2012). Thus, alongside various optimization (Miller *et al.*, 2007; Doyon *et al.*, 2011), the ZFN platform enables precisely targeting sequences of 18-36 nucleotides, excluding the spacer which contains the cut site. However, generating ZFNs with different specificity for different loci remains complex, long, and costly. Additionally, because ZFPs cannot accommodate all possible triplet combinations, this technology is restricted by limited targeting potential (Bae *et al.*, 2003). Regardless, ZFNs have found potential clinical applications, including the inactivation of the chemokine receptor type 5 (CCR5) to hamper HIV susceptibility (Tebas *et al.*, 2014).

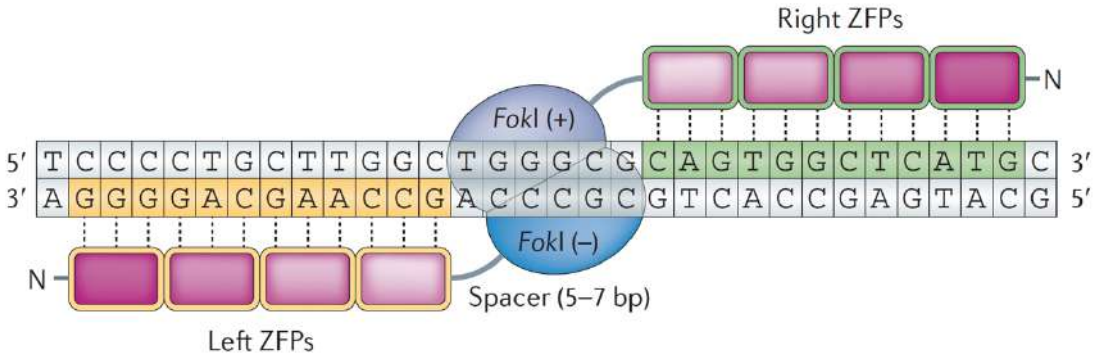


Figure 7. Zinc-finger nucleases. *ZFNs are dimeric nucleases consisting of zinc-finger protein (ZFP) arrays responsible for sequence specificity and an endonuclease domain of the FokI enzyme. ZFN pairs recognize target sequences that span between 18 and 36 base pairs, generating a DSB with overhangs in the spacer region* (adapted from Kim and Kim, 2014).

Similarly to ZFNs, TALENs have a modular design composed of an array of Transcription Activator-Like Effector (TALE) repeats connected to the FokI endonuclease, thus requiring dimerization for inducing the DSB (Joung and Sander, 2013; Pruett-Miller, 2013). TALEs are 33-35 amino acids long, and different TALEs recognize a different nucleotide through different repeated variable di-residue (RVD), which are the two amino acids at positions 12 and 13, respectively (Moscou and Bogdanove, 2009). Thus, the combination of four distinct TALEs enables the targeting of virtually any genomic sequence comprised in the spacer, as long as the condition of having a 5'-T residue at the end of the target site is fulfilled (Mak *et al.*, 2013). Despite their potency, TALENs can generate recombination byproducts, given the repetitive nature of TALEs, thus potentially generating multiple DSBs at undesired loci (Cermak *et al.*, 2011; Morbitzer *et al.*, 2011; Reyon *et al.*, 2012).

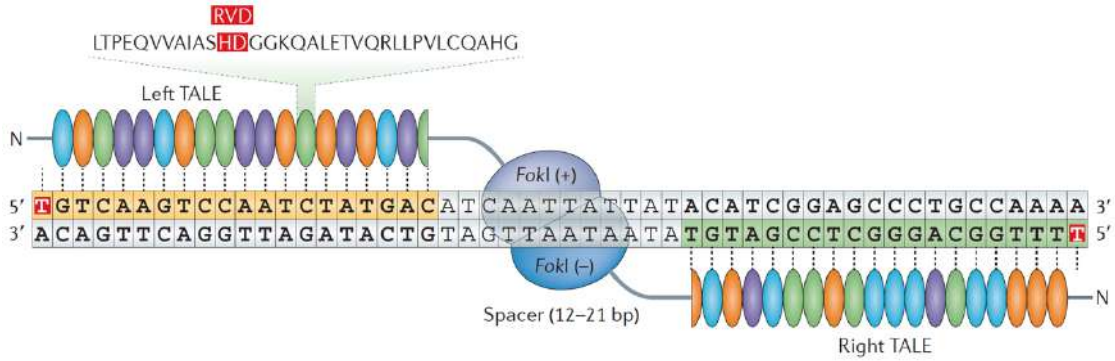


Figure 8. Transcription activator-like effector nucleases. *TALENs are dimeric nucleases consisting of TALE modules responsible for sequence specificity through the RVD region (in red) and an endonuclease domain of the FokI enzyme. TALENs generate a DSB with overhangs in the spacer region embedded in a 30-40 nucleotide-long specific sequence* (adapted from Kim and Kim, 2014).

The CRISPR/Cas system is the most widely adopted and engineered technology for GE applications. Originally, this system evolved as a sort of bacterial adaptive immune system, exploiting RNA-directed nucleases to degrade foreign nucleic acids upon a second pathogen exposure (Makarova *et al.*, 2006; Barrangou *et al.*, 2007). Engineering of the CRISPR/Cas9 system from *Streptococcus pyogenes* has revolutionized GE applications, enabling precise and versatile DSB induction across multiple loci and cell types (Jinek *et al.*, 2012). Cas9 endonuclease preferentially generates blunt-ended DSBs (although 30% of the cuts may originate overhangs) (Longo *et al.*, 2024) 3-4 nucleotides upstream of a protospacer adjacent motif (PAM), usually a 5'-NGG-3' sequence (where N is A, T, C, or G), exploiting the sequence encoded in the guide RNA (gRNA) to bind the target locus. Differently from ZFNs and TALENs, which require protein engineering and dimerization of two monomers to form an active nuclease, Cas9 acts as a single-protein complex, and its specificity is completely driven by the gRNA, thus not requiring protein engineering. gRNAs are dual RNA molecules, composed of a CRISPR RNA (crRNA), complementary to the target locus, and a trans-activating CRISPR RNA (tracrRNA), which is necessary for nuclease activity (Figure 9) (Deltcheva *et al.*, 2011). The breakthrough improvement to this editing platform was the generation of a single-guide RNA (sgRNA), merging the crRNA and tracrRNA into a single molecule (Jinek *et al.*, 2012). In addition, further gRNA optimizations include the addition of chemical modifications to improve gRNA stability (Kim and Kim, 2014; Hendel *et al.*, 2015) and the implementation of truncated gRNAs (tru-gRNAs) (Fu *et al.*, 2014). Finally, multiple Cas variants were engineered to obtain relaxed or altered PAM requirements, thus expanding the range of targetable sites (Kleinstiver *et al.*, 2016; Hu *et al.*, 2018; Nishimasu *et al.*, 2018; Walton *et al.*, 2020).

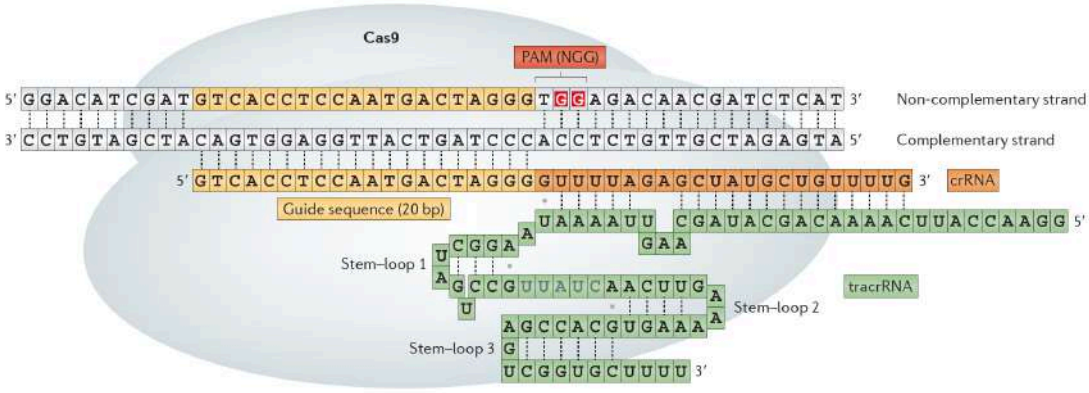


Figure 9. The CRISPR/Cas9 system. *Cas9 exploits the gRNA to bind its genomic target, allowing efficient DNA cleavage near the PAM sequence, primarily inducing a precise blunt-ended DSB* (adapted from Kim and Kim, 2014).

The potential of programmable nucleases lies in their ability to induce precise DNA double-strand breaks (DSBs), which can be exploited for genetic engineering purposes, including gene disruption and precise insertion of exogenous DNA cassettes, depending on the choice of DNA repair pathway engaged to sealing the break (Porteus, 2019). In general, DSBs are resolved primarily by non-homologous end joining (NHEJ) and homology-directed repair (HDR).

Indeed, DSBs are sealed mostly through NHEJ (Lieber *et al.*, 2003), which is a DNA repair pathway active throughout the entire cell cycle (Burma, Chen and Chen, 2006). NHEJ is initiated by Ku70/80 heterodimer that sits on and stabilizes DSB ends and recruits the DNA-dependent protein kinase catalytic subunit (DNA-PKcs), generating a particular structure that holds the two DNA ends together (Soutoglou *et al.*, 2007). This complex retrieves several other proteins, such as x-ray repair cross-complementing protein 4 (XRCC4), DNA Ligase IV (LIG4), XRCC4-like factor (XLF), and paralogue of XRCC4 and XLF (PAXX), which bring the two DNA fragments closer, inducing a short-range synapse (Scully *et al.*, 2019). Finally, Artemis, Pol λ, and Pol μ cleave the DNA lesion to generate compatible blunt ends, ultimately ligated by LIG4 (Povirk *et al.*, 2007; Chang *et al.*, 2017). Both end-modification and end-ligation require phosphorylation of DNA-PKcs (Jiang *et al.*, 2015), and once the DSB is repaired, the complex is disassembled (Figure 10). NHEJ is an extremely efficient repair mechanism, although it promotes small sequence insertions and deletions, thus being error-prone (Weston and Poirier, 2014). For this reason, in the context of GE, this repair pathway is exploited to induce small indels and thus inactivate the target locus. Remarkably, this principle is at the basis of the first market-approved CRISPR-based GT product, Casgevy, that exploits NHEJ to disrupt the erythroid-specific enhancer of the *BCL11A* gene and restore fetal hemoglobin expression in

patients affected by β-thalassemia and sickle cell disease (Frangoul *et al.*, 2021; Sheridan, 2024). Additionally, NHEJ allows simultaneous KO and homology-independent targeted integration (HITI) of corrective DNA sequences in both proliferating and non-replicating tissues, such as the retina and liver (Tornabene *et al.*, 2022).

Unlike NHEJ, HDR is restricted to S and G2 phases (Takata *et al.*, 1998) and error-free, as it exploits homologous recombination (HR) between a donor template, which could be the sister chromatid or an exogenous DNA, and the sequence carrying the DSB. During HDR initiation, the MRN complex (MRE11, RAD50, and NBS1) induces a SSB 15-300 bp upstream the 5'-end of the DSB, which is then exploited by MRN and CtBP-interacting protein (CtIP) to perform short-range resection of the damaged DNA filament, which ultimately inhibits NHEJ through Ku70/80 displacement (Scully *et al.*, 2019). This short-range resection is then further elongated to generate a long ssDNA filament through the activity of exonuclease 1 (EXO1), in combination with DNA replication helicase/nuclease 2 (DNA2) and Bloom Syndrome protein (BLM). The newly synthesized ssDNA is then stabilized by replication protein A (RPA), which protects the filament from further fragmentation. RPA is then exchanged with RAD51, thanks to the recruitment of multiple proteins, including breast cancer 1 (BRCA1), breast cancer 2 BRCA2, partner and localizer of BRCA2 (PALB2), and BRCA2 BRCA-associated RING domain protein 1 (BARD1). At this point, RAD51 vehicles the broken ssDNA filament towards a dsDNA sequence with high/complete homology, generating an intermediate synapsis that is then converted in a displacement-loop (D-loop) upon BRCA1-BARD1 stabilization (Stark *et al.*, 2002). Once the D-loop is formed, the ssDNA of the broken filament is released from its protein coating, enabling the binding of a non-replicative polymerase, often Pol δ (McVey *et al.*, 2016), which will synthesize the complementary sequence and generate a complex four-way DNA structure known as Holliday junction. Finally, HDR concludes with the resolution of this complex DNA structure, often achieved by synthesis-dependent strand annealing (SDSA). SDSA occurs primarily in somatic cells and does not enable crossing-over of DNA fragments between the two DNA molecules, while second-end capture often takes place during meiosis, generating a second Holliday junction and frequent allele crossover (Figure 10) (Punatar *et al.*, 2017). In the context of GE, this repair pathway is exploited to precisely insert an exogenous DNA cassette or restore the correct DNA sequence of a faulty gene through the administration of a donor DNA (Genovese *et al.*, 2014).

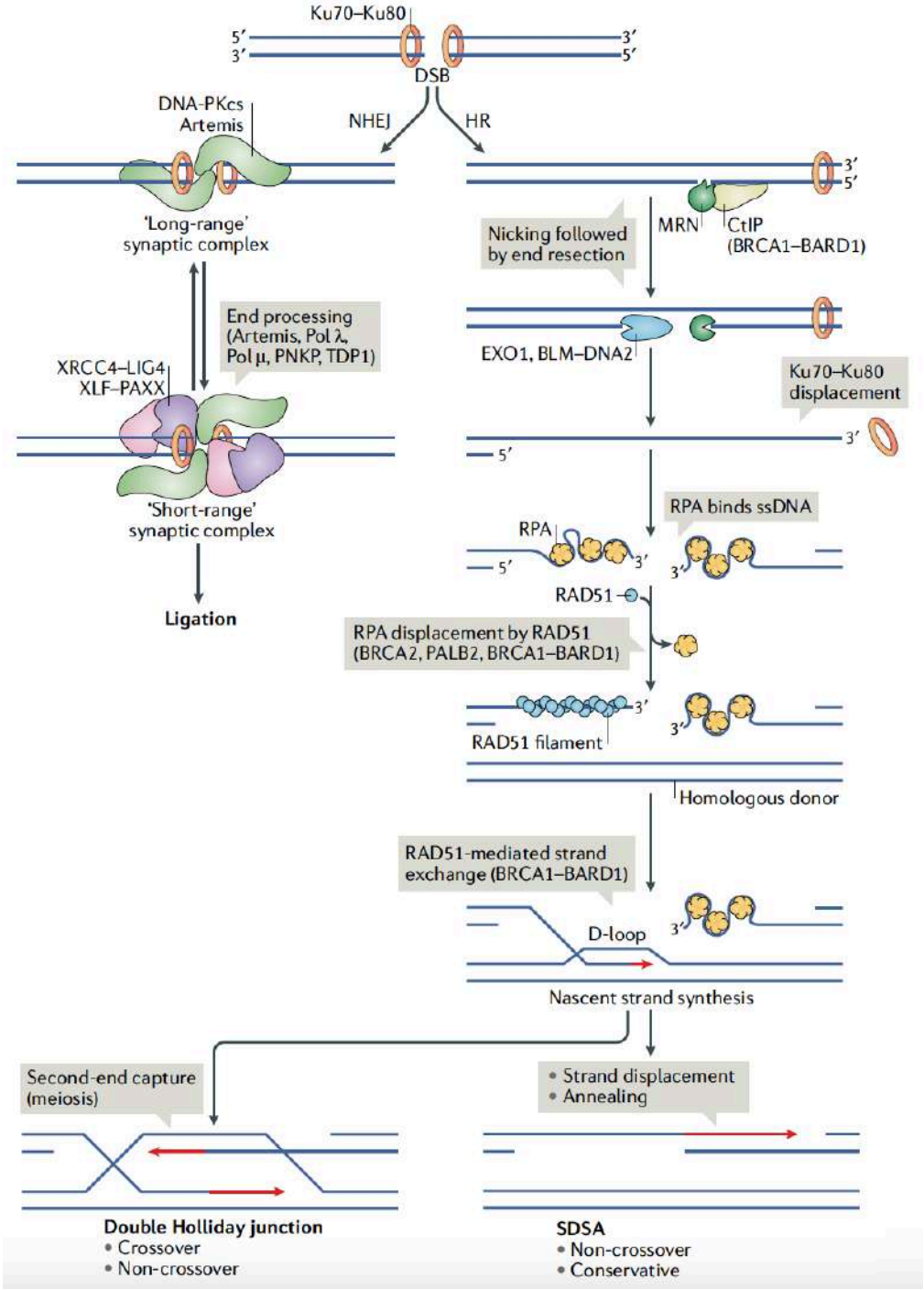


Figure 10. The two major DSB repair pathways. *Schematic representation of the error-prone NHEJ (left) and the high-fidelity HDR (right) pathways* (adapted from Scully *et al.*, 2019).

In parallel to NHEJ and HDR, cells possess other mechanisms of DSB repair can be found, including i) microhomology-mediated end joining (MMEJ or alternative end joining), which involves short-range resection and shares multiple molecules involved in NHEJ - error-prone (Wang and Xu, 2017); ii) single-strand annealing (SSA), based on recombination and that occurs within the damaged DNA duplex only if the DSB is

present between two repeated sequences (does not require a homologous template) - error-prone (Bhargava, Onyango and Stark, 2016); and iii) long-tract gene conversion (LTGC) and iv) break-induced replication (BIR), based on recombination and that occur mainly at DSBs at replication forks or in case of abortive HDR - error-prone (Chumki *et al.*, 2016; Malkova, 2018). Generally, while NEHJ and HDR are conventionally used to repair DSBs, these other repair pathways are more activated in specific situations, often to fix aborted repair byproducts.

The choice of NHEJ engagement over HDR and vice versa depends primarily on the cell cycle state, chromatin architecture around the DSB, and the type of DNA ends (blunt vs. overhangs) (Scully *et al.*, 2019). Molecularly, DSB repair pathway activation depends on the generation of short-range resection and Ku70/80 displacement (Symington, 2016). Indeed, alongside the above-mentioned molecular players, RIF1 and Shieldin prevent end resection upon p53 binding protein 1 (53BP1)-mediated recruitment (Bothmer *et al.*, 2010). Conversely, CtIP phosphorylation, mediated by cyclin-dependent kinase (CDK) 1/2 during the S/G2 phases, releases 53BP1 from the DSB (Escribano-Díaz *et al.*, 2013), allowing MRN recruitment and Ku70/80 removal. Besides preventing short-range resection, various mechanisms impair HR activity during the G1 phase, including several post-translational modifications of several HDR proteins (Zhao *et al.*, 2017). In summary, during GE applications in HSPCs, NHEJ is primarily exploited for gene disruption strategies, while HDR for targeted integration of therapeutic cassettes and gene correction, generally relying on adeno-associated viral vector serotype 6 (AAV6) delivery of the donor template (Figure 11).

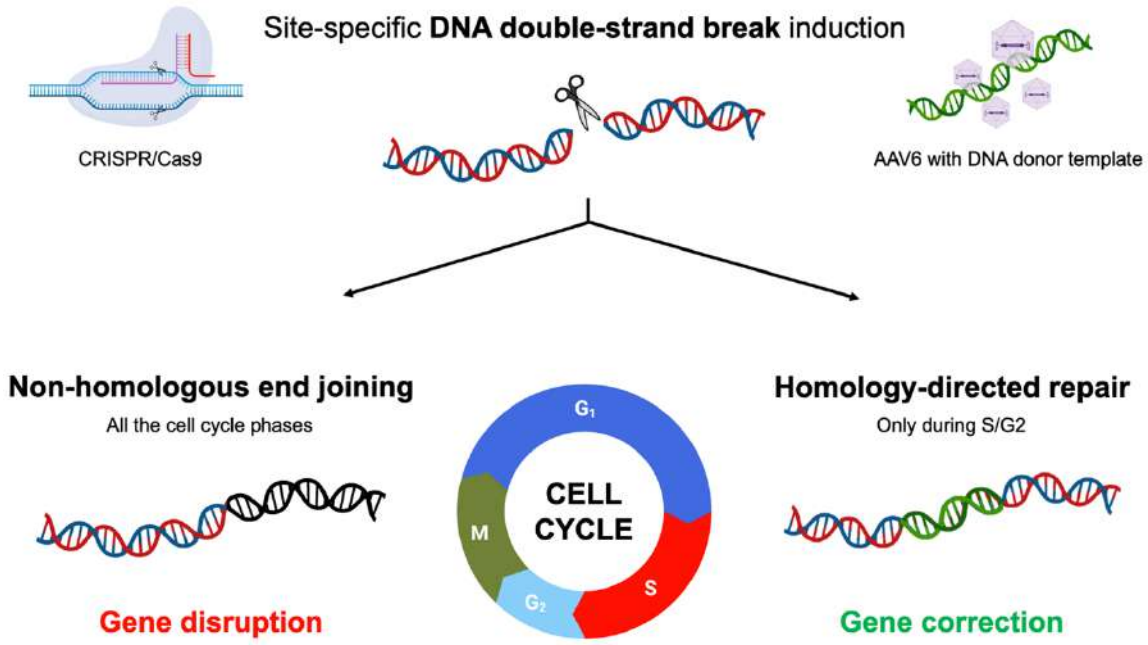


Figure 11. General outcomes of nuclease-based gene editing. *Depending on the cell cycle state and the consequent DNA repair mechanism engaged, the nuclease-induced DSB can be repaired by NHEJ to inactivate the target gene or by HDR to correct a faulty gene or allow targeted integration of a therapeutic cassette, usually delivered with an AAV6 vector (created with Biorender).*

Recently, the extensive knowledge gained on the Cas nucleases of the CRISPR system, coupled with the capacity of engineering and play with this pair of molecular scissors, led to the generation of a completely novel class of genome editors that includes base-, prime- and epi-genome editors.

Base editors (BEs) empowered precise single-point mutation editing without the requirement for DSBs and HDR. Indeed, BEs are engineered from a catalytically inactive Cas9 nuclease (dCas9), which has been modified to prevent DSB formation at the target sequence, fused with a DNA deaminase (Komor *et al.*, 2016). In this way, the dCas9 moiety localizes the deaminase on the target site, thus allowing targeted DNA modification. In particular, the fusion of different deaminases allowed the generation of two classes of BE: adenine BEs (ABEs) and cytosine BEs (CBEs). ABEs catalyze the conversion of A-T base pairs to G-C, while CBEs convert C-G into T-A. Thus, BE enables all four possible transition mutations. In detail, the binding of the dCas9 and the respective gRNA exposes PAM-distal ssDNA nucleotides, making them accessible for deamination. In contrast, the 4-8 PAM-adjacent nucleotides are occluded by the dCas9 moiety, thus impeding their modification. ABEs mediate A deamination, generating inosines (I), while CBEs convert C into uraciles (U). Thus, the presence of I and U generates a mismatch on the WT strand, and stable BE requires the correction of the non-deaminated strand using the edited one as a

reference. However, I and U are rapidly excised from the genomic DNA. Hence, to increase the likelihood of selecting the newly introduced mutation, dCas9 has been substituted with a Cas9 nickase (Cas9n), which is able to induce only a single-strand break (SSB) instead of a DSB, to nick only the non-deaminated strand. In this way, DNA repair is stimulated to use the edited strand as a reference, resulting in stable conversion of the targeted base (Satomura *et al.*, 2017). Moreover, further engineering of CBEs with U glycosylase inhibitors (UGIs) delayed the excision of the CBE-induced U, thus favoring the fixation of the desired base conversion (Figure 12) (Wang *et al.*, 2017). Finally, the optimization of more efficient and precise BEs involves the evolution of new deaminase enzymes, modification of the linker regions between the Cas protein and the deaminase or the UGI, and minimizing bystander base-conversions (Anzalone, Koblan and Liu, 2020). In the context of HSPC-GT, BE has demonstrated its efficacy in the treatment of hemoglobinopathies (Zeng *et al.*, 2020; Antoniou *et al.*, 2022; Everette *et al.*, 2023). Indeed, these promising results led to the approval of the first clinical trial employing BE for sickle cell disease (NCT05456880).

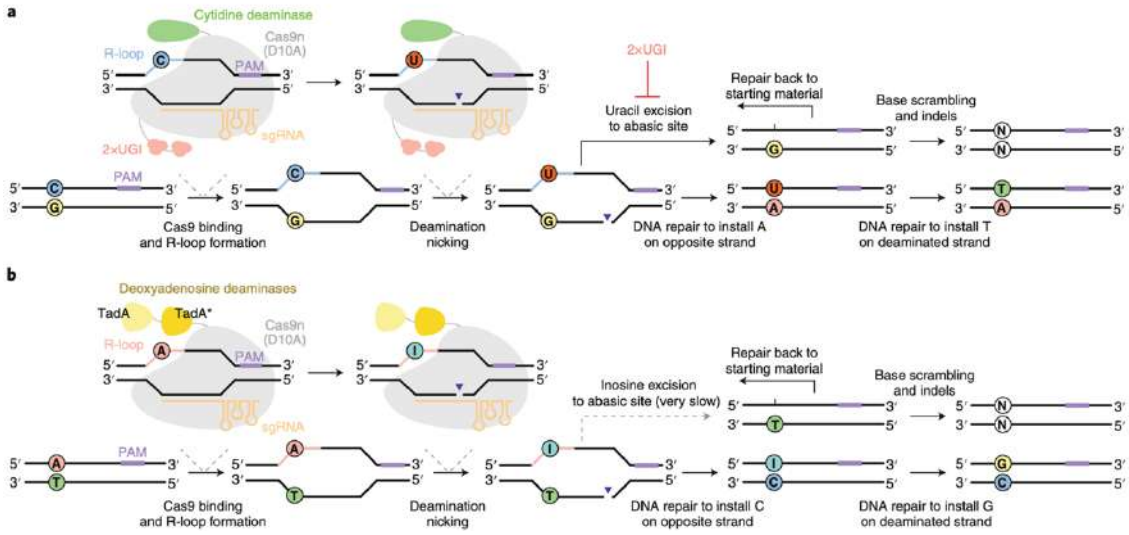


Figure 12. Base editors enable single nucleotide conversions. *(A) CBE and (B) ABE deaminates target C and A, generating U and I, respectively, and ultimately allowing C-G to T-A and A-T to G-C conversion* (adapted from Anzalone, Koblan and Liu, 2020).

Further evolution of this system has come with the advent of prime editors (PEs), which allow editing of the target DNA sequence by retrotranscription of an RNA-based template. PEs are composed of a Cas9n fused with an engineered reverse transcriptase enzyme, and their activity is controlled by the pegRNA, which contains the sequences for the specific genomic target locus and the desired editing template

(Anzalone *et al.*, 2019). Upon binding to its target, the Cas9n nicks the DNA strands containing the PAM sequence, and the generated 3'-end is first primed and then elongated by retrotranscription using the pegRNA as a template. Thus, the non-edited 5'-end is thought to be cleaved to allow the sealing of the newly synthesized 3'-end into the original strand, generating a heteroduplex containing one edited and one non-edited DNA filament. At this point, fixation of the edited strand is promoted by a second nick on the non-edited strand (dependent on a different nicking gRNA), which stimulates DNA repair to use the edited strand as a reference (Figure 13). In the HSPC-GT frame, PEs have been exploited to correct sickle cells (Kelcee A Everette 2023), but their clinical transition has yet to occur.

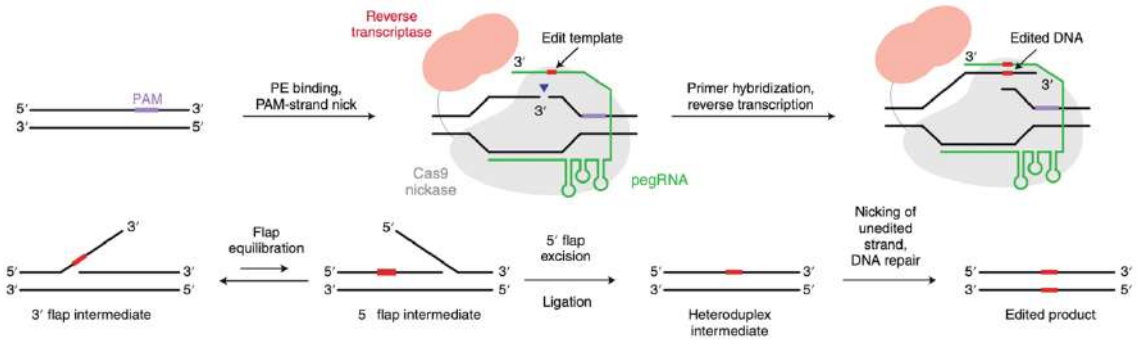


Figure 13. Prime editing relies on retrotranscription to induce all types of genetic modifications. *PE contains a Cas9n fused with a reverse transcriptase that relies on pegRNA to precisely edit the target locus, introducing the desired modification encoded in the RNA template* (adapted from Anzalone, Koblan and Liu, 2020).

Finally, the CRISPR/Cas system has also been engineered with transposase domains to favor HDR insertions of long DNA sequences without DSBs induction and without relying on the entire endogenous DNA repair machinery (Klompe *et al.*, 2019). Moreover, another layer of genetic engineering is represented by epigenome editors, which allow efficient activation or silencing of target genes without inducing DNA modifications through the fusion to catalytically inactive programmable nucleases and various histone writers, epigenetic activators/repressors, and DNA methylation editors (Amabile *et al.*, 2016; Liao *et al.*, 2017). Thus, epigenome editors may allow broadening GT applications beyond DNA editing, paving the way for new clinical approaches, such as the silencing of *Pcsk9* for hypercholesterolemia (Cappelluti *et al.*, 2024).

Delivery of editing reagents

Apart from integrating viral vectors that exploit the respective viral infection machinery to deliver the transgene, precise genome editors need to be inserted into

target cells via external delivery methods. Non-viral approaches include physical delivery and carrier-mediated delivery. In general, editors are delivered *ex vivo* in HSPCs primarily by electroporation, which employs a high-intensity electric pulse that transiently opens micropores on the cell membrane, thus allowing the internalization of the editing tools (Hendel *et al.*, 2015). Despite this strategy being widely used, its toxicity may be exacerbated in different cell types (Young and Dean, 2015). Thus, alternative methods have been developed for harmless and more versatile delivery. Nanoparticles have nano-scale dimensions around 1 to 100 nm and exploit cellular endocytosis to deliver their cargo. Nanoparticle components and formulations depend on the desired size, surface properties, and cargo. Indeed, both gold nanoparticles, polymer-based nanoparticles, and lipid nanoparticles (LNPs) have been designed to efficiently target HSPCs, endowing successful genetic modification with low toxicity (Shahbazi *et al.*, 2019; Vavassori *et al.*, 2023). Additionally, while simpler methods, such as lipofection, are generally used for preliminary experiments in cell lines given their limited efficacy in primary cells, there is increasing interest in the generation of cell-penetrating peptides and virus-like particles (Foss *et al.*, 2023; An *et al.*, 2024).

Genetic engineering tools can be delivered in the form of plasmid DNA, mRNA, or recombinant protein complexed with the gRNA (RNP). Despite being the cheapest option, plasmid can accommodate and stably express larger constructs. However, they can be actively replicated and accidentally integrate into the genomic DNA of the cells. Moreover, the persistency of the nuclease increases the risk of off-target events (Glass *et al.*, 2018). On the contrary, mRNA delivery allows transient expression of the editor, reducing the risk of unwanted non-specific editing but suffering from potential degradation as exogenous mRNAs are rapidly eliminated within the host cells (Xu *et al.*, 2019). For these reasons, purified RNPs are now the preferred choice, bypassing both transcription and translation inside the cell and reducing the risk of off-targets due to their transient nature. However, genome editors have a high molecular weight in general, thus posing challenges for their delivery (Kim et al, 2014), particularly for the new generation of BE, PE, and epigenome editors.

Differently from the other genetic engineering strategies, HDR-mediated GE relies not only on nuclease-induced DSB induction but also on the presence of a donor DNA template, which is generally delivered through non-integrating viral vectors, such as integrase-defective lentiviral vectors (IDLV), adenoviruses (AdVs), and AAVs (Athanasopoulos, Munye and Yáñez-Muñoz, 2017). AAV6 is indeed the most widely employed delivery method for HDR-GE in HSPCs, supporting high editing efficiencies in primitive HSPCs (Wang *et al.*, 2015; Schiroli *et al.*, 2017). However, recent

improvements in IDLV manufacturing and the discovery of LV transduction enhancers (Zonari *et al.*, 2017; Petrillo *et al.*, 2018) have proposed a promising alternative to AAV6 to mitigate detrimental HSPC responses to viral exposure (Ferrari *et al.*, 2022). In addition, short HDR templates can also be delivered through single-stranded chemically modified oligodeoxynucleotide (ssODN) electroporation (De Ravin *et al.*, 2017; Pattabhi *et al.*, 2019; Romero *et al.*, 2019). However, due to their limited length, they are primarily applied for correcting short mutations, while AAV6 and IDLV are more suitable for long-range GE. Nevertheless, longODNs are currently under development and may potentially replace the use of viral vectors.

Current challenges in HSPC-GT

Cellular constrains to genetic engineering and safety concerns

Genetic engineering requires high doses of viral vectors, delivery of foreign proteins, such as nucleases and nickases, and exogenous nucleic acids, that will be sensed by cellular defense mechanisms active in HSPCs. Indeed, HSPCs express several pattern recognition receptors (PRRs), which sense the presence of pathogen-associated molecular patterns (PAMPs), including viral vector components and foreign nucleic acids, and trigger the release of several pro-inflammatory cytokines, such as type I interferon (IFN I) (Piras and Kajaste-Rudnitski, 2021). This inflammatory response is associated with cell cycle entry, proliferation, differentiation, and potential apoptosis of HSPCs (Essers *et al.*, 2009; Liu *et al.*, 2012). Thus, inflammatory responses may arise from the sensing of virtually any editing reagent, including mRNAs encoding for the editors, gRNAs, the HDR-donor DNA template, and LV, IDLV, and AAV6 (Hendel *et al.*, 2015; Mu *et al.*, 2019; Piras and Kajaste-Rudnitski, 2021).

In addition, nuclease-induced SSBs and DSBs in particular, which represent the most cytotoxic DNA lesion, trigger the activation of the DNA damage response (DDR), which promotes and orchestrates DNA repair while inducing cell cycle arrest (Turnell and Grand, 2012). SSBs and DSBs are sensed by specialized DDR sensor complexes that recruit and promotes activation of ataxia telangiectasia mutated (ATM) or ataxia telangiectasia and RAD3-related (ATR), which represent the apical kinases of the DDR pathway (Shiloh, 2006), that block cell cycle progression to prevent replication of damaged DNA, which could potentially degenerate in fork stalling and mutagenesis (Campisi and D'Adda Di Fagagna, 2007). ATM and ATR recruitment is initiated by phosphorylation of a specific residue (serine 139) of H2AX (hereafter referred as

yH2AX), MRN, RPA, and 53BP1, which initiate a positive feedback loop that sustain ATM/ATR activation and yH2AX spreading in the proximity of the DNA lesion (Celeste *et al.*, 2002; Zou and Elledge, 2003). ATM phosphorylates several substrates, including p53, BRCA1, Nijmegen breakage syndrome 1 (NBS1), structural maintenance of chromosomes 1 (SMC1), and the checkpoint kinase protein 2 (CHK2) (Carson *et al.*, 2003; Uziel *et al.*, 2003; Kitagawa *et al.*, 2004). Instead, ATR phosphorylates several substrates, such as the ATR-interacting protein (ATRIP), RPA, yH2AX, BRCA1, and the checkpoint kinase 1 (CHK1). CHK1 and CHK2, together with ATR and ATM, are responsible for the activation of a broad range of effector proteins that are involved in DNA repair, cell cycle control, and apoptosis (Bartek, Lukas and Lukas, 2004). Depending on the extent of the lesion, repair outcome, and persistence of DDR activation, cells may undergo apoptosis or enter a state of permanent cell cycle arrest, defined as cellular senescence (Figure 14) (Sulli, Di Micco and Di Fagagna, 2012).

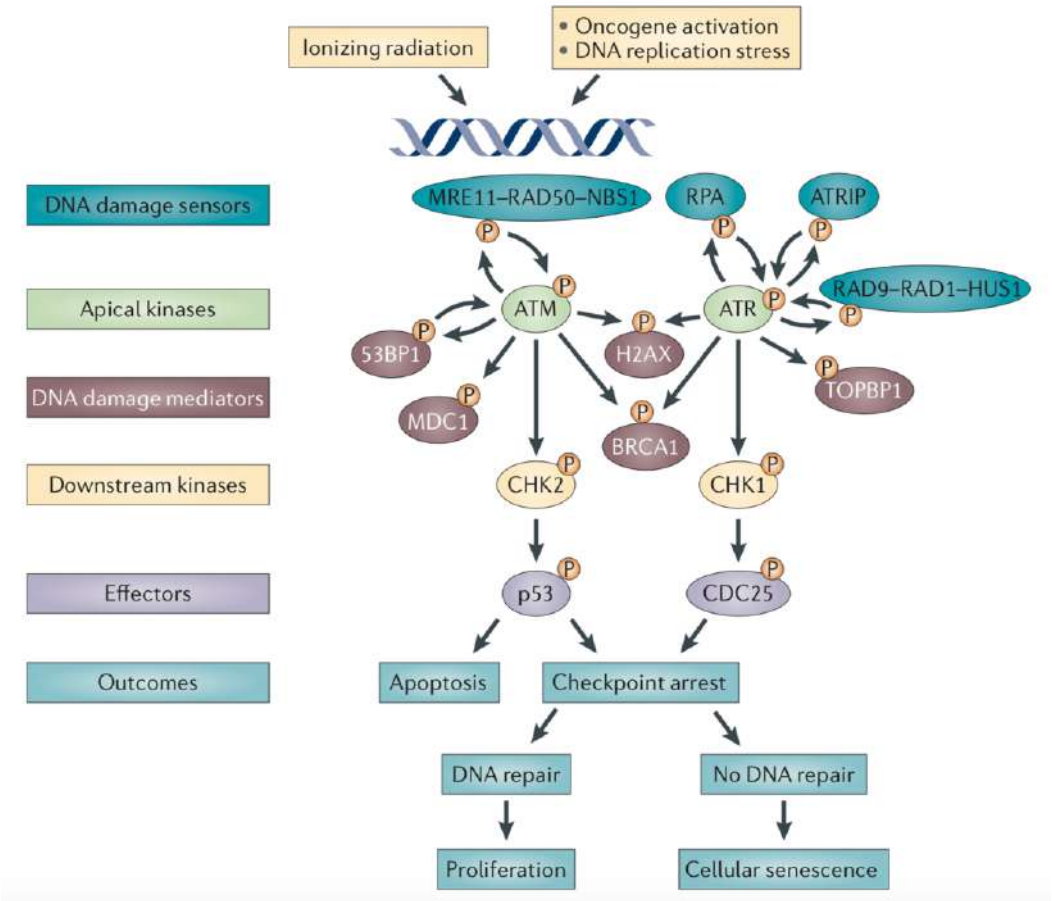


Figure 14. Schematic representation of DDR pathway. *The DDR cascade is a complex cellular response triggered by multiple DNA lesions, which are sensed by DNA damage sensors that promote apical kinases ATM and ATR activation. These two proteins phosphorylate multiple DNA damage mediators and the major downstream kinases CHK2 and CHK1,*

stimulating DNA repair while inhibiting cell cycle progression (adapted from Sulli, Di Micco and Di Fagagna, 2012).

Importantly, in parallel with SSBs and DSBs, multiple engineering reagents trigger the activation of the DDR in HSPCs, including the exposure to LV, IDLV, and AAV6 vectors, promoting the activation of p53 and loss of stemness properties (Piras *et al.*, 2017; Schiroli *et al.*, 2019). This results in the oligoclonal reconstitution of engineered cells upon transplantation (Ferrari *et al.*, 2020), posing safety concerns for the emergence of clonal hematopoiesis (Jaiswal and Ebert, 2019).

Despite several optimizations to increase the specificity of engineered nucleases, DSB induction, and to lesser extent SSBs (Fiumara *et al.*, 2023), at off-target sites may have genotoxic effects, such as transgene incorporation at undesired loci, KO of tumor suppressor or proto-oncogene activation, or other complex chromosomal rearrangements (Kosicki, Tomberg and Bradley, 2018; Hanlon *et al.*, 2019; Nelson *et al.*, 2019; Leibowitz *et al.*, 2021). Therefore, gRNA specificity assessment is mandatory for clinical applications and different strategies have been implemented to evaluate off-target activity, including GUIDE-seq (Tsai *et al.*, 2015), DIGENOME-seq (Kim *et al.*, 2015), CIRCLE-seq (Tsai *et al.*, 2017), SITE-Seq (Cameron *et al.*, 2017), DISCOVER-Seq (Wienert *et al.*, 2019), and CAST-Seq (Turchiano *et al.*, 2021).

Moreover, on-target DSB induction per se increases genomic instability, which can be associated with small, up to megabase-scale deletions, micronuclei, and chromosome bridge formation, which can ultimately determine extensive chromosome rearrangements known as chromothripsis (Cullot *et al.*, 2019; Leibowitz *et al.*, 2021). In addition, randomly occurring or nuclease-induced DSBs may be hotspots for the integration of viral vector fragments, such as long terminal repeats (LTR) of LV and the inverted terminal repeats (ITR) of AAV vectors (Knight *et al.*, 2010; Dalwadi *et al.*, 2021).

In the clinic, integrations of gRV and LV vectors into proto-oncogenes or tumor suppressors led to leukemia establishment in a few patients subject to HSPC-GT (Cesana *et al.*, 2024; Klapwijk *et al.*, 2024). Moreover, the first HDR-based HSCP-GT trial designed for sickle cell disease (nula-cel, Graphite Bio) was recently interrupted for safety and efficacy issues.

Strategies to improve genetic engineering efficiency

Integrating viral vectors has shown clinical efficacy in numerous clinical trials. However, gene addition strategies require high viral vector doses and, in some cases,

multiple transduction cycles to achieve sufficient engineering efficiency given the limited permissiveness of HSPCs to viral transduction (Cavazzana-Calvo *et al.*, 2000; Aiuti *et al.*, 2002; Ferrua *et al.*, 2019). For this reason, multiple transduction enhancers have been developed, including coating with retronectin, administration of 16,16-dimethyl prostaglandin E2 (PGE2), cyclosporin H (CsH), poloxamer F108 (LentiBOOST), and deoxynucleosides (dNs) supplementations (Budak-Alpdogan and Rivière, 2009; Zonari *et al.*, 2017; Petrillo *et al.*, 2018; Jang *et al.*, 2020). For instance, CsH has been shown to degrade interferon-induced transmembrane protein 3 (IFITM3), which is a potent inhibitor of VSVG-pseudotyped LV entry used for HSPC-GT applications (Petrillo *et al.*, 2018). Instead, administration of exogenous dNs allows faster LV transduction in quiescent cells, which do not actively synthesize dNTPs and thus have only a limited pool of nucleotides available for LV retrotranscription (Valeri *et al.*, 2024). Thus, transduction enhancers and their combinatorial administration may allow efficient gene addition while dramatically reducing viral vector doses, which represent a major bottleneck for the cost of current HSPC-GTs.

Regarding HDR-mediated GE, while we can achieve high editing levels in more committed HSPC progenitors, primitive HSCs display low HDR rates, which limits the efficiency of precise gene insertion or gene correction (Lombardo *et al.*, 2007; Genovese *et al.*, 2014). Manipulation of the DNA repair mechanisms and cell cycle progression enhanced HDR efficiency in different cell types (M. Liu *et al.*, 2019). Indeed, suppression of key NHEJ factors through small molecules or shRNAs, such as LIG4, Ku70/80, and DNA-PKcs, resulted in a 2- to 20-fold increase in HDR efficiency during gene editing procedures (Chu *et al.*, 2015; Maruyama *et al.*, 2015; Robert *et al.*, 2015; Li *et al.*, 2018). However, NHEJ is instrumental in maintaining genome integrity and its inhibition could severely worsen genomic instability, which may be deleterious for the cells. Thus, HDR agonists offer a potentially more relevant clinical strategy (Yang *et al.*, 2020). The small molecule RS-1 enhances RAD51 binding capability, significantly improving HDR-mediated gene modification in multiple settings (Jayathilaka *et al.*, 2008; Zhang, Zhang and Ge, 2018; Kurihara *et al.*, 2020). Interestingly, also the fusion of Cas9 with CtIP, RAD52, and MRE11 significantly increased GE efficiency in human cells and induced pluripotent stem cells (iPSCs) (Charpentier *et al.*, 2018; Tran *et al.*, 2019). Additionally, a few small molecules have been identified in HTS screening to enhance HDR efficiency, including L755505 and Brefeldin, although their mechanism of action is yet unclear (Yu *et al.*, 2015). Moreover, the regulation of end resection at DSBs can also be exploited to promote HDR over NHEJ. Indeed, the suppression of 53BP1 accumulation at DSBs or

BRCA1 overexpression increased HDR efficiency (Pinder, Salsman and Dellaire, 2015; Canny *et al.*, 2018). Since HDR is restricted to the S/G2 phases, delivery of the gene editing platforms in cell cycle-arrested cells has proven to improve HDR efficiency (Lin *et al.*, 2014; Yang *et al.*, 2016; Lomova *et al.*, 2019; Wienert *et al.*, 2020). In addition, cell cycle progression stimulation by Ad5-E4orf6/7 viral proteins has been associated with the upregulation of the HDR machinery in an E2F-dependent manner (Ferrari *et al.*, 2020). Furthermore, the Cas9-geminin fusion protein improves HDR rates by promoting Cas9 degradation during the G1 phase, when NHEJ is predominant (Gutschner *et al.*, 2016). Of note, HDR intimately depends on the availability of the donor template. Thus, all-in-one HDR complexes of Cas9-RNP linked to the HDR template improved gene editing efficiency in several experimental settings by facilitating HR in the proximity of the DSB (Carlson-Stevermer *et al.*, 2017; Ma *et al.*, 2017; Savic *et al.*, 2018). Finally, while not directly affecting editing efficiency, counteracting p53-mediated detrimental responses to GE by transient delivery of the mRNA encoding for a p53 dominant negative form (GSE56) increases the engraftment and the clonal repertoire of edited HSPCs (Schiroli *et al.*, 2017; Ferrari *et al.*, 2020).

Finally, constant optimization of Cas9 moieties with relaxed PAM specificity, improved specificity, lower dimensions, and the evolution of deaminase and activator/repressor enzymes, together with optimization of BE, PE, and epigenome editor assembly allows to further generate more efficient and safer genome editors for improved clinical applications (Anzalone, Koblan and Liu, 2020).

HSPC responses to ex vivo culture and optimization of culture conditions

In current GT protocols, *ex vivo* culture is not only required for activating HSPCs and delivering the editing reagents but also, in some cases, to increase the number of transplantable cells, considering that the average dose for GT products generally consists of 2-30$\times10^6$ CD34+ cells/kg (Morgan *et al.*, 2017; Canarutto *et al.*, 2021). However, exposure to culture conditions and cytokines is associated with rapid HSC differentiation (Johnson *et al.*, 2024) and HSPCs exhaustion, leading to a significant reduction of their multilineage reconstitution potential in the long term (Mazurier *et al.*, 2004; Zonari *et al.*, 2017). Thus, alongside the development of more efficient and precise editing tools and enhancers (Petrillo *et al.*, 2018; Ferrari *et al.*, 2020; Fiumara *et al.*, 2023; Baik *et al.*, 2024), significant efforts are spent to constantly advance culture conditions to ensure the maintenance, or potentially the expansion, of HSCs *ex vivo*, such as fine-tuning the supporting cytokine-cocktail, supplementing small molecules like nicotinamide riboside and UM171, and, more recently,

introducing only chemically-defined reagents to avoid batch-to-batch variability and diminishing possible contaminants (Horwitz *et al.*, 2014; Fares *et al.*, 2017; Zonari *et al.*, 2017; Rai *et al.*, 2023; Sakurai *et al.*, 2023). In addition, there is increasing interest in the field of 3D culture systems, which represent a promising strategy to counteract culture stress (Bai *et al.*, 2019) (Figure 15).

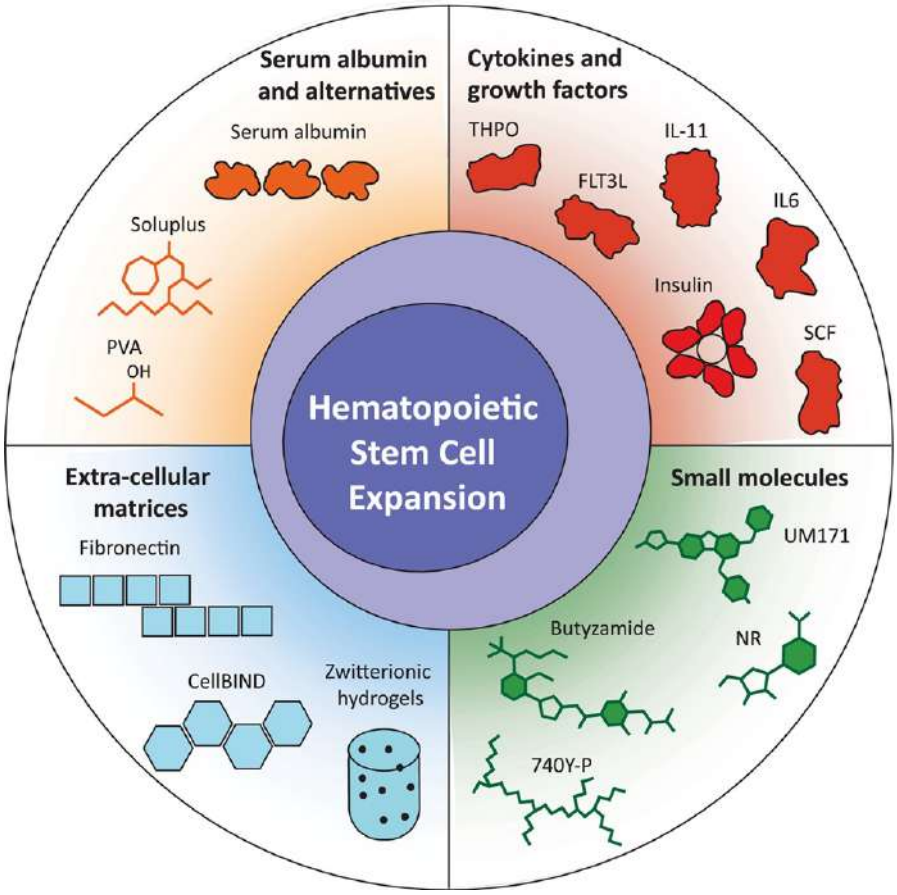


Figure 15. Strategies to facilitate ex vivo culture and expansion of HSCs. *The advancement of ameliorating HSC culture conditions focuses on substituting serum albumin with chemically stable compounds, fine-tuning the cytokine cocktail, introducing anti-differentiation small molecules, and, recently, developing more advanced culture systems with synthetic matrixes and scaffolds* (adapted from Meaker and Wilkinson, 2024).

HSCs rely on several specific mechanism to mitigate oxidative, metabolic, protein, replicative, and genotoxic stress. For instance, HSPC activation and exit from quiescence lead to the accumulation of DNA damage and replication stress, and exposure to stress stimuli promote rapid proliferation and skewing towards faster and discontinuous DNA synthesis (Walter *et al.*, 2015; Ahuja *et al.*, 2016; Jacobs *et al.*, 2022). Indeed, recent studies identified proliferative stress as a potential driver of the aging process in HSPCs (Flach et al, 2014; Yanai and Beerman, 2020), and loss of engraftment potential upon transplant has been linked to *in vitro* proliferation

and cell cycle progression (Glimm, Oh and Eaves, 2000). Moreover, elevated ROS levels and oxidative stress contribute to HSC decline (Ito *et al.*, 2004). Indeed, proliferating cells show higher mitochondrial activity compared to quiescent LT-HSC (Simsek *et al.*, 2010; Takubo *et al.*, 2013), and ROS production as oxidative phosphorylation byproduct is associated with accumulation of 8-oxo-2'-deoxyguanosine (8-oxo-dG) lesions, which can be rapidly degenerate into DSBs (Walter *et al.*, 2015). Thus, antioxidants, such as Tempol, N-acetyl cysteine (NAC), and Resveratrol, can be used to counteract culture-induced stress and increase HSC reconstitution potential upon transplantation (Ito *et al.*, 2006; Henry *et al.*, 2023). Similarly, oxidative stress is associated with p38 mitogen-activated protein kinase (MAPK) activation, which can be triggered by different stress stimuli, including UV radiation, heat and osmotic shock, PAMPs, and inflammation. p38 MAPK activation may have opposite effects on HSPCs, such as promoting beneficial homeostasis recovery upon mild and transient stressors or impairing HSC function upon chronic inflammation or stronger damaging stimuli (Canovas and Nebreda, 2021). Importantly, several works, mostly in the murine setting, have shown beneficial effects of p38 MAPK inhibition, counteracting oxidative stress, favoring HSC quiescence maintenance, and preserving their hematopoietic reconstitution potential (Ito *et al.*, 2006; Jang and Sharkis, 2007). Along this line, *ex vivo* cultured HSCs rapidly increase protein translation, and the disruption of proteo-homeostasis could contribute to stem cell aging (Signer *et al.*, 2014; Hidalgo San Jose *et al.*, 2020; Kruta *et al.*, 2021). Together, these stress responses to *ex vivo* culture may implicate premature aging of HSPCs during manipulation for GT applications. Finally, *ex vivo* culture modifies the adhesion molecules exposed on the HSPC surface, negatively affecting cellular homing or retention into the BM niche (Kallinikou *et al.*, 2012).

Traditional 2D culture vs. 3D systems

Despite continuous advances in tailoring culture conditions, traditional 2D cultures are unlikely to fully recapitulate all the essential supportive elements of the complex endogenous HSC niche. Indeed, although the HSPC mechanobiology field is still relatively in its infancy, several studies have demonstrated the critical role of 3D cues and mechanical forces in HSC specification and maintenance under both physiological and *ex vivo* conditions (Adamo *et al.*, 2009; Holst *et al.*, 2010; Altrock *et al.*, 2012; Ni *et al.*, 2019; Zhang *et al.*, 2019; Lundin *et al.*, 2020; Li *et al.*, 2021). For this reason, artificially engineered 3D systems represent an appealing solution to model the intricate architecture of the native BM niche and provide mechanical support to HSCs during *ex vivo* manipulation.

The first attempts to increase traditional 2D culture complexity included the co-culture of HSPCs and other BM cell types. Indeed, OP9 cells, fibroblasts, and MSCs guaranteed short-term expansion and increased survival of HSCs (Holmes and Zuñiga-Pflücker, 2009; Torisawa *et al.*, 2014), likely due to both direct cell-to-cell interactions and paracrine signals (Alakel *et al.*, 2009; Sharma *et al.*, 2011). Recently, MSCs/HSPCs co-culture has been exploited in the context of GE, endowing edited cells with superior repopulating capacity and polyclonal graft composition (Crippa *et al.*, 2023). In addition, organoids provide further increased complexity in mimicking the native BM microenvironment. However, very few successes have been made in the context of HSPCs, although functional organoids from blood-borne fibroblasts supported the engraftment of human HSCs and hematopoiesis *in vivo* upon subcutaneous injection (Pievani *et al.*, 2017). Interestingly, also decellularized bones have been exploited to culture human HSPCs, although ECM ultrastructure variability and the obvious reproducibility limitations of this system have limited their applications (Bianco *et al.*, 2019).

Complex systems that include multiple cell types and faithfully reproduce the native BM microenvironment are ideal for studying HSC biology and modeling physiological or pathological conditions. However, clinical applications require easy fabrication, scale-up capability, and uniformity. Thus, only some essential niche elements can be introduced into culture conditions to avoid contaminating the purity of the HSPC-GT product and achieve good manufacturing practice (GMP) compliance. In this context, synthetic scaffolds represent a more attractive and feasible approach (Congrains *et al.*, 2021). Thanks to the improvements in biomaterials engineering, various scaffolds have been designed to mimic the biophysical properties of the BM niche, including tissue rigidity and elasticity, composition, patterning, and mechanical properties (Li *et al.*, 2021). Artificial scaffolds include hydrogels, synthetic matrixes, and bioprinted structures (Rubio-Lara *et al.*, 2023). Hydrogels, as three-dimensional hydrophilic polymers, mimic the biochemical properties of the extracellular matrix. They have shown the potential to preserve HSPC stemness and mitigate adverse cellular responses in preclinical models (Bai *et al.*, 2019; Zhou *et al.*, 2020). However, hydrogels often undergo chemical modifications due to enzyme secretion by cells and lack the mechanical strength necessary to mimic the stiffness of native tissues accurately and affect the diffusion of nutrients, oxygen, and waste products within the gel matrix, leading to concentration gradients and cell death in the inner regions of the gel. Conversely, synthetic matrices composed of materials such as polystyrene, polyethylene glycol (PEG), polycaprolactone (PCL), or polydimethylsiloxane (PDMS) can be used as alternatives to natural extracellular matrix components. These

matrices offer tunable properties and can be functionalized with bioactive molecules to modulate cell behavior, potentially allowing HSPC expansion *in vitro* (Marx-Blümel *et al.*, 2021; Li *et al.*, 2023). Bioprinting enables the fabrication of complex three-dimensional structures using biomaterials and living cells, providing a customizable 3D microenvironment for stem cell culture. However, the general resolution of classical 3D printing techniques of 100-500uM may not be sufficient to replicate the intricate features of native tissues like the BM, leading to limitations in the accuracy and fidelity of printed scaffolds (Zandrini *et al.*, 2023). Another emergent 3D nanoengineered substrate with geometrical architecture has been developed exploiting two-photon laser polymerization of SZ2080, a biocompatible and inert negative photo-curable polymeric resin (Nava *et al.*, 2016). This system, called nichoid, allowed mouse embryonic stem cells, human-derived bone marrow stromal cells, and mouse neural precursor cells expansion with increased expression of pluripotency markers (Nava *et al.*, 2016; Ricci *et al.*, 2017; Messa *et al.*, 2021). Finally, engineered scaffolds can be perfused and integrated into scalable bioreactors, thus mimicking the blood flow, cardiovascular forces, and fluid shear stress (Di Buduo *et al.*, 2015, 2021; Kim *et al.*, 2019).

In conclusion, while exciting and groundbreaking works demonstrated that 3D substrates can efficiently sustain HSC maintenance and ameliorate HSPC functionality compared to standard 2D culture, the feasibility of integrating these innovative 3D systems into genetic engineering strategies and clinical practices remains to be validated.

Aim of the work

Despite the proven therapeutic efficacy of HSPC-GT in numerous clinical trials (Cavazzana-Calvo *et al.*, 2000; Aiuti *et al.*, 2002; Biffi *et al.*, 2013; Río *et al.*, 2019; Kohn *et al.*, 2020) considerable challenges prevent its universal adoption, including reaching high genetic engineering efficiency and ensuring the functionality and safety of HSPCs throughout the manipulation process. Indeed, current gene transfer and GE technologies trigger different adverse reactions, such as the activation of the DDR and the formation of genotoxic byproducts (Piras *et al.*, 2017; Schiroli *et al.*, 2019; Leibowitz *et al.*, 2021; Fiumara *et al.*, 2023). Moreover, despite significant efforts spent to constantly advance culture conditions to ensure their maintenance or potentially their expansion (Horwitz *et al.*, 2014; Fares *et al.*, 2017; Zonari *et al.*, 2017; Rai *et al.*, 2023; Sakurai *et al.*, 2023), long-term HSCs rapidly lose self-renewal potential and differentiate upon *ex vivo* exposure (Glimm, Oh and Eaves, 2000; Johnson *et al.*, 2024). Altogether, these detrimental responses may diminish the functionality of engineered cells and compromise therapy efficacy and safety by delaying hematopoietic reconstitution and affecting the clonal repertoire of repopulating stem cells (Masiuk *et al.*, 2017; Ferrari *et al.*, 2020, 2023; Tucci *et al.*, 2021).

During our work, we aimed to identify and counteract molecular determinants causing HSPC functional decline during GT protocols. First, we focused on the activation of the p38 MAPK, which has been reported to affect HSPC functionality in different contexts (Ito *et al.*, 2006; Jang and Sharkis, 2007; Tesio *et al.*, 2015; Henry *et al.*, 2020). Once we elucidated the molecular axis triggered by this stress kinase and established the beneficial effects achieved by its inhibition during Cas9/AAV6 GE, we reasoned that additional detrimental responses may arise from the removal of HSPCs from the hypoxic BM niche and be exacerbated by the loss of 3D support. Indeed, although the HSPC mechanobiology field is still relatively in its infancy, several studies have demonstrated the critical role of 3D cues and mechanical forces in HSC specification and maintenance under both physiological and *ex vivo* conditions (Adamo *et al.*, 2009; Holst *et al.*, 2010; Altrock *et al.*, 2012; Ni *et al.*, 2019; Zhang *et al.*, 2019; Lundin *et al.*, 2020; Li *et al.*, 2021). For this reason, we tested an innovative biomimetic 3D scaffold (Nava *et al.*, 2017) to counteract culture stress during genetic engineering across multiple platforms, including Cas9/AAV6, BE, PE, and lentiviral gene addition, endowing engineered HSPCs with superior long-term and polyclonal repopulating capacity for more effective and safer therapeutic applications.

Results

As stated in the Declaration, all the data reported in the section "A p38 MAPK-ROS axis fuels proliferation stress and DNA damage during CRISPR/Cas9 gene editing in HSPCs" are part of the manuscript *della Volpe, Midena et al.* accepted in principle at *Cell Reports Medicine*, in which I am listed as the co-first author.

A p38 MAPK-ROS axis fuels proliferation stress and DNA damage during CRISPR/Cas9 gene editing in HSPCs

p38 MAPK-induced ROS mediate fast cell cycle progression leading to DNA damage and DDR activation

To characterize HSPC cellular responses and identify putative molecular triggers determining the loss of stem cell functionality induced by *ex vivo* culture required for GT applications, we focused our attention on p38 MAPK, as the exposure to several cytokines, growth factors, and stress stimuli has been associated with the phosphorylation and consequent activation of this mitogen-activated protein kinase in both hematopoietic and non-hematopoietic cell types (Ezumi *et al.*, 1999; Desterke *et al.*, 2011; Tesio *et al.*, 2015; Shen *et al.*, 2017; Henry *et al.*, 2020). Thus, we found that phospho-p38 MAPK (p-p38) levels cumulatively increased upon culture time (Figure 16A) in CB-derived human CD34+ HSPCs, so we then reasoned to test SB203580 (p38i), a highly-specific and widely used ATP-competitive inhibitor of p38 MAPK activity (Cuenda *et al.*, 1995). We optimized a two-dose treatment on the first two days of *ex vivo* culture (Figure 16B) that, according to its mechanism of action, reduced the phosphorylation of p38-direct target MAPKAPK2 (MK2) without affecting HSPC viability (Appendix 1A,B).

Because p38 MAPK activation is correlated with the exposure to reactive oxygen species (ROS) (Ito *et al.*, 2006), we then measured cytosolic ROS and mitochondrial superoxides and reported that HSPCs progressively accumulated oxidative stress upon *ex vivo* culture, which was counteracted by p38i administration (Figure 16C,D). As ROS can act as key signaling molecules that stimulate cell proliferation (Ogrunc *et al.*, 2014), we reasoned that the primary trigger for adverse HSPC responses *ex vivo* may be the sudden onset of ROS-mediated cell proliferation in previously quiescent cells. Therefore, we asked whether p38 MAPK may influence HSPC proliferation dynamics via mitogenic ROS. First, we measured the number of cell divisions in vehicle- or p38i-treated cells by using a CellTrace dye. Interestingly, we found that across different donors, individual HSPCs performed slightly fewer rounds

of cell divisions when treated with p38i (on average each p38i-treated cell divided 0.36 times less than control cells) (Figure 16E). This relatively modest effect resulted in an evident reduction in cumulative proliferation upon p38 inhibition measured by live imaging cell confluence analysis (Figure 16F), suggesting that ROS may act as mitogenic signals in this experimental setting. To confirm this hypothesis, we supplemented the ROS scavenger N-acetyl cysteine (NAC) during the first two days of *ex vivo* culture, in analogy with p38i treatment. Although NAC administration was able to reduce oxidative stress only transiently, as its effect shrank at a later time point (Appendix 1C), we reported a significant slowdown in HSPC proliferation (Appendix 1D). Nevertheless, NAC treatment did not affect the percentage of phospho-p38 MAPK-positive cells (Appendix 1E). Similarly, additional antioxidants, including Resveratrol and Tempol, and their combinations with NAC showed a transient decrease of ROS accumulation (Appendix 1F) and consequent reduction of proliferation rates across all conditions (Appendix 1G). However, ROS scavenging was not sufficient to dampen the phosphorylation of p38 MAPK (Appendix 1H), implying that ROS are produced downstream of p38 MAPK activation in *ex vivo* cultured HSPCs. In addition, consistent with the well-known ability of ROS to oxidize DNA bases, we reported a cumulative increase of 8-oxo-2'-deoxyguanosine (8-oxo-dG) induction in control cells, which was counteracted by p38 inhibition (Figure 16G).

Once established the mitogenic properties of ROS, we asked whether p38/ROS-dependent proliferation may cause proliferative stress. Thus, we investigated the accumulation of physical DNA single- and double-strand breaks by comet assay and found that *ex vivo* culture is accompanied by a noticeable increase of DNA lesions, which was significantly mitigated by inhibition of p38 MAPK (Figure 16H). Importantly, both transient cell cycle inhibition via CDK4/6 inhibitor (CDK4/6i) and NAC treatments decreased physical DNA damage accumulation (Appendix 1I) according to the extent of proliferation slowdown (Appendix 1J), confirming the link between HSPC *ex vivo* proliferation and the insurgence of DNA damage. Then, to assess if proliferation-induced DNA damage could be associated with canonical DDR activation, we performed immunofluorescence analysis of phosphorylated histone variant H2AX (yH2AX), an established DDR sensor, and phosphorylated form of replication protein A (pRPA), a ssDNA binding protein (Sulli, Di Micco and Di Fagagna, 2012). Thus, we reported increasing DDR sensor accumulation during *ex vivo* culture, which was rescued by p38 inhibition (Figure 16I,J, Appendix 1K). Consistently with proliferation slowdown and diminished physical DNA breaks, p38 MAPK inhibition also alleviated the activation of the apical DNA replication stress kinase ATR (phospho-ATR, Ser428) and its downstream target CHK1 (phospho-CHK1, Ser345) (Figure

16K). Finally, mitigation of oxidative and proliferative stress led to a slight but persistent increase in the proportion of phenotypically defined primitive HSPCs (CD34+133+90+ cells) in the p38i condition (Figure 16L).

Altogether, our data highlight that *ex vivo* culture of HSPCs required for GT applications triggers a complex multi-step process initiated by p38 MAPK activation, generating oxidative stress and mitogenic ROS that mediates excessive proliferation, leading to consequent replication stress and activation of the DDR signaling cascade. Importantly, the inhibition of p38 MAPK limits the activation of this intricate molecular axis, counteracting culture stress and better preserving primitive HSPCs.

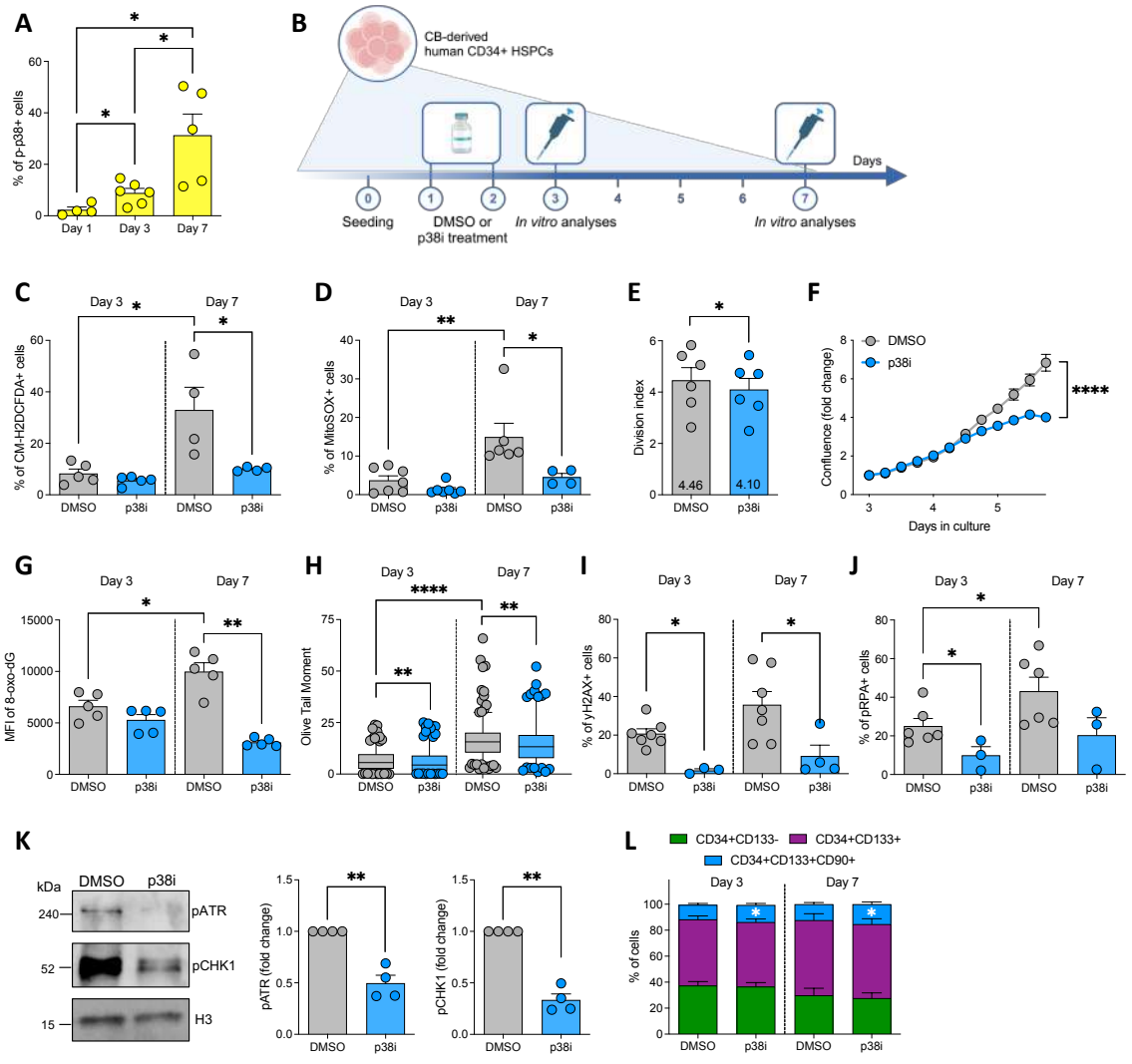


Figure 16. p38-induced ROS mediate fast cell cycle progression leading to DNA damage and DDR activation. *(**A**) Percentage of p-p38+ cells (n=4,6,5). Mann-Whitney test. (**B**) Experimental workflow. Human CB-derived HSPCs were treated with p38i or vehicle (DMSO) in the first two days and collected for downstream analyses on days 3 and 7. (**C,D**) Percentage of cytosolic (**C**) and mitochondrial (**D**) ROS+ cells ((**C**), n=5,5,4,4; (**D**), n=6,7,6,4). Mann-Whitney test. (**E**) Division index measured from CellTrace dye dilution on day 7 (n=6). Wilcoxon test. (**F**) Confluence analysis over time reported as fold change to the*

*first time point (n=3). Mann-Whitney test. (**G**) MFI of 8-oxo-dG on day 7 (n=5). Mann-Whitney test. (**H**) Quantification of SSBs and DSBs by alkaline comet assay; each dot represents a single cell (more than 300 cells were analyzed for each condition). Median ± 95% CI. Mann-Whitney test. (**I,J**) Percentage of (**I**) γH2AX or (**J**) pRPA positive HSPCs ((**I**), n=9,7,3,7,4; (**J**), n=6,6,3,6,3). Mann-Whitney test. (**K**) Western Blot analysis of pATR (left) and pCHK1 (right) on day 7 (n=4). Histone H3 was used as a loading control, and fold change relative to control is reported. One-sample T-test. (**L**) Percentage of phenotypically defined HSPC subsets (n=7). Wilcoxon test. Unless otherwise specified, Mean ± SEM. *p < 0.05; **p < 0.01; ****p < 0.0001.*

p38 inhibition improves gene-edited HSPC repopulating capacity and clonal output long-term post-transplantation

We then reasoned that by decreasing proliferation-associated endogenous DNA damage, p38 inhibitor treatment could directly benefit current HSPC-based clinical applications, especially in the context of genetic engineering, which involves additional steps of manipulation such as the administration of editing tools and viral vectors that may affect HSPC functionality *per se* (Piras *et al.*, 2017; Schiroli *et al.*, 2019). Thus, on the third day of cytokine stimulation, upon p38i or DMSO treatments, we collected CB-derived HSPCs and performed nucleofection with Cas9 ribonucleoprotein complexes (RNP) pre-assembled with synthetic base-modified gRNA targeting the *AAVS1* genomic safe harbor. Subsequently, electroporated HSPCs were transduced with an AAV6 to allow for HDR-mediated precise insertion of a GFP reporter cassette within the targeted locus (Figure 17A).

While p38i administration did not affect cell viability and GE efficiency across HSPC subsets (Figure 17B, Appendix 2A,B), it was sufficient to increase the fraction of the more primitive CD34+CD133+CD90+ compartment upon genetic engineering (Figure 17C). In addition, we reported increased numbers of white and mixed colonies generated by cells edited upon p38 inhibition (Figure 17D), suggesting the amelioration of HSPC functionality. To confirm this finding, we transplanted equal doses of edited CD34+ cells upon DMSO or p38i administration at 24h post-editing into immunodeficient mice. By monitoring the PB of the mice at different time points (from 6 to 15 weeks), we found higher human engraftment in the p38i group (Figure 2E), which was then confirmed by the analyses of the other hematopoietic organs, including the BM and SP (Figure 17F, Appendix 2C). Thus, while graft composition was comparable between treatments across the different organs (Appendix 2D-F), we confirmed the amelioration of the functionality of edited HSPC upon p38 MAPK inhibition. In addition, to track HDR-edited HSPCs within the human graft, we measured GFP-expressing cells and detected similar percentages in the PB, BM, and SP from all the analyzed mice (Figure 17G,H, Appendix 2G), in line with the *in vitro* data.

Given that we found increased graft size of p38i-treated edited cells and because genetic engineering affects the yield and clonal output of edited HSPCs (Schiroli *et al.*, 2019; Ferrari *et al.*, 2020), we asked whether p38 inhibition could impact the number and reconstitution of edited HSPC clones. First, we quantified the number of unique indels by deep sequencing the *AAVS1* target locus in the human graft from the BM of the mice and reported improved clonal diversity in the p38i condition (Figure 17I). Then, to determine the HDR-clonal repertoire, we used an AAV6 donor repair template pool carrying a 22bp degenerated heritable "barcode" sequence (BAR) downstream of the GFP reporter cassette (Ferrari *et al.*, 2020) and selected for further analyses transplanted mice with detectable engraftment (>0.1%) of GFP+ cells. Interestingly, we found that the number of BARs was significantly increased upon p38 inhibition, suggesting an enhanced polyclonal reconstitution of HDR-edited cells upon p38i treatment (Figure 17J).

Finally, we specifically tested the repopulating capacity of long-term HSCs by injecting BM-derived CD34+ cells from primary mice into secondary recipients. Thus, we reported that the p38i group outperformed the percentage of human cells in PB and SP of the DMSO group, while similar engraftment was found in the BM (Figure 17K, Appendix 2H,I). In addition, when analyzing the impact of p38i on graft composition within the different organs, we found that the p38i-treated group showed fewer myeloid cells, with increased T cell output in the PB and more B cells in the BM and SP (Appendix 2J-L). Most importantly, only the p38i group retained a sizable fraction of HDR-edited cells (Figure 17L, Appendix 2M,N), indicating improved long-term maintenance of HDR-edited cells upon p38 MAPK inhibition.

Overall, our data indicate that p38i treatment counteracts culture stress occurring during *ex vivo* culture required for HSPC genetic engineering, better preserving the quality of edited cells and improving the polyclonal reconstitution of HDR-edited HSCs in the long term.

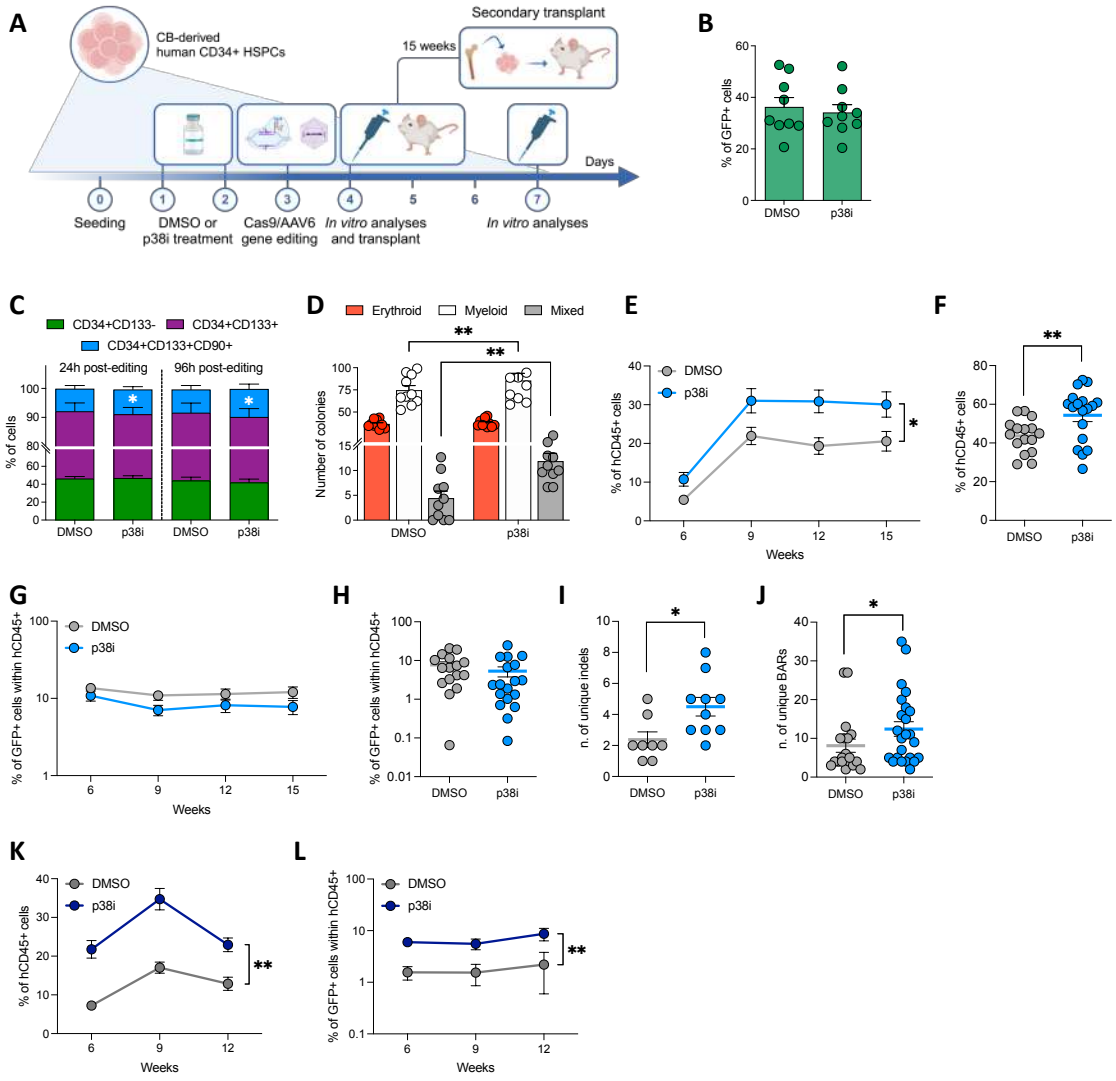


Figure 17. p38 inhibition improves gene-edited HSPC repopulating capacity and clonal output long-term post-transplantation. *(**A**) Experimental workflow. Human CB-derived HSPCs were treated with p38i or vehicle (DMSO) in the first two days and and collected on day 3 for Cas9/AAV6 gene editing to insert a GFP reporter within the AAVS1 locus. Edited cells were collected for downstream analyses on days 4 and 7 (24h and 96h post-editing, respectively). After 15 weeks post-injection, CD34+ cells were purified from the BM of the mice and transplanted into secondary recipients. (**B**) Percentage of GFP+ cells (within CD34+ cells) by FACS analysis on day 7 (n=9). (**C**) Percentage of phenotypically defined HSPC subsets (n=8). Wilcoxon test. (**D**) Number of erythroid, myeloid, and mixed colonies generated in CFU-C assay (n=10). Wilcoxon test. (**E,F**) Percentage of human CD45+ (hCD45+) cells measured in the PB (**E**) over time and BM (**F**) at the endpoint of transplanted mice (n=16,18). Mann-Whitney test (calculated at the last time point for PB). (**G,H**) Percentage of GFP+ cells (within hCD45+ cells) in the PB (**G**) over time and BM (**H**) from mice in (**E,F**) (n=16,18). Mann-Whitney test (calculated at the last time point for PB). (**I,J**) Number of unique indels (**I**) and BARs (**J**) in the BM of mice from (**F**) at the endpoint ((**I**), n=8,10; (**J**), n=19,24). Mann-Whitney test (**K**) Percentage of hCD45+ cells measured in the PB over time of transplanted secondary recipients (n=9,11). Mann-Whitney test (calculated at the last time). (**L**) Percentage of GFP+ cells (within hCD45+ cells) in the PB over time from mice in (**K**) (n=9,11). Mann-Whitney test. Mean ± SEM. *p < 0.05; **p < 0.01.*

3D scaffolds enable polyclonal and long-term engraftment of genetically engineered HSPCs

Nichoids increase the functionality of HSPCs upon ex vivo manipulation

We reasoned that the detrimental responses occurring in *ex vivo* cultured HSPCs may arise from their removal from the bone marrow niche and be exacerbated by growth on bidimensional substrates. Indeed, although the HSPC mechanobiology field is still relatively in its infancy, several studies have demonstrated the critical role of 3D cues and mechanical forces in HSC specification and maintenance under both physiological and *ex vivo* conditions (Adamo *et al.*, 2009; Holst *et al.*, 2010; Altrock *et al.*, 2012; Ni *et al.*, 2019; Zhang *et al.*, 2019; Lundin *et al.*, 2020; Li *et al.*, 2021). Thus, to provide mechanical support and ameliorate the functionality of HSPCs upon *ex vivo* exposure and prolonged time in culture required for GT applications, we tested an innovative nano-engineered 3D culture substrate with cell-scale resolution called "nichoid" (Nava *et al.*, 2016). This advanced micrometric scaffold is made of SZ2080, a biocompatible and inert negative photo-curable polymeric resin fabricated by two-photon polymerization on a glass slide, with a miniaturized lattice architecture organized by the repetition of elementary units of 10-30×15 µm (Nava *et al.*, 2017) (Figure 18A). Specifically, CB-derived CD34+ human HSPCs were seeded either on standard culture wells (2D) or nichoids (3D) immediately after thawing and collected after three or seven days of *ex vivo* culture for downstream analyses, including transplant into immunocompromised mice (Figure 18B). Of note because HSPCs tend to interact and adhere to the scaffold, we optimized a detachment protocol with a citrate solution that did not affect cell viability nor HSPC ability to generate colonies in the standard CFU-C (Appendix 3A-C).

First, we found similar percentages of phenotypically defined HSPC subsets and viable cells across the different culture systems (Figure 18C, Appendix 3D,E). However, 3D culture increased HSPC clonogenic potential due to a higher mixed-colony output, the progeny of more primitive and multipotent cells (Figure 18D) (Miller and Lai, 2005). As the nichoid substrate is fabricated on a glass support that may affect HSPC behavior *per se*, we also compared the clonogenic potential of HSPCs grown in 3D culture or 2D on standard tissue culture plates or cell culture glass coverslips. Importantly, we reported higher mixed-colony output exclusively in the nichoid condition, while the clonogenic potential of 2D cultured HSPCs was comparable between the two substrates (Appendix 3F). Of note, we observed the expansion of the mixed colonies only if HSPCs were immediately seeded on 3D after

thawing and not after a brief period of one or two days of initial 2D culture (Appendix 3G), highlighting the importance of 3D stimuli during the early stage of *ex vivo* culture adaptations.

To gather some insights on the fitness of the more primitive HSC compartment upon 3D culture, we FACS sorted HSC-enriched single cells (defined as CD34+CD133+CD90+CD45RA-) on the third day of culture to assess their multi-lineage differentiation potential along the myeloid (My), erythroid (Ery), megakaryocytic (Meg), and natural killer (NK) branches (Belluschi *et al.*, 2018) (Appendix 3H). First, we reported a slight increase in the numbers of different lineages present within single colonies derived from 3D cultured HSCs compared to the 2D counterpart (Figure 18E), thus suggesting better preservation of their multi-lineage potential. Moreover, nichoid pre-cultured cells gave rise to colonies with higher cellularity (Figure 18F), further supporting enhanced fitness of the stem cells compartment upon 3D culture. In terms of lineage specification, by analyzing in detail the composition of uni-lineage and multi-lineage colonies, we found an expansion of the Ery-only and MyNK output in the 3D condition, balanced by a decrease in the fraction of My-only and EryMeg colonies (Appendix 3I,J).

We next transplanted equal numbers of 2D or 3D cultured HSPCs into immunocompromised mice to assess their hematopoietic reconstitution potential. Importantly, we reported consistent and higher human chimerism in the PB of the mice transplanted with nichoid-cultured HSPCs throughout the different time points analyzed (Figure 18G), with superior engraftment across multiple hematopoietic organs, including the BM and SP (Figure 18H,I). Additionally, PB analyses revealed higher fractions of myeloid and T cells present in the 3D condition at the latest time point (Appendix 3K,L), although we observed similar graft composition in the BM and SP (Appendix 3M,N). We then purified human CD34+ cells from the BM of the mice and found a higher clonogenic output of nichoid pre-cultured transplanted HSPCs upon further re-challenging in the CFU-C assay (Figure 18J). At last, we mathematically assessed the relative number of HSCs required to give rise to comparable engraftments by a maximum likelihood estimation (MLE) model as previously reported (Goyal *et al.*, 2015; Zhao *et al.*, 2024). Strikingly, we found that the 2D condition required almost double the quantity of HSCs than the 3D group (Figure 18K), further highlighting the importance of 3D stimuli and mechanical support for the maintenance of functional stem cells during *ex vivo* culture.

Altogether, our findings demonstrate that the nichoid 3D culture system significantly enhances HSPC functionality compared to traditional 2D cultures. The improved clonogenic output and multi-lineage differentiation up to single-cell

resolution and superior *in vivo* repopulating capacity demonstrate the critical role of 3D cues in preserving stem cell properties during *ex vivo* manipulation.

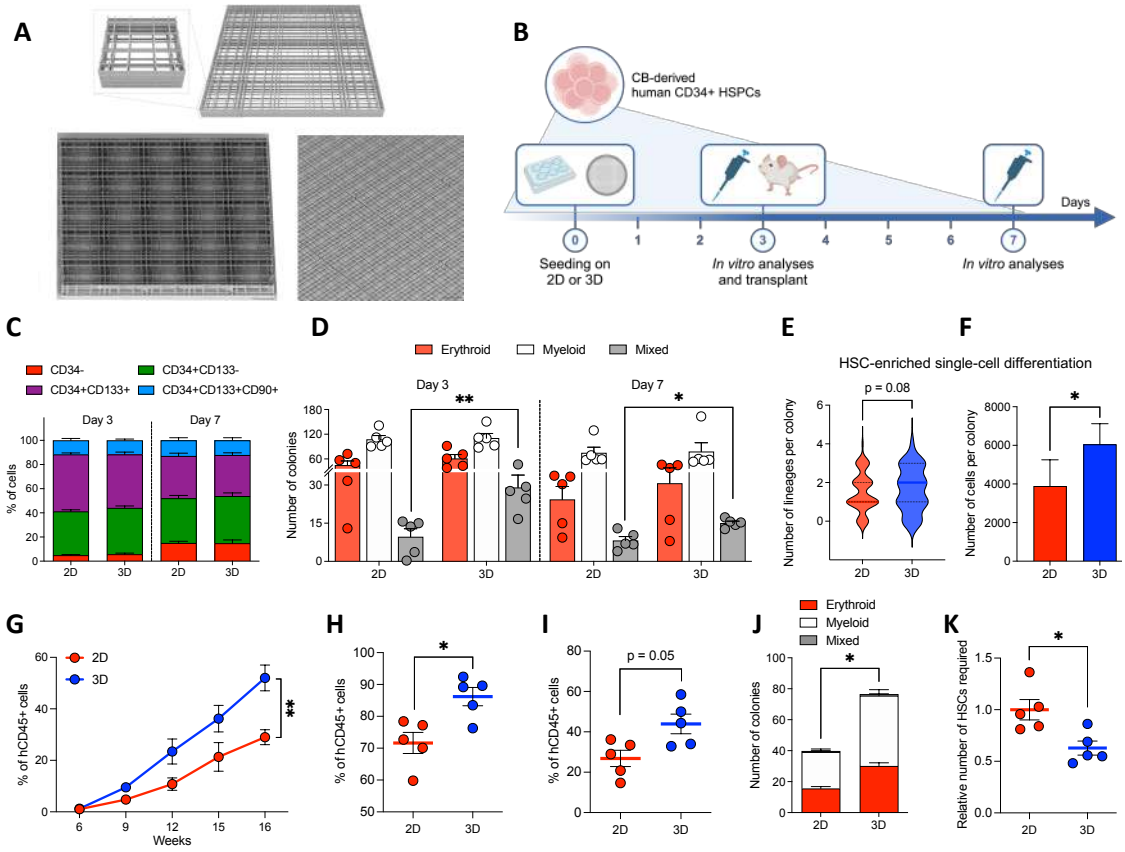


Figure 18. Nichoids increase the functionality of HSPCs upon ex vivo manipulation. *(**A**) Representative image (top) and scanning electron microscopy (bottom) of the nichoid culture substrate. (**B**) Experimental workflow. Human CB-derived HSPCs were seeded on 2D or 3D immediately after thawing and collected for downstream analyses on days 3 and 7. (**C**) Percentage of phenotypically defined HSPC subsets (n=9,9,10,10). (**D**) Number of erythroid, myeloid, and mixed colonies generated in CFU-C assay (n=5). Mann-Whitney test. (**E,F**) Number of lineages (**E**) and cells (**F**) per colony generated by HSC-enriched single cells (more than 250 colonies analyzed for each condition). Median ± 95% CI. Mann-Whitney test. (**G-I**) Percentage of human CD45+ (hCD45+) cells measured in the PB (**G**) over time, and BM (**H**) and SP (**I**) at the endpoint of transplanted mice (n=5). Mann-Whitney test (calculated at the last time point for PB). (**J**) Number of erythroid, myeloid, and mixed colonies generated by BM-derived CD34+ cells purified from mice in (**H**) (n=5). Mann-Whitney test. (**K**) Relative number of HSCs required to generate comparable engraftment calculated by MLE from (**H**) (n=5). Mann-Whitney test. Unless otherwise specified, Mean ± SEM. *p < 0.05; **p < 0.01.*

3D culture preserves cellular morphology and polarity, profoundly reshaping the HSPC transcriptional profile

To investigate the molecular changes dictated by nichoids that endow *ex vivo* cultured HSPCs with enhanced functionality, we performed transcriptional analysis on CD34+ cells cultured on 2D or 3D for four- and seven days post-thawing. Surprisingly, nichoids induced a profound reshaping of the HSPC transcriptional

profile, with differential modulation of 5399 and 5255 genes at day 4 and 7, respectively (Appendix 4A). When performing gene set enrichment analysis (GSEA), we found upregulation of cellular pathways related to the extracellular matrix (ECM), cell adhesion, and cytoskeleton organization in the 3D condition, although the latter was significantly modulated only in the later time point (Figure 19A). Conversely, we reported downregulation of genes belonging to DNA replication, cell division, transcription, protein synthesis and degradation, and oxidative respiration, features associated with more primitive and dormant stem cells (Cabezas-Wallscheid *et al.*, 2014; Lauridsen *et al.*, 2018; García-Prat *et al.*, 2021). Importantly, we also reported downregulation of pathways involved in DDR signaling and DNA repair (Figure 19A), suggesting a possible interplay between the loss of 3D stimuli and genomic instability.

To narrow down our analysis, we focused on specific genes involved in cell adhesion, cytoskeletal rearrangements and signaling, and other HSPC-related pathways (Figure 19B). Thus, we found upregulation of multiple integrin subunits (*ITGA1*, *ITGA3*, *ITGA5*, and *ITGB1*), combined with differential modulation of microfilament and microtubule remodelers (such as *CLF1*, *CAPG*, *VIL1*, *STMN1*, and *CLIP1*), and upregulation of focal adhesion genes and GPCRs (such as *PTK2*, also known as focal adhesion kinase 1, *PAK4*, *ROCK1*, and *GPRC5C*), indicating a crosstalk between the 3D scaffold and HSPC mechano-sensing. Importantly, we also reported downregulation of *CDC42*, a small GTPase of the Rho-subfamily that regulates HSC aging and rejuvenation (Florian *et al.*, 2012). Moreover, we detected upregulations of genes of the Notch and Wnt signaling pathways (such as *NOTCH3*, *CREBBP*, *FZD2*, and *WNT5A*), *HLF*, *SLC2A1* (Glut1), *EPAS1* (Hif2a), *FOXO1* and *FOXO3*, Akt, Yap/Taz, and *PTPN21*, which are fundamental for HSC specification and maintenance (Tothova *et al.*, 2007; Miyamoto *et al.*, 2007; Butler *et al.*, 2010; Pajcini, Speck and Pear, 2011; Famili *et al.*, 2015; Staal, Chhatta and Mikkers, 2016; Chabi *et al.*, 2019; Ni *et al.*, 2019; Liang *et al.*, 2020; Lundin *et al.*, 2020; Araki *et al.*, 2021; Lehnertz *et al.*, 2021; Kim *et al.*, 2022).

To experimentally validate some of the transcriptional programs modulated by 3D culture, we characterized nichoid-cultured HSPCs through multiple molecular analyses. First, we assessed cell proliferation and confirmed that individual HSPCs grown on nichoids from both the bulk CD34+ and the more primitive CD34+CD133+CD90+ subsets performed fewer rounds of cell division compared to traditional 2D culture, as supported by the heightened CellTrace dye retainment (Figure 19C, Appendix 4B). Moreover, we found reduced oxidative stress in the nichoid condition with decreased accumulation of ROS and 8-oxo-dG DNA lesions (Figure 19D,E). In addition, alkaline comet assay revealed fewer DNA single- and

double-strand breaks in the 3D condition (Figure 19F). In accordance with transcriptomic analysis and consequently with diminished physical DNA breaks accumulation, we found fewer foci *per* cell of the upstream mediators of DNA damage sensing and DDR activation pRPA and yH2AX (Appendix 4C), confirming the amelioration of genome integrity in the presence of 3D stimuli provided by the nichoid substrate. Interestingly, we also reported reduced activation of the p38 MAPK kinase (Figure 19G).

We then performed z-stacked confocal immunofluorescence microscopy to investigate HSPC morphology in the presence of the 3D scaffold. Strikingly, we found a completely different phenotype between the two conditions as nichoids endowed *ex vivo* cultured cells with a small and spherical morphology, whereas HSPCs grown on 2D were enlarged and flattened (Figure 19H). Indeed, measurement of physical parameters such as the volume and squashing (defined as the ratio between the long and short axis of each cell, where squashing values close to 1 reflect spherical objects) confirmed that not only single cells but also their respective nuclei remain smaller and more rounded in the presence of the nichoid substrate (Figure 19I,J). When performing this analysis, we also observed a different architecture of the microtubule cytoskeleton. Specifically, 3D cultured HSPCs showed a defined tubulin organization, which was either polarized or equally distributed on the outer layer of the cell, while the 2D condition displayed multiple microtubule bundles spread across the whole cellular volume (Figure 19K). Thus, we assigned a tubulin score to single HSPCs based on the intensity of the tubulin signal along the cell diameter (1 for multiple bundles, 2 for symmetrical distribution underneath the plasma membrane, and 3 for polarized cells) and reported a distinct architecture of the microtubule cytoskeleton between the two conditions, with the majority of nichoid-cultured HSPCs with polarized tubulin distribution (Figure 19L), likely resulting from the interactions with the scaffold microenvironment or the exposure to different mechanical forces between the two culture systems.

Overall, nichoids induced a profound transcriptional rewiring of *ex vivo* cultured HSPCs, upregulating molecular pathways related to cytoskeleton remodeling and adhesion, with a concomitant decrease in cell proliferation, oxidative stress, and DNA damage accumulation. Mechanistically, 3D scaffolds prevented HSPC deformation and squashing occurring in 2D culture, conserving nuclei morphology and tubulin polarity, thus potentially facilitating adaptation to *ex vivo* culture with consequent preservation of stemness properties.

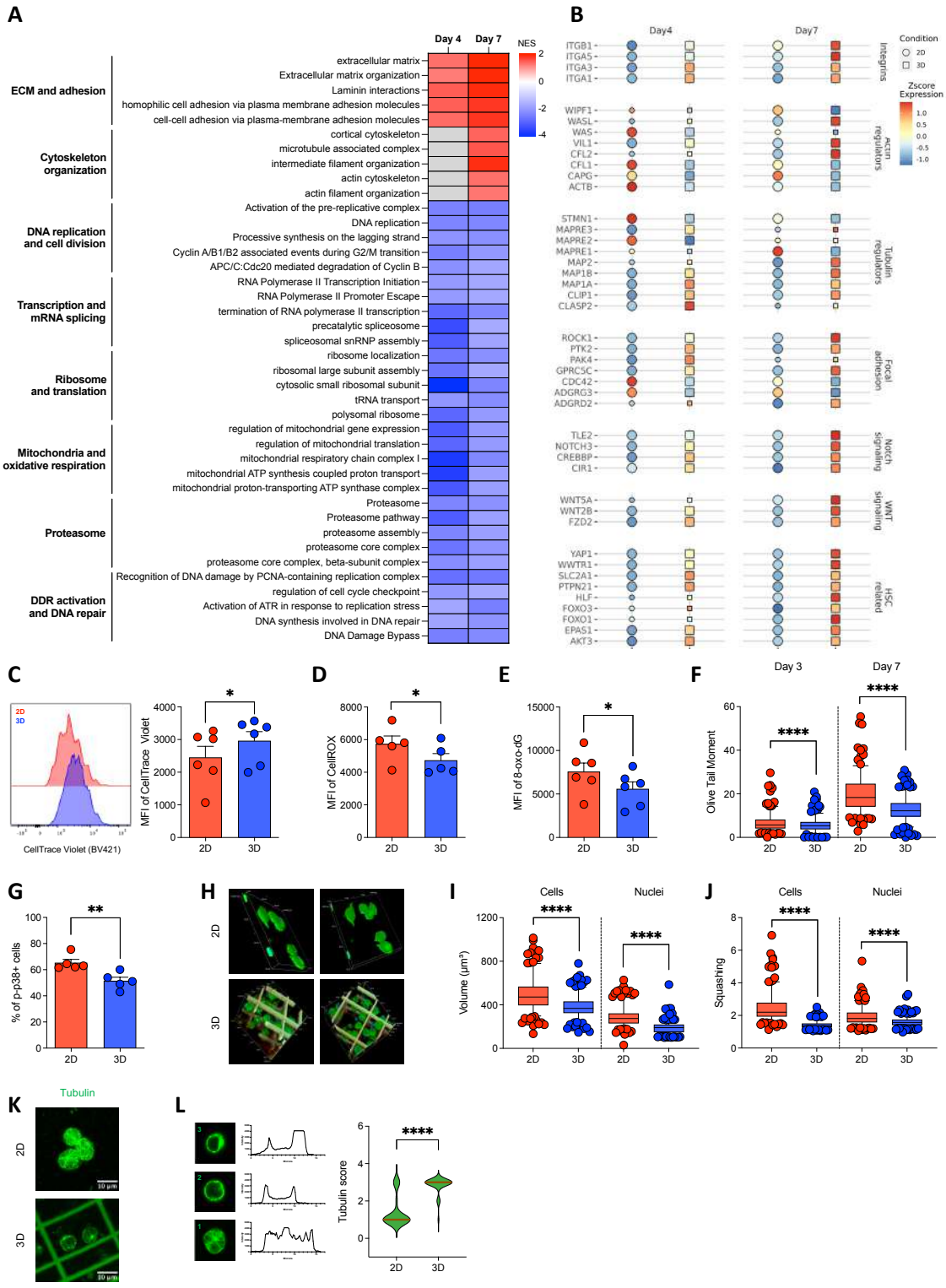


Figure 19. 3D culture preserves cellular morphology and polarity, profoundly reshaping the HSPC transcriptional profile. *(**A**) Differentially modulated categories from GSEA (FDR < 0.05) of 3D- vs. 2D-cultured HSPCs. Color gradient reflects the normalized enrichment score (NES). (**B**) Average gene expression (Zscore). Differentially expressed genes (FDR < 0.05) are represented with larger symbols. (**C**) Representative plot (left) and MFI (Median Fluorescence Intensity) (right) of CellTrace dye dilution on day 7 (n=6). Wilcoxon*

*test. (**D**) MFI of ROS (by CellROX staining) on day 7 (n=5). Mann-Whitney test. (**E**) MFI of 8-oxo-dG on day 7 (n=6). Wilcoxon test. (**F**) Quantification of SSBs and DSBs by alkaline comet assay; each dot represents a single cell (more than 200 cells were analyzed for each condition). Median ± 95% CI. Mann-Whitney test. (**G**) Percentage of phospho-p38 (p-p38)-positive cells on day 7 (n=5). Mann-Whitney test. (**H**) Representative 3D renderings of HSPCs on day 7 of 2D or 3D culture. (**I,J**) Quantification of (**I**) volume and (**J**) squashing morphological parameters on day 7; each dot represents a single cell or nucleus (more than 250 cells were analyzed for each condition). Median ± 95% CI. Mann-Whitney test. (**K**) Representative immunofluorescence staining of tubulin spatial localization on day 7. (**L**) Representative images (left) and quantification (right) of tubulin score on day 7 (more than 100 cells were analyzed for each condition). Median Value. Mann-Whitney test. Unless otherwise specified, Mean ± SEM. *p < 0.05; **p < 0.01; ****p < 0.0001.*

Nichoid pre-culture allows efficient genetic engineering with multiple editing platforms

Encouraged by these data showing that 3D cues improve the fitness of *ex vivo* cultured HSPCs, we reasoned that nichoids could directly benefit current HSPC engineering protocols. First, we implemented these innovative 3D scaffolds into our established long-range GE protocol. Immediately after thawing, we seeded human CB-derived CD34+ cells either on 2D or 3D and, on the third day of cytokine stimulation, we collected the cells and performed Cas9/AAV6 GE to introduce a GFP reporter in the *AAVS1* locus (Figure 20A). In parallel, given the recent advances in the field of genetic engineering, we tested whether nichoids implementation could benefit multiple GE strategies, such as BE and PE. To this aim, we electroporated recently-optimized mRNAs encoding for an adenine base editor (ABE8.20-m) or prime editor (PE3max) (Fiumara *et al.*, 2023) to KO the *B2M* gene in HSPCs pre-cultured in 2D or 3D for three days. For BE and PE, we decided to move from CB to mPB-derived HSPCs to test an additional source of HSPCs, which is nowadays the preferred choice for clinical applications (Ferrari *et al.*, 2023) (Figure 20A). Of note, HSPCs from both conditions were seeded on 2D post-nucleofection to avoid repetitive cycles of seeding and detachment from the scaffold.

As expected, nichoid pre-culture did not affect the viability of genetically engineered HSPCs nor the fractions of phenotypically defined HSPC subsets (Appendix 5A,B), and the GE efficiency across editing strategies was comparable between the two conditions both in the bulk CD34+ and the more primitive CD34+CD133+CD90+ fractions (Figure 20B, Appendix 5C-D). Intriguingly, nichoid pre-culture was sufficient to slow down HSPC proliferation even upon re-plating on standard 2D wells (Appendix 5E). However, the fraction of cells in the HDR-permissive S/G2 phases of the cell cycle at the time of nucleofection was similar between the 2D and 3D conditions (Appendix 5F), thus explaining the comparable HDR-mediated editing levels of the different culture systems. Importantly, nichoid

culture prior to GE enhanced the clonogenic potential of edited cells by increasing their mixed-colony output across the different editing platforms (Figure 20C).

Finally, we assessed the impact of nichoid pre-culture on the hematopoietic reconstitution capacity of gene-edited HSPCs. We focused on long-range GE, which employs nuclease-induced DSBs and viral vectors that trigger stronger detrimental cellular responses compared to BE and PE (Schiroli *et al.*, 2019; Fiumara *et al.*, 2023), and we transplanted equal doses of 2D or 3D pre-cultured HSPCs at 24h post-editing into immunodeficient mice. Thus, we found consistently higher engraftment of nichoid pre-cultured edited cells across the different hematopoietic organs analyzed (Figure 20D,E, Appendix 5G). Looking at GFP+ cells within the human fraction of the PB of the transplanted mice, we reported stable persistence of HDR-edited cells in the 3D condition, while the fraction of GFP+ cells shrank over time in the 2D group (Figure 20F), but ultimately reaching comparable levels in the BM and SP at the endpoint of the experiment (Appendix 5H,I). In addition, we found similar percentages of the various hematopoietic cell types present in the human graft across the three organs analyzed (Appendix 5J-L). Moreover, we then recovered BM-derived human CD34+ edited cells and reported that the 3D group retained a higher clonogenic potential upon further re-challenging in the CFU-C assay (Figure 20G). Most importantly, we found that the 3D condition required half the amount of input HSCs than the 2D group to give rise to comparable engraftment levels (Figure 20K), thus confirming the beneficial effects of nichoid pre-culture for preserving functional stem cells upon genetic manipulation.

Collectively, our data demonstrates that nichoids implementation into multiple GE strategies, including Cas9/AAV6, BE, and PE, significantly enhances the functionality of engineered HSCPs, endowing edited cells with improved clonogenic potential and superior hematopoietic reconstitution.

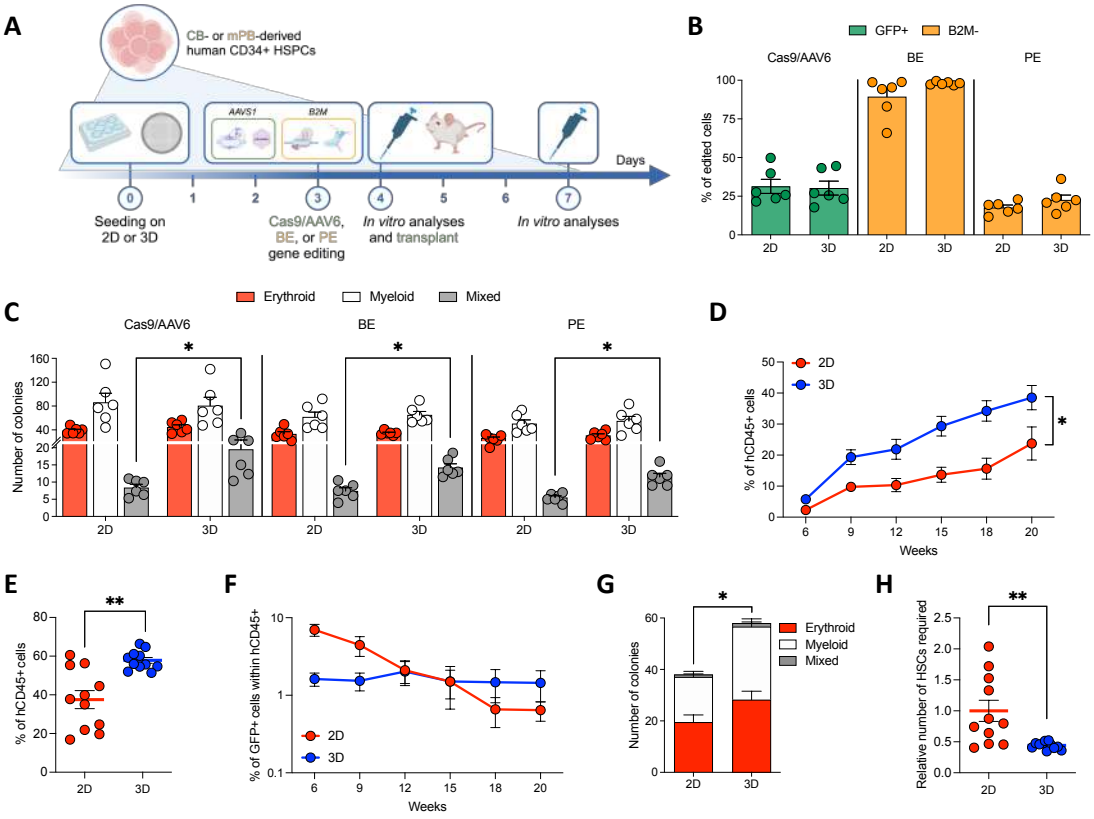


Figure 20. Nichoid pre-culture allows efficient genetic engineering with multiple editing platforms. *(**A**) Experimental workflow. Human CB- or mPB-derived HSPCs were seeded on 2D or 3D immediately after thawing and collected on day 3 for nucleofection. Specifically, CB-derived cells were edited with Cas9/AAV6 to insert a GFP reporter within the AAVS1 locus, while mPB-derived cells were edited with BE or PE to disrupt the B2M gene. HSPCs from both the 2D and 3D conditions were seeded in 2D after nucleofection and collected for downstream analyses on days 4 and 7. Transplantation was performed only for the Cas9/AAV6 treatment. (**B**) Percentage of CD34+ edited cells by FACS analysis on day 7 (n=6). (**C**) Number of erythroid, myeloid, and mixed colonies generated in CFU-C assay from edited HSPCs seeded on day 4 (n=6). Wilcoxon test. (**D,E**) Percentage of hCD45+ cells measured in the PB (**D**) over time and BM (**E**) at the endpoint of transplanted mice (n=11). Mann-Whitney test (calculated at the last time point for PB). (**F**) Percentage of GFP+ cells (within hCD45+ cells) in the PB over time from mice in (**D**) (n=11). (**G**) Number of erythroid, myeloid, and mixed colonies generated by BM-derived CD34+ cells purified from mice in (**E**) (n=11). Mann-Whitney test. (**H**) Relative number of HSCs required to generate comparable engraftment calculated by MLE from (**E**) (n=11). Mann-Whitney test. Mean ± SEM. *p < 0.05; **p < 0.01.*

3D culture enables superior long-term engraftment of HDR-edited HSPCs

Despite nichoid pre-culture generally ameliorating the engraftment of HSPC subject to the long-range GE procedure, the overall fraction of HDR-edited cells within the human graft was still relatively low. Thus, together with Cas9/AAV6 delivery to precisely insert the GFP reporter within the *AAVS1* locus, we incorporated the electroporation of the mRNA encoding for the GSE56 and Ad5-E4orf6/7 editing enhancers (Figure 21A). Specifically, this previously validated strategy allows

transient expression of a dominant-negative p53 variant (GSE56) to counteract GE-induced DDR activation and an adenoviral helper protein (Ad5-E4orf6/7) to favor HDR engagement (Schiroli *et al.*, 2019; Ferrari *et al.*, 2020).

Even in this setting, nichoid pre-culture did not affect cell viability upon genetic engineering nor the phenotypic composition of the HSPC culture (Appendix 6A,B). Similarly, GE efficiency across HSPC subsets was comparable between the 2D and 3D conditions (Appendix 6C,D), although, as expected, the presence of editing enhancers increased the overall fraction of GFP+ cells with respect to the standard protocol (Figure 19B, Appendix 5E). Moreover, in line with previous observations, we reported a higher colony-forming potential for edited HSPCs pre-cultured on nichoids with increased mixed-colony output (Appendix 6E).

We then transplanted equal numbers of 2D or 3D pre-cultured gene-edited HSPCs into immunocompromised mice at 24h post-editing. Similarly to the previous GE setting, nichoids outperformed conventional 2D culture as we found significantly higher human chimerism in the PB, BM, and SP of the mice transplanted from the 3D condition (Figure 21B,C, Appendix 6F), with comparable levels of GFP+ edited cells (Figure 21D, Appendix 6G,H) and graft composition (Appendix 6I-K) between the two groups. Moreover, nichoid pre-cultured CD34+ edited cells purified from the BM of the mice maintained a higher clonogenic potential upon re-challenging (Figure 21E), and the MLE model showed an almost two-fold increase in the relative number of edited input HSCs required from the 2D condition to reach the engraftment level of 3D pre-cultured cells (Figure 21F).

At this point, we specifically tested the repopulating capacity of long-term edited HSCs by injecting BM-derived CD34+ cells from primary mice into secondary recipients. Thus, we found significantly higher human engraftment in the 3D condition across all the different hematopoietic organs analyzed (Figure 21G,H, Appendix 6L). Strikingly, the nichoid condition showed superior persistence of HDR-edited cells through serial transplantation, with a three- to six-fold increase in the percentage of GFP+ cells compared to the 2D group (Figure 21I,J, Appendix 6M). Finally, while graft composition was similar across conditions (Appendix 6N-P), the relative number of predicted input HSCs required for comparable human chimerism was doubled in the 2D group (Figure 21K), further confirming the results obtained from the primary transplant.

Altogether, nichoids pre-culture represents a valuable strategy for preserving functional stem cells during long-range GE, improving long-term reconstitution of edited HSPCs and increasing the persistence of HDR-edited cells through serial transplantation.

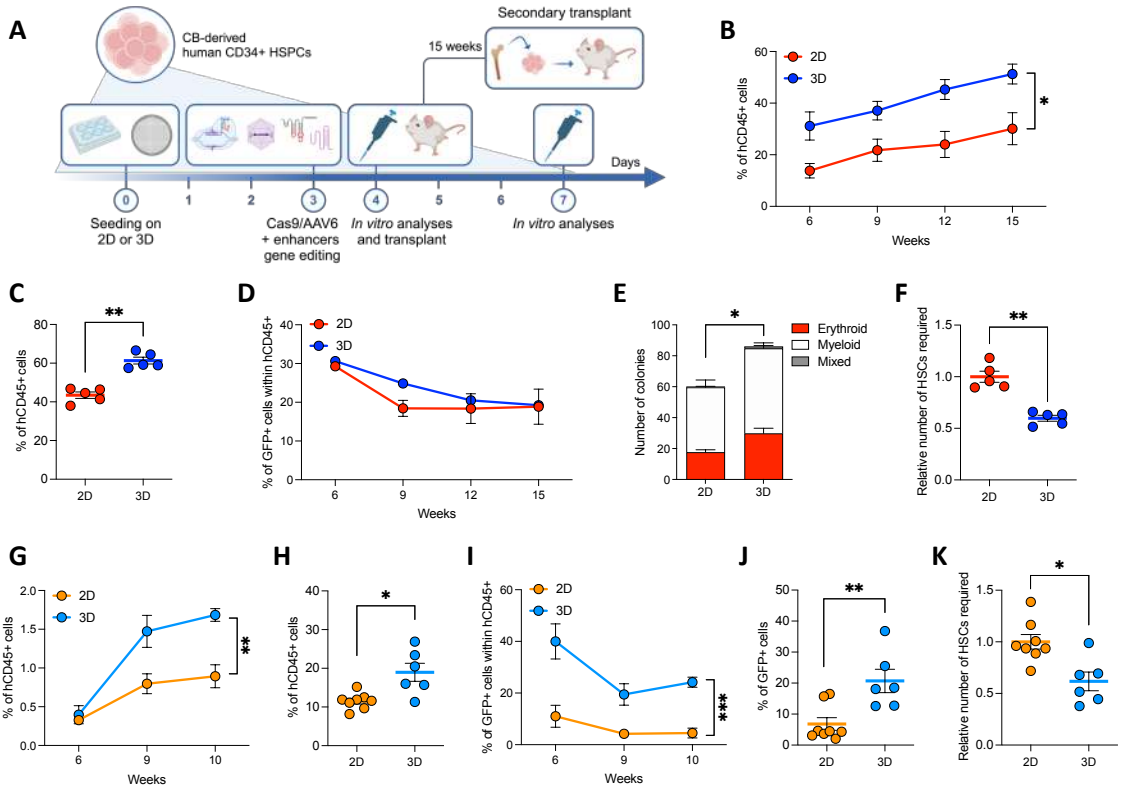


Figure 21. 3D culture enables superior long-term engraftment of HDR-edited HSPCs. *(**A**) Experimental workflow. Human CB-derived HSPCs were seeded on 2D or 3D immediately after thawing and collected on day 3 for Cas9/AAV6 gene editing in the presence of GSE56 and Ad5-E4orf6/7 editing enhancers to insert a GFP reporter within the AAVS1 locus. HSPCs from both the 2D and 3D conditions were seeded in 2D after nucleofection and collected for downstream analyses on days 4 and 7. After 15 weeks post-injection, CD34+ cells were purified from the BM of the mice and transplanted into secondary recipients. (**B,C**) Percentage of hCD45+ cells measured in the PB (**B**) over time and BM (**C**) at the endpoint of transplanted mice (n=5). Mann-Whitney test (calculated at the last time point for PB). (**D**) Percentage of GFP+ cells (within hCD45+ cells) in the PB over time from mice in (**B**) (n=5). (**E**) Number of erythroid, myeloid, and mixed colonies generated by BM-derived CD34+ cells purified from mice in (**C**) (n=5). Mann-Whitney test. (**F**) Relative number of HSCs required to generate comparable engraftment calculated by MLE from (**C**) (n=5). Mann-Whitney test. (**G,H**) Percentage of hCD45+ cells measured in the PB (**G**) over time and BM (**H**) at the endpoint of transplanted secondary recipients (n=8,6). Mann-Whitney test (calculated at the last time point for PB). (**I,J**) Percentage of GFP+ cells (within hCD45+ cells) in the PB (**I**) over time and BM (**J**) from mice in (**G,H**) (n=8,6). Mann-Whitney test (calculated at the last time point for PB). (**K**) Relative number of HSCs required to generate comparable engraftment calculated by MLE from (h) (n=8,6). Mann-Whitney test. Mean ± SEM. *p < 0.05; **p < 0.01.*

Nichoids increase the clonal output of repopulating HSPCs upon LV-mediated gene addition

To date, most market-approved HSPC-GT products and those in advanced stages of clinical development are based on LV-mediated gene addition, which has proven to be an effective strategy to treat primary immunodeficiencies, metabolic disorders, hemoglobinopathies, and BM-failure syndromes (Biffi *et al.*, 2013; Marktel *et al.*,

2019; Río *et al.*, 2019; Kohn *et al.*, 2021; Magnani *et al.*, 2022). Therefore, we asked whether nichoid incorporation into pre-existing gene addition protocols could benefit current GT approaches. Thus, upon a short 24h *ex vivo* pre-stimulation on 2D or 3D, we performed a single-round of LV transduction of mPB-derived CD34+ cells in the presence of PGE2 alone (Zonari *et al.*, 2017; Gentner *et al.*, 2021) or in combination with the transduction-enhancer CsH (Petrillo *et al.*, 2018) to achieve the insertion of a GFP reporter (Figure 22A).

As expected, cell viability was not affected by CsH administration and similar between the two conditions (Appendix 7A). Moreover, while we reported similar fraction of transduced cells across subsets and vector-copy number (VCN) in 2D or 3D, the sole addition of CsH allowed to reach saturating levels of GFP+ cells even at much lower LV MOI (30 with CsH vs. 100 without) (Figure 22B, Appendix 7B,C). Importantly, nichoids improved the erythroid and mixed colony-forming potential of transduced cells compared to 2D culture, and this increase was maintained even in the presence of CsH, which did not affect HSPC clonogenic output *per se* (Figure 22C).

To validate this data in the xenotransplantation setting, we injected equal doses of 2D or 3D cultured CD34+ cells transduced in the presence of CsH and reported higher human chimerism in the PB, BM, and SP of mice from the nichoid group (Figure 22D,E, Appendix 7D). Of note, almost the entire grafts were composed by GFP+ cells (Figure 22F, Appendix 7E,F). Additionally, nichoid culture increased the T cell output in the PB of the mice (Appendix 7G), while the fractions of the various hematopoietic cell types were similar to the 2D counterpart in the BM and SP (Appendix 7H,I). Moreover, BM-derived CD34+ cells from the 3D group maintained a higher clonogenic potential upon further re-challenging in the CFU-C assay (Figure 22G), and the relative number of transduced input HSCs required was drastically reduced in comparison to the 2D condition (Figure 22H), indicating that even a brief period of *ex vivo* culture as short as 36h on nichoids can benefit the functionality of HSPCs in long-term experiments.

To study the efficacy and safety of 3D scaffold implementation into LV-based GT approaches, we monitored the clonal dynamics of engrafting HSPCs by tracking vector genomic integrations through integration site (IS) analyses over time in the human graft (Biffi *et al.*, 2011, 2013). First, we retrieved a high number of unique integrations across the PB, BM, and BM-purified CD34+ cells of both conditions, which were generally more abundant in the 3D group (Appendix 8A). In line with the relatively short half-life of engrafting hematopoietic progenitors, we found only a moderate persistence of PB-repopulating clones across the different time points, with

the highest clonal sharing reported between the BM and BM-derived CD34+ HSPCs (Figure 22I, Appendix 8B). Importantly, no clonal dominance expansion events were reported in any of the engrafted mice (Figure 22I, Appendix 8B). Focusing on the clonal repertoire, we found a higher number of estimated engrafting clones and clonal diversity in the 3D condition (Figure 22J,K), indicating that nichoids increased the fraction of functional HSPCs capable of reconstituting the host hematopoietic system upon transplant. These results were further supported by IS gene frequency analyses, which confirmed no preferential common ISs (CIS) within oncogene or tumor suppressor loci in any of the analyzed mice (Figure 22L, Appendix 9A).

Collectively, our data extend the beneficial properties of nichoid implementation beyond precise GE, increasing the number and diversity of engrafting HSPC clones in LV-mediated gene addition protocols.

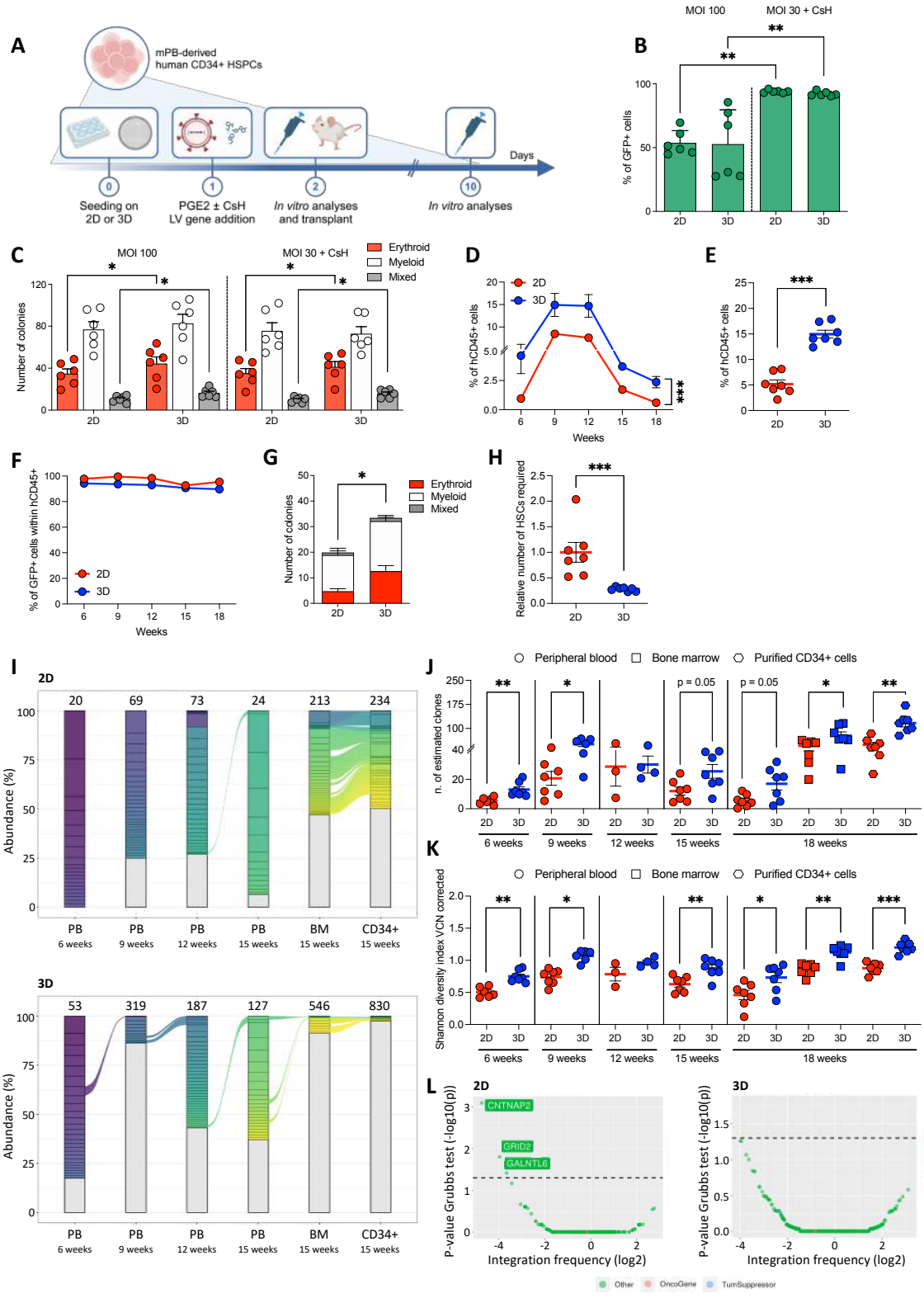


Figure 22. Nichoids increase the clonal output of repopulating HSPCs upon LV-mediated gene addition. *(**A**) Experimental workflow. Human mPB-derived HSPCs were seeded on 2D or 3D immediately after thawing and transduced on day 1 with a GFP-expressing LV vector in the presence of PGE2 alone or in combination with CsH. Specifically, transduction was performed at MOI 100 for PGE2 alone and MOI 30 with CsH. After 14h post-transduction (day 2), HSPCs from both the 2D and 3D conditions were seeded in 2D and collected for*

*downstream analyses on days 2 and 10. Transplantation was performed only for the CsH condition. (**B**) Percentage of GFP+ cells (within CD34+ cells) by FACS analysis on day 10 (n=6). Mann-Whitney test. (**C**) Number of erythroid, myeloid, and mixed colonies generated in CFU-C assay from transduced HSPCs seeded on day 2 (n=6). Wilcoxon test. (**D,E**) Percentage of hCD45+ cells measured in the PB (**D**) over time and BM (**E**) at the endpoint of transplanted mice (n=7). Mann-Whitney test (calculated at the last time point for PB). (**F**) Percentage of GFP+ cells (within hCD45+ cells) in the PB over time from mice in (**D**) (n=7). (**G**) Number of erythroid, myeloid, and mixed colonies generated by BM-derived CD34+ cells purified from mice in (**E**) (n=7). Mann-Whitney test. (**H**) Relative number of HSCs required to generate comparable engraftment calculated by MLE from (**E**) (n=7). Mann-Whitney test. (**I**) Representative plots of tracked ISs and their relative abundance over time from mice of the 2D (top, mouse A4) and 3D (bottom, mouse B12) conditions. Each colored bar univocally identifies an IS with ≥1% representation in at least one time point, with its abundance proportional to the height of the bar; a colored ribbon connects two neighboring time points for each recaptured clone. The total number of unique ISs is reported on top of each bar. (**J,K**) Number of estimated clones (**J**) and clonal population diversity measured by Shannon index normalized on VCN (**K**) from IS analyses. Mann-Whitney test. (**L**) Representative plots of CIS from mice of the 2D (left, mouse A4) and 3D (right, mouse B12) conditions. Each dot represents a gene, which is labeled with the corresponding color if observed as significant. The dashed line is the alpha value 0.05. Grubbs test. Mean ± SEM. *p < 0.05; **p < 0.01; ***p < 0.001.*

3D scaffolds ameliorate the functionality of patient-derived HSPCs for GT applications

Finally, we aimed to validate our findings on the beneficial effects of nichoids in a clinically relevant setting, specifically in a genetic disease for which a GT protocol is already available. To this end, we obtained a small sample of mPB-derived CD34+ cells from two young Wiskott-Aldrich Syndrome (WAS) patients. Thus, we seeded the cells on 2D or 3D and performed two rounds of LV transduction to transfer a functional copy of the human Wiskott-Aldrich syndrome protein (WASP) under the control of a reconstituted WAS promoter using GMP-compliant vectors and reagents, according to the clinically approved protocol under development in our institute (Ferrua *et al.*, 2019; Magnani *et al.*, 2022) (three independent technical replicates were performed for each donor) (Figure 23A). Of note, similar to the clinical manufacturing, HSPCs from the 2D condition cells were seeded upon coating with retronectin.

First, we found comparable percentages of cell viability and phenotypically defined HSPC subsets upon transduction between the two culture systems (Appendix 10A,B). However, the VCN was lower in the nichoid condition (Figure 23B), likely due to the lack of retronectin coating (Figure 23B). Nevertheless, even in a diseased-background setting, transduction on 3D scaffolds increased the mixed-colony output of engineered HSPCs (Figure 23C).

To further corroborate these data, we transplanted equal numbers of 2D or 3D cultured transduced HSPCs into immunocompromised mice. Surprisingly, we found faster human hematopoietic reconstitution of the PB of the mice from the 3D group

(Figure 23D), suggesting that nichoid culture may potentially facilitate a faster hematopoietic recovery of HSPC GT-treated patients. Moreover, while the engraftment in the PB was comparable between the two conditions at the later time points, we found significantly higher human chimerism in both the BM and the SP of the mice from the 3D group (Figure 23E, Appendix 10C). When looking at graft composition, we found a modest expansion of myeloid cells in the PB and CD34+ cells in the BM of mice transplanted with 3D cultured HSPCs, while the composition of the SP was comparable between the two groups (Appendix 10D-F). Finally, although VCN analyses of the human graft are currently still ongoing, the MLE model showed a two-fold decrease in the relative number of input HSCs required from the 3D condition to achieve comparable engraftment levels of the traditional 2D culture (Figure 23N), further confirming the beneficial effects of nichoid incorporation into current HSPC GT protocols even in the setting of diseased background.

In conclusion, our study sheds light on the critical role of 3D cues and mechanical support in preserving stem cell functionality during HSPC *ex vivo* manipulation for multiple clinical scopes. We propose an innovative nano-engineered 3D culture substrate that can be directly implemented into different pre-existing GT protocols, endowing engineered HSPCs with superior long-term and polyclonal repopulating capacity for more effective and safer therapeutic applications.

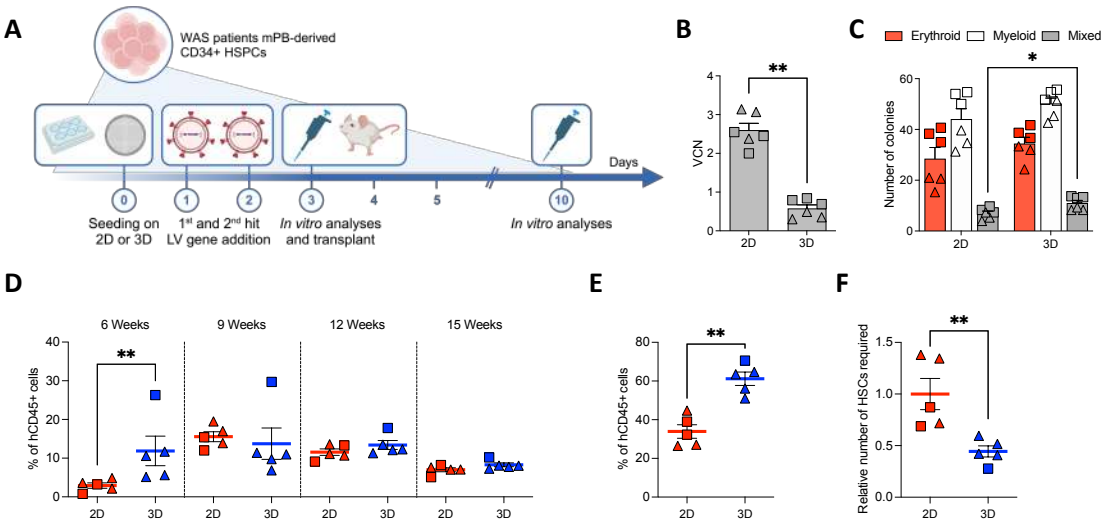


Figure 23. 3D scaffolds ameliorate the functionality of patient-derived HSPCs for GT applications. *(**A**) Experimental workflow. mPB-derived HSPCs from WAS patients were seeded on 2D (upon coating with retronectin) or 3D immediately after thawing and transduced with two hits of WASP-expressing LV on day 1 and 2 at MOI 100. After 14h from the second round of transduction (day 3), HSPCs from both the 2D and 3D conditions were seeded in 2D and collected for downstream analyses on days 3 and 10. Three independent technical replicates were performed for each donor (different symbols identify the two patients). (**B**) VCN of transduced HSPC on day 10 (n=6). (**C**) Number of erythroid, myeloid, and mixed colonies generated in CFU-C assay from transduced HSPCs seeded on day 3 (n=6). Mann-*

*Whitney test. (**D,E**) Percentage of hCD45+ cells measured in the PB (d) over time and BM (e) at the endpoint of transplanted mice (n=5). Mann-Whitney test. (**F**) Relative number of HSCs required to generate comparable engraftment calculated by MLE from (**E**) (n=5). Mann-Whitney test. Mean ± SEM. *p < 0.05; **p < 0.01.*

Discussion

The advent of autologous HSPC-GT has revolutionized the medical field, offering a promising one-time solution for the treatment of multiple immune-hematologic and genetic diseases, as well as enabling potential cross-correction of some non-hematological disorders (Naldini, 2015; Morgan *et al.*, 2017; Ferrari, Thrasher and Aiuti, 2021; Ferrari *et al.*, 2023). Genetic engineering of HSPCs was first achieved through semi-randomly integrating viral vectors, such as gRVs and LVs (Cavazzana-Calvo *et al.*, 2000; Aiuti *et al.*, 2002; Biffi *et al.*, 2013), while nowadays we can induce targeted genetic modifications with up to single-nucleotide resolution thanks to the constant improvements of GE platforms, such as programmable nucleases like CRISPR/Cas9, and base- or prime-editors (Genovese *et al.*, 2014; Zeng *et al.*, 2020; Everette *et al.*, 2023) In current GT protocols, *ex vivo* culture is not only required for activating HSPCs and delivering the editing reagents but also, in some cases, to increase the number of transplantable cells, considering that the average dose for GT products generally consists of 2-30$\times 10^6$ CD34+ cells/kg (Morgan *et al.*, 2017; Canarutto *et al.*, 2021). Thus, alongside the development of more efficient and precise editing tools and enhancers (Petrillo *et al.*, 2018; Ferrari *et al.*, 2020; Fiumara *et al.*, 2023; Baik *et al.*, 2024), significant efforts are spent to constantly advance culture conditions to ensure the maintenance, or potentially the expansion, of HSCs *ex vivo*, such as fine-tuning the supporting cytokine-cocktail, supplementing small molecules like nicotinamide riboside and UM171, and, more recently, introducing only chemically-defined reagents to avoid batch-to-batch variability and diminishing possible contaminants (Fares *et al.*, 2014; Horwitz *et al.*, 2014; Zonari *et al.*, 2017; Rai *et al.*, 2023; Sakurai *et al.*, 2023). Despite these continuous advances, the more primitive HSCs, responsible for the life-long supply of the whole hematopoietic compartment, rapidly lose self-renewal and repopulating potential upon *ex vivo* exposure (Glimm, Oh and Eaves, 2000; Johnson *et al.*, 2024).

To identify molecular determinants causing HSPC functional decline during *ex vivo* culture, we focused on the activation of the p38 MAPK, which has been reported to affect HSPC functionality in different contexts (Ito *et al.*, 2006; Jang and Sharkis, 2007; Tesio *et al.*, 2015; Henry *et al.*, 2020). Distinctively from previous works, we uncover an intricate molecular axis that links p38 MAPK-induced ROS with proliferative stress and HSPC dysfunction with loss of repopulating capacity upon genetic engineering. In accordance with previous works showing that exit from quiescence, MYC activation, and divisional history (Walter *et al.*, 2015; Bernitz *et al.*, 2016; García-Prat *et al.*, 2021) affect HSC self-renewal, we identified excessive

proliferation as a main driver of HSPC dysfunction during *ex vivo* culture. Indeed, we discovered that ROS do not only cause oxidative stress but rather act primarily as mitogenic signals in HSPCs as confirmed by reduced proliferation by p38i and multiple antioxidant treatments. Subsequently, fast cell cycle progression mediates physical DNA breaks accumulation, with activation of the ATR-CHK1 axis, a marker of DNA replication stress. Accordingly, reducing HSPC proliferation by p38i, NAC, and CDK4/6i administration reduced DNA damage accumulation, confirming the detrimental effects of excessive proliferation.

Even if we cannot completely rule out the involvement of p38 MAPK in other aspects of culture adaptation, we believe p38i-induced proliferation slowdown is likely to confer cells more time to resolve DNA lesions before entering the following S-phase and replicate their genome, similarly to murine embryonic stem cells, where delaying G1 progression suppresses ssDNA accumulation (Ahuja 2016). On the same line, excessive proliferation driven by pI:pC *in vivo* administration, which simulates viral infection, modifies DNA replication patterns of murine HSCs toward a PrimPol-mediated faster and discontinuous DNA synthesis, posing a risk to genome integrity and stability (Jacobs *et al.*, 2022). Although further studies should be performed to identify the genomic distribution of proliferation-induced DNA breaks, it is likely that SSBs and DSBs would preferentially occur at highly transcribed regions, potentially determining DNA replication and transcription conflicts, which would result in replication forks stalling and genomic instability. Importantly, proliferation-induced DNA breaks may become hotspots to trap AAV structures (like the inverted terminal repeats (ITR) sequences) during genetic engineering, further raising safety concerns and increasing the genotoxicity risk of genetic engineering (Breton *et al.*, 2020; Ferrari *et al.*, 2022).

While most efforts in precise long-range gene correction have focused on promoting cell cycle progression to increase HDR engagement in the most primitive HSC subset (Lomova *et al.*, 2019; Ferrari *et al.*, 2020), our study shows that fast cell cycle progression may initiate premature exhaustion of edited HSPCs, in agreement with limited rounds of cell division that LT-HSCs can tolerate before exhausting (Wilson *et al.*, 2008; Bernitz *et al.*, 2016). Therefore, cell proliferation should be carefully tuned to avoid HSC dysfunction induced by proliferative stress, particularly in expansion protocols that are currently being developed for HSPC-GT of genetic diseases with limited HSPC harvest and mobilization, for which the number of retrieved CD34+ cells may not be sufficient to formulate the GT drug product (Ferrari, Thrasher and Aiuti, 2021; Ferrari *et al.*, 2023). Nevertheless, it is worth mentioning that in our setting, the more primitive HSCs have just completed one cell division *ex*

vivo and will likely undergo more rounds of replication *in vivo* to repopulate the host bone marrow. Thus, our data may indicate that, by reducing DNA damage accumulation, prolonging cell cycle duration during the first *ex vivo* HSC division may be sufficient to ameliorate the long-term repopulating potential of edited cells by diminishing the proliferative stress imposed by transplantation itself, especially when experiencing a higher DDR burden due to genetic engineering (Piras *et al.*, 2017; Schiroli *et al.*, 2019). Indeed, although the fraction of engrafting HDR-edited cells was comparable upon primary transplant, p38 inhibition favored the persistence of long-term edited HSCs in secondary recipients. Importantly, p38i also increased the number of edited repopulating clones, measured by deep sequencing of the human graft, which has tremendous implications for clinical applications, as an oligoclonal composition of repopulating HSPCs might delay hematopoietic recovery after conditioning, restricting the persistence of corrected HSCs in the long term, and increasing the risk for clonal hematopoiesis with augmented risk of blood disorders and malignancies (Jaiswal and Ebert, 2019).

During our work, we attempted to identify the molecular triggers of p38 MAPK activation upon *ex vivo* exposure. However, while multiple antioxidant combinations prevented the accumulation of mitogenic ROS and dampened the activation of the above-mentioned molecular axis, it was not sufficient to prevent p38 phosphorylation, confirming that ROS are generated downstream of this stress kinase. Similarly, p38 activation was not prevented by removing the cytokines present in conventional HSPC culture media in a one-by-one fashion or culturing HSPCs in a recently developed chemically-defined setting (Sakurai *et al.*, 2023) (data not shown here for simplicity). Therefore, we speculated that p38 MAPK could be triggered by the loss of 3D stimuli and mechanical support ensured by the BM niche. Indeed, among all our attempts, culturing HSPCs in a biocompatible 3D scaffold was the only strategy that reduced p38 MAPK activation.

From this observation, we reasoned that additional detrimental responses may arise from traditional 2D culture conditions, which are unlikely to fully recapitulate all the essential supportive elements of the endogenous HSC niche. Indeed, although the HSPC mechanobiology field is still relatively in its infancy, several studies have demonstrated the critical role of 3D cues and mechanical forces in HSC specification and maintenance under both physiological and *ex vivo* conditions (Adamo *et al.*, 2009; Holst *et al.*, 2010; Altrock *et al.*, 2012; Ni *et al.*, 2019; Zhang *et al.*, 2019; Lundin *et al.*, 2020; Li *et al.*, 2021). In addition, 2D culture could often lead to stem cell dysfunctions by imposing mechanical and osmotic stress, promoting DDR activation, metabolic and epigenetic rewiring, and exhaustion (Kidiyoor *et al.*, 2020;

Rey *et al.*, 2020; Messa *et al.*, 2021). Given these premises, we continued testing an innovative nano-engineered 3D culture substrate with cell-scale resolution called "nichoid" (Nava *et al.*, 2016), which has a relatively simple geometry with a miniaturized lattice architecture organized by the repetition of elementary units of 10-30×15 µm (Ricci *et al.*, 2017). Thus, we investigated how HSPC responded to different culture settings and compared traditional 2D culture conditions with the 3D nichoids.

Intriguingly, the sole addition of a simple geometric scaffold increased the colony output and multi-lineage differentiation of the HSC-enriched fraction up to single-cell resolution *in vitro*, which was then validated in xenotransplantation experiments. Because previous studies in murine and human HSCs pointed out a new concept of early-phase adaptation in culture, according to which the first 24 hours of *ex vivo* culture are crucial for shaping HSC fate specification through profound transcriptional remodeling (Choi and Harley, 2017; Johnson *et al.*, 2024), we investigated whether 3D culture may have different outcomes based on the time windows in which HSPCs are seeded on the scaffold. Surprisingly, we observed increased clonogenic potential only when 3D scaffolds were applied from the very beginning of the *ex vivo* culture, suggesting that the loss of 3D stimuli and interactions with the niche may be responsible for HSPC rewiring early upon *ex vivo* exposure.

Consequently, we interrogated the transcriptional profile of HSPC grown in different culture settings to elucidate the molecular alterations induced by nichoids. Importantly, through transcriptomic analyses, we found a massive rewiring of the gene expression status as a direct consequence of 3D culture, with more than 5000 differentially expressed genes among the two different conditions. GSEA analysis revealed the involvement of pathways related to DNA integrity, metabolism, and cytoskeletal regulators. In particular, we found a downregulation of gene categories belonging to DNA damage, DDR, and DNA repair upon nichoid culture, in accordance with our molecular analyses of physical DNA breaks and yH2AX and pRPA foci. Moreover, nichoids reduced the expression of genes involved in oxidative phosphorylation, protein translation, DNA replication, and proliferation. Therefore, our data suggest a switch in the cellular metabolic profile, particularly in reducing the use of oxidative phosphorylation for energy production. Indeed, it is well-established that, at homeostasis, the most primitive subsets of HSC maintain a dormant state, characterized by low mitochondrial activity and higher glycolysis, minimal presence of ROS, and reduced protein synthesis (Signer *et al.*, 2014; Itkin *et al.*, 2016; Morganti, Cabezas-Wallscheid and Ito, 2022). Altogether, we can speculate that HSPC cultured on nichoids display a slow-cycling and more dormant profile than the

2D counterpart, with reduced metabolic activity and lower energy requirements overall, as suggested by our molecular analyses on cellular proliferation and ROS accumulation. Nevertheless, analysis of mitochondrial respiration and glycolytic rate through the Seahorse assay may validate this hypothesis (Gu *et al.*, 2020). Regardless, even in the context of 3D culture, we reported the link between p38 MAPK activation, mitogenic ROS, proliferation-induced DNA damage, and DDR activation.

On the other hand, HSPCs seeded on nichoids were characterized by an upregulation of genes encoding for proteins of the ECM, adhesion, and cytoskeletal organization. Interestingly, similar results were found in rat mesenchymal stem cells and murine neural precursor cells cultured on nichoids, where whole transcriptomic analyses revealed many DEGs enriched in pathways related to cytoskeleton, ECM, and cell adhesion molecules (Rey *et al.*, 2020; Testa *et al.*, 2023). Indeed, the loss of adhesion molecules is one of the drivers of HSPC dysfunction, responsible for impeding cellular homing into the niche and driving lineage differentiation (Kallinikou *et al.*, 2012; Larochelle *et al.*, 2012). For instance, the expression of integrin α3 (ITGA3) is associated with more primitive and functional HSC (Tomellini *et al.*, 2019). Interestingly, RNA-seq analysis on ITGA3+ cells revealed, other than an enrichment in genes associated with stemness and quiescence, an upregulation of transcripts involved in cell-cell adhesion, ECM organization, Hippo signaling, and actin filament-based movements. Therefore, we could speculate that ITGA3 is involved in the crosstalk between HSPC and the niche, as well as the mechanoperception of external stimuli. These results perfectly overlap with our RNA sequencing analyses, as we found upregulation of *ITGA3* expression in the nichoid condition, together with multiple HSC-related categories.

Since we detected an enrichment in categories related to cytoskeleton organization, we focused on changes in HSPC morphological organization that could be driven by nichoid culture. Indeed, z-stacked confocal immunofluorescence analysis of tubulin revealed that 3D culture endowed HSPC with a smaller and more rounded morphology at both cytoplasmic and nuclei levels. Importantly, HSPC cell size is a determinant of stem cell potential, with HSPC enlarging under stress conditions, including repetitive cell divisions and aging (Lengefeld *et al.*, 2021). Moreover, squashed cellular morphology, as we reported upon prolonged HSPC *ex vivo* culture in standard 2D settings, is associated with higher mechanical forces imposed on cell nuclei (Gonzalez *et al.*, 2018) that can determine chromatin remodeling, DDR activation, and exhaustion (Kidiyoor *et al.*, 2020). Because nichoids are decellularized scaffolds and are not functionalized with ECM proteins, we can

speculate that 3D morphology preservation is solely conferred by the regulation of mechanical forces. Indeed, recent works correlated the alterations in cell morphology with changes in F-actin organization, nuclear membrane permeability, and spatial organization of lamina and chromatin (Donnaloja *et al.*, 2019; Remuzzi *et al.*, 2020; Jacchetti *et al.*, 2021). By studying rat MSC cultured on nichoids or flat substrates, they demonstrated that 3D culture determines a roundish nuclear shape, a reduced nuclear envelope permeability guided by a diminished opening of nuclear pores, with consequent cytoplasmic retention of mechanotransducer transcription factors (such as *YAP* and *MyoD*), regulating different chromatin profiles and gene expression. They correlated these effects to a reduction in intracellular force transmission in cells grown on nichoids, meaning that 3D culture preserves cells from culture-mediated mechanical stress. These data are coherent with our observations with human HSPC, thus suggesting a conserved mechanism across cell types and species. We envisage investigating other components of the nucleo/cytoskeleton, such as F-actin and lamin A/C, and the localization of mechano-regulated transcription factors as a readout of nuclear permeability. Overall, this could add another piece of information about the influence of 3D scaffolds on diminishing mechanical force transmission imposed by *ex vivo* culture, facilitating the preservation of HSPC biomechanical properties and identity.

Additionally, our imaging analyses revealed that 2D culture caused significant alterations in tubulin spatial organization, while nichoids prevented the loss of tubulin polarity. The implications of cytoskeletal remodeling, with a focus on microtubule architecture, have been previously investigated in the context of aged and young murine HSC (Florian *et al.*, 2012, 2020; Mejia-Ramirez and Florian, 2020). These works introduced the concept of cellular polarity as an HSPC fitness determinant, focusing on the localization of tubulin, the Rho GTPase CDC42, and the histone H4K16ac. Indeed, elevated activity of CDC42 in aged HSC was causally linked to HSC aging and correlated with a loss of tubulin polarity and reduction of H4K16ac, while pharmacological inhibition of CDC42 activity functionally rejuvenated aged HSC by increasing the percentage of polarized cells and restoring the levels and spatial distribution of H4K16ac. Moreover, this concept was further extended by studies on osteopontin, *WNT*, and *Yap/Taz* signaling (Florian *et al.*, 2013; Guidi *et al.*, 2017; Kandi *et al.*, 2021), which correlated the aging process with a progressive loss of cell polarity that ultimately leads to the functional deterioration of stem cells. Importantly, together with tubulin remodeling, nichoids decreased the expression of *CDC42*, upregulating *WNT* and *Yap/Taz* signaling upon *ex vivo* culture, further extending our molecular findings. Hence, we could speculate that 3D culture can

preserve a young-like and more functional phenotype in HSPCs, and it would be interesting to characterize the spatial organization of these proteins in our context. Furthermore, in murine hematopoiesis, molecules that control HSC polarity have been shown to act as modulators of stem cell division through the regulation of open chromatin inheritance. Indeed, through single-cell ATAC-seq, it was discovered that aged non-polar HSCs undergo self-renewing symmetric divisions, while young polar HSCs undergo preferentially asymmetric divisions (Florian *et al.*, 2018). Notably, the number of HSCs increases upon aging while their regenerative potential decreases (Chambers *et al.*, 2007; Pang, Schrier and Weissman, 2017). According to these observations, asymmetric cell division may act as a protective mechanism against cell exhaustion. Therefore, it would be interesting to investigate the modality of cell division in our context and determine if human HSPC grown on nichoids tend to divide asymmetrically. Indeed, there is growing interest in the field of human hematopoiesis in understanding the mechanisms interfering with the spatial localization and polarity of different factors and their implications in driving cellular stemness, aging, and pathology. Thus, we plan to expand our study to integrate how mechanoregulation influences subcellular spatial organization, building up novel valuable knowledge on HSPC biology.

Alongside ameliorating HSPC functionality upon *ex vivo* manipulation, nichoid culture supported efficient genetic engineering of HSPCs in multiple GT strategies, including Cas9/AAV6, BE, and PE gene correction and LV-mediated gene addition. Most importantly, nichoid pre-cultured engineered cells showed higher and increased persistence upon long-term xenotransplantation experiments in secondary recipients, further confirming the importance of 3D interactions and mechanical support during the *ex vivo* culture step required for HSPC-GT applications. Moreover, IS analyses revealed higher clonal output and diversity in the 3D condition, with no signs of pre-malignant clonal expansion, indicating superior preservation of HSPCs capable of engrafting and reconstituting the hematopoietic system upon reinfusion post-genetic engineering. These data have terrific implications for clinical translation, as the introduction of 3D scaffolds into pre-existing GT protocols may increase the quality of engineered cells, facilitating fast hematopoietic reconstitution upon transplant and broadening the clonal repertoire of repopulating stem cells for more effective and safer therapeutic scopes (Masiuk *et al.*, 2017; Ferrari *et al.*, 2020, 2023; Tucci *et al.*, 2021). While the effects of 3D culture may be different across different genetic-diseased backgrounds, we showed that nichoid ameliorated the engraftment of WAS patient-derived HSPCs treated according to the clinically approved protocol under development in our institute. Indeed, it would be interesting to exploit nichoids

to culture HSPCs from BM-failure syndromes, in which HSPCs are progressively lost during *ex vivo* culture, such as Dyskeratosis Congenita and Fanconi anemia (Siegner *et al.*, 2022; Savage and Niewisch, 2023).

Additionally, although we found a general reduction of DNA damage upon 3D culture, a specific assessment of genotoxic events associated with genetic engineering should be performed before moving to clinical transition. Indeed, whether or not nichoids could impact on on- and off-target events, large deletions, chromosomal rearrangements, and chromothripsis remains to be elucidated (Kosicki, Tomberg and Bradley, 2018; Leibowitz *et al.*, 2021; Turchiano *et al.*, 2021; Cullot *et al.*, 2023). Moreover, GT protocols currently exploit cell-culture bags to manipulate and expand patient-derived HSPCs. While we performed our experiments using standard cell culture wells due to the research scale capability of our study (as at least 10 million cells are required to be seeded in culture bags), plastic bags likely present the same limitations linked to 2D culture systems (Congrains *et al.*, 2021). Indeed, our preliminary experiments on a side-by-side comparison between culture bags and nichoids showed enhanced *in vitro* functionality of 3D cultured HSPCs, even when compared to clinical standards for cell culture (data not shown). Additionally, it will be interesting to compare the nichoid substrate with other 3D scaffolds fabricated, such as hydrogels and other polymer-based scaffolds (Bai *et al.*, 2019; Rubio-Lara *et al.*, 2023).

It is worth mentioning that nichoids currently have a few limitations, including their fragility, cell recovery (as we can recover around 70-80% of all the cells enclosed in the scaffold), and scale-up feasibility of their fabrication. Indeed, despite continuous technological improvements in two-photon polymerization, manufacturing of synthetic nichoids is still time-consuming. Indeed, it takes approximately 40 minutes to fabricate a complete nichoid structure, and some nichoids do not pass quality control due to production faults (Ricci *et al.*, 2017). Thus, the industrial scale-up is challenging, particularly considering the large number of nichoids that would be required to meet clinical demands of $2\text{-}30\times10^6$ CD34+ cells/kg. However, challenging mainstream efforts to scale up the GT process by expanding the number of genetically engineered HSPC *ex vivo* prior to transplantation, we could potentially envision a revolutionary approach based on scale-down. Indeed, because engineered HSPCs cultured on nichoids show enhanced long-term hematopoietic reconstitution and clonal output upon transplant, we may think of infusing a reduced number of cells to achieve successful engraftment of gene-corrected cells, with potential astonishing implications for reducing the cost of HSPC-GT. As of today, these advanced therapies are priced in the millions (Tucci *et al.*, 2021), with a single-

patient dose costing between 600,000-3,000,000 $, significantly impeding accessibility. These costs encompass extensive research and development, manufacturing expenses for viral vectors, genome editing tools, clinical-grade materials, HSPC isolation and expansion, and clinical trial expenditures. Due to these extremely high costs, novel therapies may be withdrawn from consideration or face delays in market approval due to the inability to overcome manufacturing bottlenecks, particularly those that hinder the production process. Consequently, lowering cell doses by ameliorating HSPC functionality by culture on nichoids may significantly reduce the manufacturing price of the ultimate GT drug product. Whether the feasibility of this revolutionary approach would allow reaching comparable results to current standards remains to be proven, and we plan to perform limiting dilution assays in xenotransplantation experiments to get a first preliminary assessment of its feasibility.

In conclusion, this study deepens our understanding of the molecular determinants causing functional decline of human HSPCs upon *ex vivo* culture required for GT approaches. We uncover that p38 MAPK activation, likely triggered by the absence of 3D constraints and mechanical support in traditional 2D cultures, promotes the generation of mitogenic ROS that fuel fast cell cycle progression, causing proliferative stress with accumulation of physical DNA damage and consequent activation of the DDR. In addition, we found that 3D scaffolds better preserve HPSC functional properties by profoundly reshaping their transcriptional profile, mitigating endogenous DNA damage accumulation, and preventing HSPC deformation and squashing, conserving nuclei morphology and tubulin polarity. We proposed innovative strategies like p38 inhibition and integration of the nichoid culture substrate to mitigate *ex vivo* culture-induced detrimental responses in GT protocols, endowing genetically engineered HSCs with superior long-term hematopoietic reconstitution and polyclonal output for more effective and safer therapeutic scopes.

Materials and methods

Cell cultures

Cord blood-derived CD34+ HSPCs: Cells were either freshly purified from human CB after obtaining informed consent and upon approval by the San Raffaele Hospital ethical committee or purchased frozen from Lonza or StemExpress. After thawing, HSPCs were seeded at the concentration of $5x10^5$ cells/ml in serum-free StemSpan SFEM medium (StemCell Technologies) supplemented with 2mM L-glutamine and Penicillin-Streptomycin (100IU/ml penicillin, 100mg/ml streptomycin), 1μM SR-1 (Biovision), 50nM UM171 (STEMCell Technologies), and recombinant human cytokines (100ng/ml SCF, 100ng/ml Flt3-L, 20ng/ml TPO, and 20ng/ml IL-6; Peprotech). 10μM 16,16-Dimethyl Prostaglandin E2 (Cayman) was added only at thawing.

Mobilized peripheral blood-derived CD34+ HSPCs: Cells were purified in-house with the CliniMACS CD34 Reagent System (Miltenyi Biotec) from Mobilized Leukopak (AllCells, mobilized with G-CSF or G-CSF+Plerixafor) according to the TIGET-HPCT protocol approved by OSR Ethical Committee and following the manufacturer's instructions. After thawing, HSPCs were seeded at the concentration of $5x10^5$ cells/ml in serum-free StemSpan SFEM medium (StemCell Technologies) supplemented with 2mM L-glutamine and Penicillin-Streptomycin (100IU/ml penicillin, 100mg/ml streptomycin), 1μM SR-1(Biovision), 35nM UM17 (STEMCell Technologies), and recombinant human cytokines (300ng/ml SCF, 300ng/ml Flt3-L, and 100ng/ml TPO; Peprotech). 10μM 16,16-Dimethyl Prostaglandin E2 (Cayman) was added only at thawing only for base- and prime-editing.

Wiskott-Aldrich Syndrome-derived CD34+ HSPCs: Cells were purified with human CD34 MicroBead Kit (Miltenyi Biotec) from a small volume (1-5ml) of G-CSF+Plerixafor leukapheresis from patients undergoing gene therapy in the Pediatric immunohematology unit in the San Raffaele Hospital after obtaining informed consent and upon approval by the San Raffaele Hospital ethical committee. After thawing, HSPCs were seeded at the concentration of $5x10^5$ cells/ml in SCGM medium (CellGenix/Sartorius) supplemented with Penicillin-Streptomycin (100IU/ml penicillin, 100mg/ml streptomycin) and recombinant human cytokines (100ng/ml TPO, 60ng/ml IL3, 300ng/ml SCF, and 300ng/ml FLT3L; CellGenix/Sartorius). Only for the 2D condition, coating with retronectin (Takara) was performed according to the manufacturer's instructions. GMP-grade reagents were provided by Erika Zonari (Marina Radrizzani's group, SR-TIGET).

All cells were cultured in a 5% CO_2 humidified atmosphere at 37°C.

Where indicated, on day 1 and day 2 post-thawing, HSPCs were treated with 4μM p38 inhibitor (SB-203580; Sigma-Aldrich), 2mM NAC (A9165; Sigma-Aldrich) 10μM Resveratrol (A9165; Sigma-Aldrich), 300μM Tempol (SRT501, 4-Hydroxy-TEMPO; MedChemExpress), or the combination of the three. 2μM CDK4/6 inhibitor (Palbociclib-PD0332991, Selleck Chemicals) treatment was performed for 24h on day 1 before washing out. For all treatments, negative control was obtained treating cells with the same volume of DMSO or DPBS vehicle.

Nichoids fabrication

Nichoids were fabricated by Claudio Conci (Manuela Raimondi, Politecnico di Milano) as previously described (Ricci *et al.,* 2017).

Genetic engineering

Cas9/AAV6: After three days of *ex vivo* culture, cells were nucleofected with 2.5-1.25μM of RNPs and electroporation enhancer (Integrated DNA Technologies) according to manufacturer's instructions using P3 Primary Cell 4D-Nucleofector X Kit and program EO-100 (Lonza). RNPs were assembled by incubating for 10 min at room temperature at 1:1.5 molar ratio S.p. Cas9 protein (Aldevron) with synthetic gRNAs (Integrated DNA Technologies) targeting *AAVS1* locus (Schiroli *et al.,* 2019). Transduction with AAV6 (purchased from AAV vector core, TIGEM) was performed at a dose of $1x10^4$ vg/cell after electroporation. The design of AAV6 donor templates encoding for a PGK.GFP reporter cassette with homologies for the *AAVS1* locus was previously reported (Schiroli *et al.,* 2019). BAR-coded AAV6 and GSE56-Ad5-E4orf6/7 mRNA were provided by Samuele Ferrari (Luigi Naldini's group, SR-TIGET) (Ferrari *et al.,* 2020). Editing efficiency was assessed by FACS analyses.

Base-editing: After three days of *ex vivo* culture, cells were nucleofected with 75pmol of synthetic gRNA (Synthego) targeting the exon 1 of *B2M* and 3.5μg of ABE8.20-m optimized RNA (provided by Martina Fiumara, Luigi Naldini's group, SR-TIGET) according to manufacturer's instructions using P3 Primary Cell 4D-Nucleofector X Kit and program EO-100 (Lonza) (Fiumara *et al.,* 2023). Editing efficiency was assessed by FACS analyses using anti-human B2M FITC (BioLegend).

Prime-editing: After three days of *ex vivo* culture, cells were nucleofected with 186 pmol of *B2M* pegRNA (Integrated DNA Technologies), 75pmol of synthetic gRNA (Synthego) targeting the exon 1 of *B2M* and 7.5μg of PEmax optimized mRNA (provided by Martina Fiumara, Luigi Naldini's group, SR-TIGET) according to

manufacturer's instructions using P3 Primary Cell 4D-Nucleofector X Kit and program EO-100 (Lonza) (Fiumara *et al.,* 2023). Editing efficiency was assessed by FACS analyses using anti-human B2M FITC (BioLegend).

Lentiviral gene addition: According to the experimental design described in the main text, cells were transduced for 14h with third-generation self-inactivating lentiviruses encoding for a PGK.GFP reporter cassette (Zonari *et al.,* 2017) or WASP under the control of a reconstituted WAS promoter (two rounds of transduction; GMP-grade vector, provided by Milena Perrone, Marina Radrizzani's group, SR-TIGET) (Ferrua *et al.*, 2019; Magnani *et al.*, 2022). 10μM 16,16-Dimethyl Prostaglandin E2 (Cayman) was added 2h prior to transduction. 8μM Cyclosporine H (Sigma-Aldrich) was added together with PGE2. Gene transfer efficiency was assessed by VCN analysis.

Functional assays

Colony-forming unit cell assay

CFU-C assay was performed by plating 800 cells in methylcellulose-based medium (MethoCult H4434, StemCell Technologies) supplemented with Penicillin-Streptomycin (100IU/ml penicillin, 100mg/ml streptomycin). Three technical replicates were performed for each sample, and the mean value was plotted and used for statistical analysis. Two weeks after plating, colonies were counted in a blinded fashion. Erythroid, myeloid, and mixed colonies were identified according to morphological criteria.

Myeloid-Erythroid-Megakaryocyte (MEM) single-cell differentiation assay

$CD34^+CD133^+CD45RA^-CD90^+$ population (negative to ZombieAqua viable dye) was sorted as single cells (1 cell/well) and seeded in U-bottom 96-well filled with 100 μl/well MEM cytokine medium (Belluschi *et al.*, 2018): StemPro medium with nutrients supplement (Life Technologies) supplemented with 2mM L-glutamine and Penicillin-Streptomycin (100IU/ml penicillin, 100mg/ml streptomycin), recombinant human cytokines (100ng/ml SCF, 20ng/ml Flt3-L, 100ng/ml TPO, 50ng/ml IL-6, 10ng/ml IL-3, 50ng/ml IL-11, 20ng/ml GM-CSF, 10ng/ml IL-2, 20ng/ml IL-7; Miltenyi Biotec), 3UI/ml erythropoietin (Eprex, Janssen-Cilag), and 50ng/ml h-LDL (Stem Cell Technologies). Cell sorting was performed with BD FACSAria Fusion (BD Biosciences); cells were sorted with a 100 mm nozzle.

Xenotransplantation studies

NSG and NBSGW mice were purchased from The Jackson Laboratory and maintained in specific-pathogen-free conditions. The procedures involving animals were designed and performed with the approval of the Animal Care and Use Committee of the San Raffaele Hospital and communicated to the Ministry of Health and local authorities according to Italian law (IACUC #1385). For transplantation of non-genetically manipulated HSPCs, $1x10^5$ CB-derived CD34+ cells were injected intravenously into NBSGW mice. For transplantation of Cas9/AAV6-edited HSPCs, $2x10^5$ CB-derived CD34+ cells were injected intravenously into NSG mice after sub-lethal irradiation (150-180 cGy). For transplantation of Cas9/AAV6 + GSE56 and Ad5-E4orf6/7 edited HSPCs, $5x10^5$ CB-derived CD34+ cells were injected intravenously into NSG mice after sub-lethal irradiation (150-180 cGy). For transplantation of LV-transduced HSPCs, $4x10^5$ mPB-derived CD34+ cells were injected intravenously into NSG mice after sub-lethal irradiation (150-180 cGy). For transplantation of WAS patient-derived HSPCs, $4\text{-}5x10^5$ cells (depending on donor) were injected intravenously into NSG mice after sub-lethal irradiation (150-180 cGy).

For secondary transplants of Cas9/AAV6 + GSE56 and Ad5-E4orf6/7 edited HSPCs, $1x10^6$ CD34+ cells purified from the BM of primary recipients were pooled according to the experimental group and injected intravenously into NSG mice after sub-lethal irradiation (150-180 cGy).

Mice sample size was determined by the total number of available cells. Mice were attributed to each experimental group randomly. Human engraftment and the presence of engineered cells were monitored through FACS analyses by serial collection of blood from the mouse tail and bone marrow and spleen (at endpoint).

Flow cytometry

Immunophenotypic and apoptosis analysis

For immunophenotypic analyses of *ex vivo* cultured HSPCs, $3\text{-}10x10^4$ cells were washed with 2% FBS in DPBS and stained with the following fluorescent-labeled antibodies (1:100 dilution, each) for 15 min at 4°C: anti-human CD34 PE (Miltenyi Biotec), anti-human CD133 PE-Vio 770 (Miltenyi Biotec), and anti-human CD90 APC (BD Biosciences). Cells were washed in 2% FBS in DPBS. Where indicated, immunophenotypic staining was combined with Annexin V (BioLegend) and 7-amino-actinomycin D (7-AAD) (BioLegend) viability staining according to the manufacturer's instructions (3 and 1µl *per* sample, respectively).

For immunophenotypic analyses of cells retrieved from *in vivo* organs, blood samples and purified cells were washed with 2% FBS in DPS and incubated with anti-human and anti-mouse FcR Blocking (1:100 and 1:200 dilution, respectively; Miltenyi Biotec) for 10 min at room temperature. Then, cells were stained with combinations of the following fluorescent-labeled antibodies (1:100 dilution, each) for 15 min at 4°C: anti-human CD45 APC-eFluor 780 (Invitrogen), anti-human CD19 BV510 (BD Biosciences), anti-human CD13 BV421 (BD Biosciences), anti-human CD33 PE-Cy7 (BD Biosciences), anti-human CD3 PE (BioLegend), anti-human CD8 APC (BioLegend), and anti-human CD34 PE-Cy7 (BD Biosciences). Cells were washed in 2% FBS in DPBS. 7-AAD was employed as viability staining.

Sample acquisition was performed with FACSCanto II (BD Biosciences). Single-stained and Fluorescence Minus One (FMO) stained cells were used as controls and SPHERO™ Rainbow Calibration Particles (Spherotech) were used to perform instrument calibration. Data were analyzed using the FlowJo software.

MEM single-cell differentiation assay analysis

All single-cell-derived colonies were stained directly into 96 U-bottom plates. Cells were washed with 100 µl/well 2% FBS in DPBS and then stained with 50 µl/well of the following antibody mix: anti-human CD45-PECy7 (1:300; BioLegend), anti-human CD11b-PE (1:500; BioLegend), anti-human CD41-PECy5 (1:200; BioLegend), anti-human GlyA-APC (1:1000; BD Biosciences), anti-human CD14-APCCy7 (1:500; BioLegend), anti-human CD56-BV421 (1:200; BioLegend), and anti-human CD15-BV510 (1:1000; BioLegend) for 20 min at room temperature and then washed with 100 µl/well 2% FBS in DPBS + 2% FBS. Samples acquisition was performed by high-throughput flow cytometry with FACSCanto II (BD Biosciences). Colonies were considered only if containing ≥ 30 cells.

Proliferation analysis with CellTrace Violet

Immediately after thawing, HSPCs were stained with Cell Trace Violet (Thermo Fisher Scientific) following the manufacturer's instructions. Cells were resuspended in DPBS at a concentration of $1x10^6$/mL and 1µL of Cell Trace solution was added per each mL of cell suspension for a final concentration of 5µM. Cells were incubated for 20 min in the incubator at 37°C and then for 5 min with five times the original staining volume of 2% FBS in DPBS. After centrifugation, cells were resuspended in the appropriate culture medium volume. After at least 30 min, samples were acquired with FACSCanto II (BD Biosciences) to check the effectiveness of the staining.

Proliferation analyses were subsequently performed on day 7.Data were analyzed using the FlowJo software using the Proliferation Kinetics tool.

CM-H_2DCFDA

CM-H_2DCFDA (Thermo Fisher Scientific) was dissolved in DMSO according to the manufacturer's instructions. 3-10x10^4 cells were washed and resuspended in pre-warmed DPBS and incubated with 10µM CM-H_2DCFDA for 30 min in the incubator at 37°C. Then, cells were centrifuged and resuspended in pre-warmed 2% FBS in DPBS. Samples were immediately acquired with FACSCanto II (BD Biosciences). Data were analyzed using the FlowJo software.

MitoSOX and CellROX staining

MitoSOX or CellRox (Thermo Fisher Scientific) were dissolved or pre-diluted in DMSO according to the manufacturer's instructions. 5µM MitoSOX or 1µM CellROX were directly added to the cell culture (3-10x10^4 cells). Cells were incubated for 10 and 40 min, respectively, in the incubator at 37°C. After washing in 2% FBS in DPBS, Samples were immediately acquired with FACSCanto II (BD Biosciences). Data were analyzed using the FlowJo software.

8-oxo-2'-deoxyguanosine staining

3-10x10^4 cells were washed with 2% FBS in DPBS and fixed with 4% paraformaldehyde (Santa Cruz Biotechnology) at room temperature for 15 min. Cells were washed again and denatured with 100 µL of HCl (2N) for 20 min at room temperature. After washing with 2% FBS in DPBS, cells were permeabilized with 800µL of 1X Intracellular Staining Permeabilization Wash Buffer (BioLegend) for 20 min at room temperature. Then, cells were washed with 2% FBS in DPBS and stained with 8-oxo-2'-deoxyguanosine Antibody (1:250 dilution) (Trevigen) at 4°C overnight. After washing with 2% FBS in DPBS, samples were stained with anti-mouse secondary antibody Alexa Fluor 488 (1:1000 dilution) (Thermo Fisher Scientific) for 45 min at room temperature. Cells were washed with 2% FBS in DPBS and sample acquisition was performed with FACSCanto II (BD Biosciences). Data were analyzed using the FlowJo software.

Phospho-p38 staining

3-10x10^4 cells were washed with 2% FBS in DPBS, eventually stained with surface markers, and fixed with 4% paraformaldehyde (Santa Cruz Biotechnology) at room temperature for 15 min. Cells were washed again with 2% FBS in DPBS and permeabilized with 100µL of 1X Click-iT saponin-based permeabilization at room temperature for 15 min. Then, cells were stained with phospho-p38 MAPK antibody (1:100 dilution) (pThr180/pTyr182; Cell Signalling) at 4°C overnight. After washing with 2% FBS in DPBS, samples were stained with anti-rabbit secondary antibodies (1:1000 dilution) (Alexa Fluor 488 or Alexa Fluor 647; Thermo Fisher Scientific) for 45 min at room temperature. After washing with 2% FBS in DPBS, sample acquisition was performed with FACSCanto II (BD Biosciences) and the collected data were analyzed using the FlowJo software.

Cell cycle analysis

Cell cycle analysis were performed by Click-iT EdU Alexa Fluor PacifiBlue Imaging Kit (Thermo-Fisher Scientific) and Hoechst (Thermo Fisher Scientific) staining. 3-10x10^4 cells were treated with 2µM 5-ethynyl-2'-deoxyuridine (EdU) for 4 hours in culture. Then, cells were washed with 2% FBS in DPBS and fixed with 100µL of Click-iT fixative for 15 min at room temperature. Cells were washed again and permeabilized with 100µL of 1X Click-iT saponin-based permeabilization for 15 min at room temperature. EdU was marked by incubating cells with 500µl of Click-iT Plus reaction cocktail for 30 min at room temperature. Finally, cells were washed and stained with DNA with 2µM Hoechst overnight at 4°C. After the incubation, sample acquisition was performed with FACSymphony A5 SORP (BD Biosciences). Data were analyzed using the FlowJo software.

Immunofluorescence analysis

For the analyses of γH2AX and pRPA DDR sensors: multitest slides (MP Biomedicals) were treated with Poly-L-lysine solution (Sigma-Aldrich) at 1mg/ml concentration for 20 min at room temperature. After two washes with DPBS solution, approximately 3-10x10^4 cells were seeded on covers for 20 min and fixed with 4% paraformaldehyde (Santa Cruz Biotechnology) for another 20 min. After washing, cells were then permeabilized with 0.3% Triton X100 for 15 min at room temperature. After blocking with 0.5% BSA and 0.2% fish gelatin in DPBS fro 30 min, cells were probed with anti-phospho Histone H2A.X (1:200 dilution; Ser139, clone JBW301; Merk) and phospho-RPA32 (1:200 dilution; S33; Bethyl Laboratories). for 1h at room temperature. After primary antibodies incubation, cells were washed three times with

DPBS and incubated with Alexa 488-, 568- and/or 647-labeled secondary antibodies (1:1000 dilution) for 45 min at room temperature (Thermo Fisher Scientific). Nuclear DNA was stained with 0.2mg/ml DAPI (Sigma-Aldrich) and covers were mounted with Aqua-Poly/Mount solution (Polysciences. Inc.) on glass slides (Bio-Optica). Fluorescent images were acquired using Leica SP5 Confocal microscope. Foci quantification was performed with the ImageJ software.

For the analysis of HSPC morphology and tubulin distribution: cells were fixed directly on nichoids or coverglasses (Bio-Optica) on day 7 of *ex vivo* culture with with 4% paraformaldehyde (Santa Cruz Biotechnology) for 20 min at room temperature. After washing, cells were then permeabilized with 0.3% Triton X100 for 15 min at room temperature. After blocking with 0.5% BSA and 0.2% fish gelatin in DPBS fro 30 min, cells were probed with anti-alpha tubulin (1:200 dilution; Abcam) for 1h at room temperature. After primary antibodies incubation, cells were washed three times with DPBS and incubated with Alexa 488-labeled secondary antibodies (1:1000 dilution) for 45 min at room temperature (Thermo Fisher Scientific). Nuclear DNA was stained with 0.2mg/ml DAPI (Sigma-Aldrich) and covers were mounted with Aqua-Poly/Mount solution (Polysciences. Inc.) on glass slides (Bio-Optica). Fluorescent images were acquired using a Nikon Confocal microscope. Z-stacked images were analyzed with the ImageJ and Arivis Vision4D with the help of Valeria Berno (ALEMBIC, San Raffaele Hospital).

Comet assay

HSPCs were suspended at 1 x 10^5 cells/ml in ice-cold DPBS and mixed with molten Comet LMAgarose (Trevigen, MD) at a ratio of 1:10 (v/v) and immediately pipetted onto CometSlides (Trevigen, MD) and placed for 30 min at 4°C. Once solidified, slides were immersed in pre-chilled Lysis Solution (Trevigen, MD) for 1 hour at 4°C. Following lysis, slides were immersed in freshly prepared Alkaline Unwinding Solution pH > 13 (300 mM NaOH, 1mM EDTA) for 1 hour at 4°C and then electrophoresed in Alkaline Electrophoresis Solution pH > 13 (300 mM NaOH, 1mM EDTA) at 300 mA for 40 min. Slides were washed twice in ddH2O and fixed with 70% ethanol for 5 min. Comets were stained with SYBR Safe (Invitrogen) for 30 min at room temperature. All steps were conducted in the dark to prevent additional DNA damage. Comets were analyzed using a Nikon Eclipse E600 microscope and a Nikon-DS-RI2 camera. Quantification of the Olive Tail Moment of individual nuclei was performed with the CaspLab software.

Western Blot

Cells were washed twice with cold DPBS and lysed for 30 min on ice with RIPA buffer containing 50 mM Tris–HCl pH 8.0, 150 mM NaCl, 1% (v/v) NP-40, 0.5% (w/v) Sodium Deoxycholate, 1 mM EDTA, 0.1% (w/v) SDS, 0.01% (w/v) Sodium azide pH 7.4, and Pierce protease and phosphatase minitablets inhibitors (Thermo Fisher Scientific). Cells were centrifuged at 13,000 rpm for 10 min at 4°C and the supernatants were quantified for protein content with Pierce's BCA protein assay kit (Thermo Fisher Scientific), according to manufacturer's instructions. The extracted proteins were resolved by SDS–PAGE before transfer onto nitrocellulose membrane (Sigma-Aldrich), followed by overnight incubation at 4°C with phospho-ATR (Ser428) (Cell Signalling, 2853, 1:250 dilution), phospho-CHK1 (Ser 345) (Cell Signalling, 2341, 1:500 dilution), phospho-MAPKAPK-2 (Thr334) (Cell Signalling, 3007, 1:500 dilution), MAPKAPK-2 (Cell Signalling, 3042, 1:1000 dilution), and Histone 3 (Abcam, AB1791, 1:1000 dilution) primary antibodies. Finally, membranes were incubated for 1h at room temperature with an anti-rabbit or anti-mouse HRP-linked secondary antibodies (Thermo Fisher Scientific, 1:3000 and 1:2000 dilution, respectively) and signals were detected using ECL Western blotting substrate (Thermo Fisher Scientific) following the recommendations of the manufacturer's instructions. Images were acquired on a ChemiDoc imager (BioRad). Images were analyzed with the ImageLab (BioRad) software.

Live imaging analysis of confluency

IncuCyte (Essen Biosciences) was used to quantify confluency in live cells for 4 days. 30.000 cells of each condition were plated in a 96-multiwell placed in an incubator to maintain standard cell culture conditions (5% CO_2 humidified atmosphere at 37°C) and images were acquired each 15'. The confluence processing analysis tool (IncuCyte Software S3 v2018A) calculated confluency for each sample. Quantification of the cellular confluence of each condition was assessed by calculating fold change to the first time point.

Relative number of HSCs by maximum likelihood estimation

The number of HSCs required for a specific extent of engraftment is calculated by the maximum likelihood estimation method (MLE) using the following formula: HSCrequired = -log(1 - fraction_stem_cells) * total_cells_transplanted / mean(log(1-donor_chimerism)), where the fraction of stem cell frequency here is assumed to be 0.005 across all groups. This number was then reported as a relative value to the

average of the 2D condition. While not providing a precise estimate of the number of HSCs in a mixed and heterogeneous population, as can be achieved with limiting dilution analyses, this approach estimates how many HSCs are required to achieve a specified level of engraftment.

BAR-Seq and Indels-based clonal tracking

Library preparation was performed by Samuele Ferrari (Luigi Naldini's group, SR-TIGET) as previously described (Ferrari *et al.,* 2020) and sequenced in the Genomic Facility of San Raffaele Hospital. Sequencing data were analyzed by Stefano Beretta (Luigi Naldini's group, SR-TIGET).

RNA sequencing analysis

RNA extraction was performed with RNeasy Plus Micro Kit (QIAGEN) following the manufacturer's instructions. RNA samples were quantified with Qubit RNA HS Assay Kit (Thermo Fischer Scientific) and sequenced by GENEWIZ (Azenta Life Sciences). Bioinformatic analyses were performed by Matteo Barcella (Bioinformatics Core, SR-TIGET).

Integration site analyses

DNA extraction was performed with QIAamp DNA Micro Kit (QIAGEN) following the manufacturer's instructions. Library preparation and downstream analyses were performed by Fabrizio Benedicenti, Sergio Arevalo Diaz, and Francesco Gazzo (Eugenio Montini's group, SR-TIGET) as previously described (Biffi *et al.*, 2011, 2013).

Statistics and Reproducibility

Measurements were taken from distinct biological samples and sample size (n) is reported in the figure legends. In the presence of more than two independent groups, the Kruskal-Wallis test was performed, followed by post hoc pairwise comparisons. For paired observations, the Wilcoxon matched-pairs signed rank test was performed. Mann-Whitney test was performed to compare two independent groups or paired samples with n<6. For WB analysis, one-sample T-test was performed on normalized data. All tests were performed with two-tail statistics. Data were analyzed using the Prism software (GraphPad Software Inc.). *p* values <0.05 were considered significant (*, $p<0.05$; **, $p<0.01$; ***, $p<0.001$; ****, $p<0.0001$).

References

Adamo, L. *et al.* (2009) 'Biomechanical forces promote embryonic haematopoiesis', *Nature 2009 459:7250*, 459(7250), pp. 1131–1135. doi: 10.1038/nature08073.

Ahuja, A. K. *et al.* (2016) 'A short G1 phase imposes constitutive replication stress and fork remodelling in mouse embryonic stem cells', *Nature Communications*, 7(1), pp. 1–11. doi: 10.1038/ncomms10660.

Aiuti, A. *et al.* (2002) 'Correction of ADA-SCID by stem cell gene therapy combined with nonmyeloablative conditioning', *Science*, 296(5577), pp. 2410–2413. Available at: https://www.science.org/doi/10.1126/science.1070104 (Accessed: 13 March 2021).

Aiuti, A. *et al.* (2013) 'Lentiviral hematopoietic stem cell gene therapy in patients with wiskott-aldrich syndrome', *Science*, 341(6148). doi: 10.1126/SCIENCE.1233151/SUPPL_FILE/AIUTI.SM.PDF.

Aiuti, A., Roncarolo, M. G. and Naldini, L. (2017) ' Gene therapy for ADA-SCID, the first marketing approval of an ex vivo gene therapy in Europe: paving the road for the next generation of advanced therapy medicinal products ', *EMBO Molecular Medicine*, 9(6), pp. 737–740. doi: 10.15252/EMMM.201707573/ASSET/0E48B325-2F1C-4357-BFD8-FA35E4289FAF/ASSETS/GRAPHIC/EMMM201707573-FIG-0001-M.PNG.

Alakel, N. *et al.* (2009) 'Direct contact with mesenchymal stromal cells affects migratory behavior and gene expression profile of CD133+ hematopoietic stem cells during ex vivo expansion', *Experimental hematology*, 37(4), pp. 504–513. doi: 10.1016/J.EXPHEM.2008.12.005.

de Almeida, M. J. *et al.* (2017) 'Dye-Independent Methods Reveal Elevated Mitochondrial Mass in Hematopoietic Stem Cells', *Cell Stem Cell*, 21(6), pp. 725-729.e4. doi: 10.1016/j.stem.2017.11.002.

Altrock, E. *et al.* (2012) 'The significance of integrin ligand nanopatterning on lipid raft clustering in hematopoietic stem cells', *Biomaterials*, 33(11), pp. 3107–3118. doi: 10.1016/J.BIOMATERIALS.2012.01.002.

Amabile, A. *et al.* (2016) 'Inheritable Silencing of Endogenous Genes by Hit-and-Run Targeted Epigenetic Editing', *Cell*, 167(1), pp. 219-232.e14. doi: 10.1016/J.CELL.2016.09.006.

An, M. *et al.* (2024) 'Engineered virus-like particles for transient delivery of prime editor ribonucleoprotein complexes in vivo', *Nature Biotechnology 2024*, pp. 1–12. doi: 10.1038/s41587-023-02078-y.

Antoniou, P. *et al.* (2022) 'Base-editing-mediated dissection of a γ-globin cis-regulatory element for the therapeutic reactivation of fetal hemoglobin expression', *Nature Communications 2022 13:1*, 13(1), pp. 1–22. doi: 10.1038/s41467-022-34493-1.

Anzalone, A. V. *et al.* (2019) 'Search-and-replace genome editing without double-strand breaks or donor DNA', 576(7785), pp. 149–157. doi: 10.1038/s41586-019-1711-4.

Anzalone, A. V., Koblan, L. W. and Liu, D. R. (2020) 'Genome editing with CRISPR–Cas nucleases, base editors, transposases and prime editors', *Nature Biotechnology 2020 38:7*, 38(7), pp. 824–844. doi: 10.1038/s41587-020-0561-9.

Appelbaum, F. R. (2007) 'Hematopoietic-cell transplantation at 50', *The New England journal of medicine*, 357(15), pp. 1472–1475. doi: 10.1056/NEJMP078166.

Aprile, A. *et al.* (2020) 'Hematopoietic stem cell function in β-thalassemia is impaired and is rescued by targeting the bone marrow niche', *Blood*, 136(5), pp. 610–622. doi: 10.1182/BLOOD.2019002721.

Araki, D. *et al.* (2021) 'NOTCH-mediated ex vivo expansion of human hematopoietic stem and progenitor cells by culture under hypoxia', *Stem Cell Reports*, 16(9), pp. 2336–2350. doi: 10.1016/J.STEMCR.2021.08.001.

Athanasopoulos, T., Munye, M. M. and Yáñez-Muñoz, R. J. (2017) 'Nonintegrating Gene Therapy Vectors', *Hematology/Oncology Clinics of North America*. W.B. Saunders, pp. 753–770. doi: 10.1016/j.hoc.2017.06.007.

Bae, K. H. *et al.* (2003) 'Human zinc fingers as building blocks in the construction of artificial transcription factors', *Nature Biotechnology*, 21(3), pp. 275–280. doi: 10.1038/nbt796.

Bai, T. *et al.* (2019) 'Expansion of primitive human hematopoietic stem cells by culture in a zwitterionic hydrogel', *Nature Medicine 2019 25:10*, 25(10), pp. 1566–1575. doi: 10.1038/s41591-019-0601-5.

Baik, R. *et al.* (2024) 'Transient inhibition of 53BP1 increases the frequency of targeted integration in human hematopoietic stem and progenitor cells', *Nature Communications 2024 15:1*, 15(1), pp. 1–14. doi: 10.1038/s41467-023-43413-w.

Barnett, M. J. *et al.* (1991) 'Human hematopoietic stem cells in long-term culture: Quantitation and manipulation', in *Bone Marrow Transplantation*, p. 70. Available at: https://europepmc.org/article/med/2043892 (Accessed: 12 March 2021).

Barrangou, R. *et al.* (2007) 'CRISPR provides acquired resistance against viruses in prokaryotes', *Science (New York, N.Y.)*, 315(5819), pp. 1709–1712. doi: 10.1126/SCIENCE.1138140.

Bartek, J., Lukas, C. and Lukas, J. (2004) 'Checking on DNA damage in S phase',

Nature Reviews Molecular Cell Biology. Nature Publishing Group, pp. 792–804. doi: 10.1038/nrm1493.

Belluschi, S. *et al.* (2018) 'Myelo-lymphoid lineage restriction occurs in the human haematopoietic stem cell compartment before lymphoid-primed multipotent progenitors', *Nature Communications*, 9(1). doi: 10.1038/s41467-018-06442-4.

Bernitz, J. M. *et al.* (2016) 'Hematopoietic Stem Cells Count and Remember Self-Renewal Divisions', *Cell*, 167(5), pp. 1296-1309.e10. doi: 10.1016/J.CELL.2016.10.022/ATTACHMENT/CF383C1C-A2BC-4121-ACA2-B258BBA869D3/MMC1.PDF.

Bhargava, R., Onyango, D. O. and Stark, J. M. (2016) 'Regulation of Single-Strand Annealing and its Role in Genome Maintenance', *Trends in Genetics*. Elsevier Ltd, pp. 566–575. doi: 10.1016/j.tig.2016.06.007.

Bianco, J. E. R. *et al.* (2019) 'Characterization of a novel decellularized bone marrow scaffold as an inductive environment for hematopoietic stem cells', *Biomaterials science*, 7(4), pp. 1516–1528. doi: 10.1039/C8BM01503A.

Biffi, A. *et al.* (2011) 'Lentiviral vector common integration sites in preclinical models and a clinical trial reflect a benign integration bias and not oncogenic selection', *Blood*, 117(20), pp. 5332–5339. doi: 10.1182/BLOOD-2010-09-306761.

Biffi, A. *et al.* (2013) 'Lentiviral hematopoietic stem cell gene therapy benefits metachromatic leukodystrophy', *Science (New York, N.Y.)*, 341(6148). doi: 10.1126/SCIENCE.1233158.

Bitinaite, J. *et al.* (1998) 'Foki dimerization is required for dna cleavage', *Proceedings of the National Academy of Sciences of the United States of America*, 95(18), pp. 10570–10575. doi: 10.1073/pnas.95.18.10570.

Bonora, M. *et al.* (2018) 'Membrane-potential compensation reveals mitochondrial volume expansion during HSC commitment', *Experimental Hematology*, 68, pp. 30-37.e1. doi: 10.1016/j.exphem.2018.10.012.

Bonora, M. *et al.* (2024) 'A mitochondrial NADPH-cholesterol axis regulates extracellular vesicle biogenesis to support hematopoietic stem cell fate', *Cell stem cell*, 31(3), pp. 359-377.e10. doi: 10.1016/J.STEM.2024.02.004.

Bothmer, A. *et al.* (2010) '53BP1 regulates DNA resection and the choice between classical and alternative end joining during class switch recombination', *Journal of Experimental Medicine*, 207(4), pp. 855–865. doi: 10.1084/jem.20100244.

Boyd, A. L. *et al.* (2014) 'Niche displacement of human leukemic stem cells uniquely allows their competitive replacement with healthy HSPCs', *The Journal of experimental medicine*, 211(10), pp. 1925–1935. doi: 10.1084/JEM.20140131.

Boyle, C., Lansdorp, P. M. and Edelstein-Keshet, L. (2023) 'Predicting the number

of lifetime divisions for hematopoietic stem cells from telomere length measurements', *iScience*, 26(7). doi: 10.1016/J.ISCI.2023.107053.

Breton, C. *et al.* (2020) 'ITR-Seq, a next-generation sequencing assay, identifies genome-wide DNA editing sites in vivo following adeno-associated viral vector-mediated genome editing', *BMC Genomics*, 21(1), p. 239. doi: 10.1186/s12864-020-6655-4.

Brunet de la Grange, P. *et al.* (2013) 'Long-term repopulating hematopoietic stem cells and "side population" in human steady state peripheral blood', *Stem Cell Research*, 11(1), pp. 625–633. doi: 10.1016/j.scr.2013.04.003.

Bruns, I. *et al.* (2014) 'Megakaryocytes regulate hematopoietic stem cell quiescence through CXCL4 secretion', *Nature medicine*, 20(11), pp. 1315–1320. doi: 10.1038/NM.3707.

Budak-Alpdogan, T. and Rivière, I. (2009) 'Genetic Modification of Human Hematopoietic Cells: Preclinical Optimization of Oncoretroviral-mediated Gene Transfer for Clinical Trials', *Methods in molecular biology (Clifton, N.J.)*, 506, p. 33. doi: 10.1007/978-1-59745-409-4_4.

Di Buduo, C. A. *et al.* (2015) 'Programmable 3D silk bone marrow niche for platelet generation ex vivo and modeling of megakaryopoiesis pathologies', *Blood*, 125(14), pp. 2254–2264. doi: 10.1182/blood-2014-08-595561.

Di Buduo, C. A. *et al.* (2021) 'Latest culture techniques: cracking the secrets of bone marrow to mass-produce erythrocytes and platelets ex vivo', *Haematologica*, 106(4), pp. 947–957. doi: 10.3324/haematol.2020.262485.

Burma, S., Chen, B. P. C. and Chen, D. J. (2006) 'Role of non-homologous end joining (NHEJ) in maintaining genomic integrity', *DNA Repair*. Elsevier, pp. 1042–1048. doi: 10.1016/j.dnarep.2006.05.026.

Bushman, F. *et al.* (2005) 'Genome-wide analysis of retroviral DNA integration', *Nature Reviews Microbiology*. Nat Rev Microbiol, pp. 848–858. doi: 10.1038/nrmicro1263.

Butler, J. M. *et al.* (2010) 'Endothelial cells are essential for the self-renewal and repopulation of Notch-dependent hematopoietic stem cells', *Cell stem cell*, 6(3), pp. 251–264. doi: 10.1016/J.STEM.2010.02.001.

Cabezas-Wallscheid, N. *et al.* (2014) 'Identification of regulatory networks in HSCs and their immediate progeny via integrated proteome, transcriptome, and DNA methylome analysis', *Cell stem cell*, 15(4), pp. 507–522. doi: 10.1016/J.STEM.2014.07.005.

Cameron, P. *et al.* (2017) 'Mapping the genomic landscape of CRISPR-Cas9 cleavage', *Nature Methods*, 14(6), pp. 600–606. doi: 10.1038/nmeth.4284.

Campisi, J. and D'Adda Di Fagagna, F. (2007) 'Cellular senescence: When bad things happen to good cells', *Nature Reviews Molecular Cell Biology*. Nature Publishing Group, pp. 729–740. doi: 10.1038/nrm2233.

Canarutto, D. *et al.* (2021) 'Peripheral blood stem and progenitor cell collection in pediatric candidates for ex vivo gene therapy: a 10-year series', *Molecular therapy. Methods & clinical development*, 22, pp. 76–83. doi: 10.1016/J.OMTM.2021.05.013.

Canny, M. D. *et al.* (2018) 'Inhibition of 53BP1 favors homology-dependent DNA repair and increases CRISPR-Cas9 genome-editing efficiency', *Nature Biotechnology*, 36(1), pp. 95–102. doi: 10.1038/nbt.4021.

Canovas, B. and Nebreda, A. R. (2021) *Diversity and versatility of p38 kinase signalling in health and disease*. Available at: www.nature.com/nrm (Accessed: 28 April 2021).

Cappelluti, M. A. *et al.* (2024) 'Durable and efficient gene silencing in vivo by hit-and-run epigenome editing', *Nature 2024 627:8003*, 627(8003), pp. 416–423. doi: 10.1038/s41586-024-07087-8.

Carlson-Stevermer, J. *et al.* (2017) 'Assembly of CRISPR ribonucleoproteins with biotinylated oligonucleotides via an RNA aptamer for precise gene editing', *Nature Communications*, 8(1), pp. 1–13. doi: 10.1038/s41467-017-01875-9.

Carson, C. T. *et al.* (2003) 'The Mre11 complex is required for ATM activation and the G2/M checkpoint', *EMBO Journal*, 22(24), pp. 6610–6620. doi: 10.1093/emboj/cdg630.

Cavazza, A., Moiani, A. and Mavilio, F. (2013) 'Mechanisms of retroviral integration and mutagenesis', *Human Gene Therapy*. Hum Gene Ther, pp. 119–131. doi: 10.1089/hum.2012.203.

Cavazzana-Calvo, M. *et al.* (2000) 'Gene therapy of human severe combined immunodeficiency (SCID)-X1 disease', *Science*, 288(5466), pp. 669–672. Available at: https://www.science.org/doi/10.1126/science.288.5466.669 (Accessed: 13 March 2021).

Celeste, A. *et al.* (2002) 'Genomic instability in mice lacking histone H2AX', *Science*, 296(5569), pp. 922–927. doi: 10.1126/science.1069398.

Cermak, T. *et al.* (2011) 'Efficient design and assembly of custom TALEN and other TAL effector-based constructs for DNA targeting', *Nucleic Acids Research*, 39(12). doi: 10.1093/nar/gkr218.

Cesana, D. *et al.* (2024) 'A case of T-cell acute lymphoblastic leukemia in retroviral gene therapy for ADA-SCID', *Nature Communications*, 15(1). doi: 10.1038/S41467-024-47866-5.

Chabi, S. *et al.* (2019) 'Hypoxia Regulates Lymphoid Development of Human

Hematopoietic Progenitors', *Cell reports*, 29(8), pp. 2307-2320.e6. doi: 10.1016/J.CELREP.2019.10.050.

Chambers, S. M. *et al.* (2007) 'Aging hematopoietic stem cells decline in function and exhibit epigenetic dysregulation', *PLoS biology*, 5(8), pp. 1750–1762. doi: 10.1371/JOURNAL.PBIO.0050201.

Chang, H. H. Y. *et al.* (2017) 'Non-homologous DNA end joining and alternative pathways to double-strand break repair', *Nature Reviews Molecular Cell Biology*. Nature Publishing Group, pp. 495–506. doi: 10.1038/nrm.2017.48.

Charlesworth, C. T. *et al.* (2018) 'Priming Human Repopulating Hematopoietic Stem and Progenitor Cells for Cas9/sgRNA Gene Targeting', *Molecular therapy. Nucleic acids*, 12, pp. 89–104. doi: 10.1016/J.OMTN.2018.04.017.

Charpentier, M. *et al.* (2018) 'CtIP fusion to Cas9 enhances transgene integration by homology-dependent repair', *Nature Communications*, 9(1), pp. 1–11. doi: 10.1038/s41467-018-03475-7.

Choi, J. S. and Harley, B. A. C. (2017) 'Marrow-inspired matrix cues rapidly affect early fate decisions of hematopoietic stem and progenitor cells', 3(1). Available at: https://pubmed.ncbi.nlm.nih.gov/28070554/ (Accessed: 14 February 2023).

Chu, V. T. *et al.* (2015) 'Increasing the efficiency of homology-directed repair for CRISPR-Cas9-induced precise gene editing in mammalian cells', *Nature Biotechnology*, 33(5), pp. 543–548. doi: 10.1038/nbt.3198.

Chumki, S. A. *et al.* (2016) 'Remarkably long-tract gene conversion induced by fragile site instability in Saccharomyces cerevisiae', *Genetics*, 204(1), pp. 115–128. doi: 10.1534/genetics.116.191205.

Congrains, A. *et al.* (2021) '3D Scaffolds to Model the Hematopoietic Stem Cell Niche: Applications and Perspectives', *Materials*, 14(3), pp. 1–18. doi: 10.3390/MA14030569.

Copelan, E. A. (2006) 'Hematopoietic Stem-Cell Transplantation', *New England Journal of Medicine*, 354(17), pp. 1813–1826. doi: 10.1056/NEJMra052638.

Copley, M. R., Beer, P. A. and Eaves, C. J. (2012) 'Hematopoietic stem cell heterogeneity takes center stage', *Cell Stem Cell*. Elsevier, pp. 690–697. doi: 10.1016/j.stem.2012.05.006.

Crippa, S. *et al.* (2023) 'Mesenchymal stromal cells improve the transplantation outcome of CRISPR-Cas9 gene-edited human HSPCs', *Molecular therapy : the journal of the American Society of Gene Therapy*, 31(1), pp. 230–248. doi: 10.1016/J.YMTHE.2022.08.011.

Crisan, M. and Dzierzak, E. (2016) 'The many faces of hematopoietic stem cell heterogeneity', *Development (Cambridge)*. Company of Biologists Ltd, pp. 4571–

4581. doi: 10.1242/dev.114231.

Cuenda, A. *et al.* (1995) 'SB 203580 is a specific inhibitor of a MAP kinase homologue which is stimulated by cellular stresses and interleukin-1', *FEBS letters*, 364(2), pp. 229–233. doi: 10.1016/0014-5793(95)00357-F.

Cullot, G. *et al.* (2019) 'CRISPR-Cas9 genome editing induces megabase-scale chromosomal truncations', *Nature Communications*, 10(1), pp. 1–14. doi: 10.1038/s41467-019-09006-2.

Cullot, G. *et al.* (2023) 'Cell cycle arrest and p53 prevent ON-target megabase-scale rearrangements induced by CRISPR-Cas9', *Nature Communications 2023 14:1*, 14(1), pp. 1–16. doi: 10.1038/s41467-023-39632-w.

Dalerba, P., Cho, R. W. and Clarke, M. F. (2007) 'Cancer Stem Cells: Models and Concepts', *Annual Review of Medicine*. doi: 10.1146/annurev.med.58.062105.204854.

Dalwadi, D. A. *et al.* (2021) 'AAV integration in human hepatocytes', *Molecular Therapy*, 29(10), pp. 2898–2909. doi: 10.1016/J.YMTHE.2021.08.031/ATTACHMENT/5829DAC4-BBCE-4DCE-A84D-B9BBA4870DA4/MMC9.PDF.

Dausset, J. (1958) 'Iso-leuco-anticorps', *Acta Haematologica*, 20(1–4), pp. 156–166. doi: 10.1159/000205478.

Deltcheva, E. *et al.* (2011) 'CRISPR RNA maturation by trans-encoded small RNA and host factor RNase III', *Nature*, 471(7340), pp. 602–607. doi: 10.1038/nature09886.

Desterke, C. *et al.* (2011) 'FLT3-mediated p38-MAPK activation participates in the control of megakaryopoiesis in primary myelofibrosis', *Cancer research*, 71(8), pp. 2901–2915. doi: 10.1158/0008-5472.CAN-10-1731.

Dexter, T. M., Moore, M. A. S. and Sheridan, A. P. C. (1977) 'Maintenance of hemopoietic stem cells and production of differentiated progeny in allogeneic and semiallogeneic bone marrow chimeras in vitro*', *Journal of Experimental Medicine*, 145(6), pp. 1612–1616. doi: 10.1084/jem.145.6.1612.

Di, X. *et al.* (2023) 'Cellular mechanotransduction in health and diseases: from molecular mechanism to therapeutic targets', *Signal Transduction and Targeted Therapy 2023 8:1*, 8(1), pp. 1–32. doi: 10.1038/s41392-023-01501-9.

Ding, L. *et al.* (2012) 'Endothelial and perivascular cells maintain haematopoietic stem cells', *Nature*, 481(7382), pp. 457–462. doi: 10.1038/NATURE10783.

Donnaloja, F. *et al.* (2019) 'Mechanosensing at the nuclear envelope by nuclear pore complex stretch activation and its effect in physiology and pathology', *Frontiers in Physiology*, 10(JUL), p. 463617. doi: 10.3389/FPHYS.2019.00896/BIBTEX.

Doudna, J. A. (2020) 'The promise and challenge of therapeutic genome editing', *Nature*, 578(7794), pp. 229–236. doi: 10.1038/s41586-020-1978-5.

Doulatov, S. *et al.* (2012) 'Hematopoiesis: A human perspective', *Cell Stem Cell*. Elsevier, pp. 120–136. doi: 10.1016/j.stem.2012.01.006.

Doyon, Y. *et al.* (2011) 'Enhancing zinc-finger-nuclease activity with improved obligate heterodimeric architectures', *Nature Methods*, 8(1), pp. 74–79. doi: 10.1038/nmeth.1539.

Durai, S. *et al.* (2005) 'Zinc finger nucleases: Custom-designed molecular scissors for genome engineering of plant and mammalian cells', *Nucleic Acids Research*, 33(18), pp. 5978–5990. doi: 10.1093/nar/gki912.

Dzierzak, E. and Speck, N. A. (2008) 'Of lineage and legacy: the development of mammalian hematopoietic stem cells', *Nature Immunology*. doi: 10.1038/ni1560.

Escribano-Díaz, C. *et al.* (2013) 'A Cell Cycle-Dependent Regulatory Circuit Composed of 53BP1-RIF1 and BRCA1-CtIP Controls DNA Repair Pathway Choice', *Molecular Cell*, 49(5), pp. 872–883. doi: 10.1016/j.molcel.2013.01.001.

Essers, M. A. G. *et al.* (2009) 'IFNα activates dormant haematopoietic stem cells in vivo', *Nature*, 458(7240), pp. 904–908. doi: 10.1038/nature07815.

Everette, K. A. *et al.* (2023) 'Ex vivo prime editing of patient haematopoietic stem cells rescues sickle-cell disease phenotypes after engraftment in mice', *Nature Biomedical Engineering 2023 7:5*, 7(5), pp. 616–628. doi: 10.1038/s41551-023-01026-0.

Ezumi, Y. *et al.* (1999) 'Thrombopoietin Potentiates Agonist-Stimulated Activation of p38 Mitogen-Activated Protein Kinase in Human Platelets', 261(1), pp. 58–63. doi: 10.1006/BBRC.1999.0979.

Famili, F. *et al.* (2015) 'Discrete roles of canonical and non-canonical Wnt signaling in hematopoiesis and lymphopoiesis', *Cell Death & Disease 2015 6:11*, 6(11), pp. e1981–e1981. doi: 10.1038/cddis.2015.326.

Fares, I. *et al.* (2014) 'Pyrimidoindole derivatives are agonists of human hematopoietic stem cell self-renewal', *Science*, 345(6203), pp. 1509–1512. doi: 10.1126/science.1256337.

Fares, I. *et al.* (2017) 'EPCR expression marks UM171-expanded CD34+ cord blood stem cells', *Blood*, 129(25), pp. 3344–3351. doi: 10.1182/blood-2016-11-750729.

Ferrai, C. and Schulte, C. (2024) 'Mechanotransduction in stem cells', *European journal of cell biology*, 103(2). doi: 10.1016/J.EJCB.2024.151417.

Ferrari, G., Thrasher, A. J. and Aiuti, A. (2021) 'Gene therapy using haematopoietic stem and progenitor cells', 22(4), pp. 216–234. Available at:

https://pubmed.ncbi.nlm.nih.gov/33303992/ (Accessed: 30 August 2024).

Ferrari, S. *et al.* (2020) 'Efficient gene editing of human long-term hematopoietic stem cells validated by clonal tracking', *Nature Biotechnology*, 38(11), pp. 1298–1308. doi: 10.1038/s41587-020-0551-y.

Ferrari, S. *et al.* (2022) 'Choice of template delivery mitigates the genotoxic risk and adverse impact of editing in human hematopoietic stem cells', *Cell stem cell*, 29(10), pp. 1428-1444.e9. doi: 10.1016/J.STEM.2022.09.001.

Ferrari, S. *et al.* (2023) 'Genetic engineering meets hematopoietic stem cell biology for next-generation gene therapy', *Cell stem cell*, 30(5), pp. 549–570. doi: 10.1016/J.STEM.2023.04.014.

Ferrua, F. *et al.* (2019) 'Lentiviral haemopoietic stem/progenitor cell gene therapy for treatment of Wiskott-Aldrich syndrome: interim results of a non-randomised, open-label, phase 1/2 clinical study', 6(5), pp. e239–e253. doi: 10.1016/S2352-3026(19)30021-3.

Fiumara, M. *et al.* (2023) 'Genotoxic effects of base and prime editing in human hematopoietic stem cells', *Nature Biotechnology 2023 42:6*, 42(6), pp. 877–891. doi: 10.1038/s41587-023-01915-4.

Fliedner, T. M. *et al.* (2002) 'Structure and function of bone marrow hemopoiesis: mechanisms of response to ionizing radiation exposure', *Cancer biotherapy & radiopharmaceuticals*, 17(4), pp. 405–426. doi: 10.1089/108497802760363204.

Florian, M. C. *et al.* (2012) 'Cdc42 activity regulates hematopoietic stem cell aging and rejuvenation', *Cell stem cell*, 10(5), pp. 520–530. doi: 10.1016/J.STEM.2012.04.007.

Florian, M. C. *et al.* (2013) 'A canonical to non-canonical Wnt signalling switch in haematopoietic stem-cell ageing', *Nature*, 503(7476), p. 392. doi: 10.1038/NATURE12631.

Florian, M. C. *et al.* (2018) 'Aging alters the epigenetic asymmetry of HSC division', *PLoS biology*, 16(9). doi: 10.1371/JOURNAL.PBIO.2003389.

Florian, M. C. *et al.* (2020) 'Inhibition of Cdc42 activity extends lifespan and decreases circulating inflammatory cytokines in aged female C57BL/6 mice', *Aging cell*, 19(9). doi: 10.1111/ACEL.13208.

Foss, D. V. *et al.* (2023) 'Peptide-mediated delivery of CRISPR enzymes for the efficient editing of primary human lymphocytes', *Nature Biomedical Engineering 2023 7:5*, 7(5), pp. 647–660. doi: 10.1038/s41551-023-01032-2.

Frangoul, H. *et al.* (2021) 'CRISPR-Cas9 Gene Editing for Sickle Cell Disease and β-Thalassemia', *The New England journal of medicine*, 384(3), pp. 252–260. doi: 10.1056/NEJMOA2031054.

Fu, Y. *et al.* (2014) 'Improving CRISPR-Cas nuclease specificity using truncated guide RNAs', *Nature Biotechnology*, 32(3), pp. 279–284. doi: 10.1038/nbt.2808.

García-Prat, L. *et al.* (2021) 'TFEB-mediated endolysosomal activity controls human hematopoietic stem cell fate', *Cell stem cell*, 28(10), pp. 1838-1850.e10. doi: 10.1016/J.STEM.2021.07.003.

Genovese, P. *et al.* (2014) 'Targeted genome editing in human repopulating haematopoietic stem cells', *Nature*, 510(7504), pp. 235–240. doi: 10.1038/nature13420.

Gentner, B. *et al.* (2021) 'Hematopoietic Stem- and Progenitor-Cell Gene Therapy for Hurler Syndrome', *New England Journal of Medicine*, 385(21), pp. 1929–1940. doi: 10.1056/NEJMOA2106596/SUPPL_FILE/NEJMOA2106596_DATA-SHARING.PDF.

Gertz, M. A. *et al.* (2010) 'Clinical impact and resource utilization after stem cell mobilization failure in patients with multiple myeloma and lymphoma', *Bone marrow transplantation*, 45(9), pp. 1396–1403. doi: 10.1038/BMT.2009.370.

Glass, Z. *et al.* (2018) 'Engineering the Delivery System for CRISPR-based Genome Editing', *Trends in biotechnology*, 36(2), p. 173. doi: 10.1016/J.TIBTECH.2017.11.006.

Glimm, H., Oh, I. H. and Eaves, C. J. (2000) 'Human hematopoietic stem cells stimulated to proliferate in vitro lose engraftment potential during their S/G(2)/M transit and do not reenter G(0)', *Blood*, 96(13), pp. 4185–4193. doi: 10.1182/blood.v96.13.4185.

Gnani, D. *et al.* (2019) 'An early-senescence state in aged mesenchymal stromal cells contributes to hematopoietic stem and progenitor cell clonogenic impairment through the activation of a pro-inflammatory program', *Aging Cell*, 18(3), p. e12933. doi: 10.1111/acel.12933.

Gonzalez, N. P. *et al.* (2018) 'Cell tension and mechanical regulation of cell volume', *Molecular biology of the cell*, 29(21), pp. 2591–2600. doi: 10.1091/MBC.E18-04-0213.

Goyal, S. *et al.* (2015) 'Mechanisms of blood homeostasis: Lineage tracking and a neutral model of cell populations in rhesus macaques', *BMC Biology*, 13(1), p. 85. doi: 10.1186/s12915-015-0191-8.

Gratwohl, A. *et al.* (2015) 'One million haemopoietic stem-cell transplants: a retrospective observational study', *The Lancet. Haematology*, 2(3), pp. e91–e100. doi: 10.1016/S2352-3026(15)00028-9.

Greenbaum, A. *et al.* (2013) 'CXCL12 in early mesenchymal progenitors is required for haematopoietic stem-cell maintenance', 495(7440), pp. 227–230. doi: 10.1038/nature11926.

Grigoryan, A. *et al.* (2018) 'LaminA/C regulates epigenetic and chromatin architecture changes upon aging of hematopoietic stem cells', *Genome biology*, 19(1). doi: 10.1186/S13059-018-1557-3.

Gu, X. *et al.* (2020) 'Measurement of mitochondrial respiration in adherent cells by Seahorse XF96 Cell Mito Stress Test', *STAR protocols*, 2(1). doi: 10.1016/J.XPRO.2020.100245.

Guidi, N. *et al.* (2017) 'Osteopontin attenuates aging-associated phenotypes of hematopoietic stem cells', *The EMBO Journal*, 36(7), pp. 840–853. doi: 10.15252/EMBJ.201694969/SUPPL_FILE/EMBJ201694969-SUP-0004-MOVIEEV2.ZIP.

Le Guiner, C. *et al.* (2017) 'Long-term microdystrophin gene therapy is effective in a canine model of Duchenne muscular dystrophy', *Nature Communications*, 8(1), pp. 1–15. doi: 10.1038/ncomms16105.

Gutschner, T. *et al.* (2016) 'Post-translational Regulation of Cas9 during G1 Enhances Homology-Directed Repair', *Cell Reports*, 14(6), pp. 1555–1566. doi: 10.1016/j.celrep.2016.01.019.

Hacein-Bey-Abina, S. *et al.* (2002) 'Sustained correction of X-linked severe combined immunodeficiency by ex vivo gene therapy', *The New England journal of medicine*, 346(16), pp. 1185–1193. doi: 10.1056/NEJMOA012616.

Hacein-Bey-Abina, S. *et al.* (2003) 'LMO2-Associated Clonal T Cell Proliferation in Two Patients after Gene Therapy for SCID-X1', *Science*, 302(5644), pp. 415–419. Available at: https://www.science.org/doi/10.1126/science.1088547 (Accessed: 13 March 2021).

Hanlon, K. S. *et al.* (2019) 'High levels of AAV vector integration into CRISPR-induced DNA breaks', *Nature Communications*, 10(1), pp. 1–11. doi: 10.1038/s41467-019-12449-2.

Hendel, A. *et al.* (2015) 'Chemically modified guide RNAs enhance CRISPR-Cas genome editing in human primary cells', *Nature Biotechnology*, 33(9), pp. 985–989. doi: 10.1038/nbt.3290.

Henry, E. *et al.* (2020) 'Human hematopoietic stem/progenitor cells display reactive oxygen species-dependent long-term hematopoietic defects after exposure to low doses of ionizing radiations', *Haematologica*, 105(8), pp. 2044–2055. doi: 10.3324/haematol.2019.226936.

Henry, E. *et al.* (2023) 'The Antioxidant TEMPOL Protects Human Hematopoietic Stem Cells From Culture-Mediated Loss of Functions', *Stem Cells Translational Medicine*, 12(10), pp. 676–688. doi: 10.1093/STCLTM/SZAD049.

Hidalgo San Jose, L. *et al.* (2020) 'Modest Declines in Proteome Quality Impair

Hematopoietic Stem Cell Self-Renewal', *Cell reports*, 30(1), p. 69. doi: 10.1016/J.CELREP.2019.12.003.

Hoffman, B. D. and Yap, A. S. (2015) 'Towards a Dynamic Understanding of Cadherin-Based Mechanobiology', *Trends in cell biology*, 25(12), pp. 803–814. doi: 10.1016/J.TCB.2015.09.008.

Holmes, R. and Zuñiga-Pflücker, J. C. (2009) 'The OP9-DL1 system: generation of T-lymphocytes from embryonic or hematopoietic stem cells in vitro', *Cold Spring Harbor protocols*, 2009(2). doi: 10.1101/PDB.PROT5156.

Holst, J. *et al.* (2010) 'Substrate elasticity provides mechanical signals for the expansion of hemopoietic stem and progenitor cells', *Nature Biotechnology 2010 28:10*, 28(10), pp. 1123–1128. doi: 10.1038/nbt.1687.

Horwitz, M. E. *et al.* (2014) 'Umbilical cord blood expansion with nicotinamide provides long-term multilineage engraftment', *Journal of Clinical Investigation*, 124(7), pp. 3121–3128. doi: 10.1172/JCI74556.

Hu, J. H. *et al.* (2018) 'Evolved Cas9 variants with broad PAM compatibility and high DNA specificity', *Nature*, 556(7699), pp. 57–63. doi: 10.1038/nature26155.

Human Methylcellulose Base Media (HSC002) by R&D Systems, Part of Bio-Techne (no date). Available at: https://www.bio-techne.com/p/stem-cell/human-methylcellulose-base-media_hsc002 (Accessed: 16 September 2024).

Isalan, M. (2012) 'Zinc-finger nucleases: How to play two good hands', *Nature Methods*. Nat Methods, pp. 32–34. doi: 10.1038/nmeth.1805.

Itkin, T. *et al.* (2016) 'Distinct bone marrow blood vessels differentially regulate haematopoiesis', *Nature*, 532(7599), pp. 323–328. doi: 10.1038/NATURE17624.

Ito, K. *et al.* (2004) 'Regulation of oxidative stress by ATM is required for self-renewal of haematopoietic stem cells', *Nature*, 431(7011), pp. 997–1002. doi: 10.1038/nature02989.

Ito, K. *et al.* (2006) 'Reactive oxygen species act through p38 MAPK to limit the lifespan of hematopoietic stem cells', *Nature Medicine*, 12(4), pp. 446–451. doi: 10.1038/nm1388.

Ito, M. *et al.* (2002) 'NOD/SCID/γcnull mouse: An excellent recipient mouse model for engraftment of human cells', *Blood*, 100(9), pp. 3175–3182. doi: 10.1182/blood-2001-12-0207.

Ivanovs, A. *et al.* (2014) 'Stem Cell Reports Repor t Identification of the Niche and Phenotype of the First Human Hematopoietic Stem Cells', *Stem Cell Reports*, 2, pp. 449–456. doi: 10.1016/j.stemcr.2014.02.004.

Jacchetti, E. *et al.* (2021) 'The nuclear import of the transcription factor MyoD is reduced in mesenchymal stem cells grown in a 3D micro-engineered niche', *Scientific*

Reports 2021 11:1, 11(1), pp. 1–19. doi: 10.1038/s41598-021-81920-2.

Jacobs, K. *et al.* (2022) 'Stress-triggered hematopoietic stem cell proliferation relies on PrimPol-mediated repriming', *Molecular cell*, 82(21), pp. 4176-4188.e8. doi: 10.1016/J.MOLCEL.2022.09.009.

Jaenisch, R. and Young, R. (2008) 'Stem Cells, the Molecular Circuitry of Pluripotency and Nuclear Reprogramming', *Cell*. Cell, pp. 567–582. doi: 10.1016/j.cell.2008.01.015.

Jaiswal, S. and Ebert, B. L. (2019) 'Clonal hematopoiesis in human aging and disease', *Science (New York, N.Y.)*, 366(6465). doi: 10.1126/SCIENCE.AAN4673.

Jang, Y. *et al.* (2020) 'Optimizing Lentiviral Vector Transduction of Hematopoietic Stem Cells for Gene Therapy', *Gene therapy*, 27(12), p. 545. doi: 10.1038/S41434-020-0150-Z.

Jang, Y. Y. and Sharkis, S. J. (2007) 'A low level of reactive oxygen species selects for primitive hematopoietic stem cells that may reside in the low-oxygenic niche', *Blood*, 110(8), pp. 3056–3063. doi: 10.1182/blood-2007-05-087759.

Jayathilaka, K. *et al.* (2008) 'A chemical compound that stimulates the human homologous recombination protein RAD51', *Proceedings of the National Academy of Sciences of the United States of America*, 105(41), pp. 15848–15853. doi: 10.1073/pnas.0808046105.

Jiang, W. *et al.* (2015) 'Differential phosphorylation of DNA-PKcs regulates the interplay between end-processing and end-ligation during nonhomologous end-joining', *Molecular Cell*, 58(1), pp. 172–185. doi: 10.1016/j.molcel.2015.02.024.

Jinek, M. *et al.* (2012) 'A programmable dual-RNA-guided DNA endonuclease in adaptive bacterial immunity', 337(6096), pp. 816–821. Available at: https://pubmed.ncbi.nlm.nih.gov/22745249/ (Accessed: 13 March 2021).

Johnson, C. S. *et al.* (2024) 'Adaptation to ex vivo culture reduces human hematopoietic stem cell activity independently of the cell cycle', *Blood*, 144(7), pp. 729–741. doi: 10.1182/BLOOD.2023021426.

Joung, J. K. and Sander, J. D. (2013) 'TALENs: A widely applicable technology for targeted genome editing', *Nature Reviews Molecular Cell Biology*. Nat Rev Mol Cell Biol, pp. 49–55. doi: 10.1038/nrm3486.

Kallinikou, K. *et al.* (2012) 'Engraftment defect of cytokine-cultured adult human mobilized CD34(+) cells is related to reduced adhesion to bone marrow niche elements', *British journal of haematology*, 158(6), pp. 778–787. doi: 10.1111/J.1365-2141.2012.09219.X.

Kamel-Reid, S. and Dick, J. E. (1988) 'Engraftment of immune-deficient mice with human hematopoietic stem cells', *Science*, 242(4886), pp. 1706–1709. doi:

10.1126/science.2904703.

Kandi, R. *et al.* (2021) 'Cdc42-Borg4-Septin7 axis regulates HSC polarity and function', *EMBO reports*, 22(12). doi: 10.15252/EMBR.202152931.

Kay, M. A. (2011) 'State-of-the-art gene-based therapies: The road ahead', *Nature Reviews Genetics*. Nature Publishing Group, pp. 316–328. doi: 10.1038/nrg2971.

Khurana, S. *et al.* (2016) 'Outside-in integrin signalling regulates haematopoietic stem cell function via Periostin-Itgav axis', *Nature Communications 2016 7:1*, 7(1), pp. 1–14. doi: 10.1038/ncomms13500.

Kidiyoor, G. R. *et al.* (2020) 'ATR is essential for preservation of cell mechanics and nuclear integrity during interstitial migration', *Nature communications*, 11(1). doi: 10.1038/S41467-020-18580-9.

Kim, D. *et al.* (2015) 'Digenome-seq: Genome-wide profiling of CRISPR-Cas9 off-target effects in human cells', *Nature Methods*, 12(3), pp. 237–243. doi: 10.1038/nmeth.3284.

Kim, H. and Kim, J. S. (2014) 'A guide to genome engineering with programmable nucleases', *Nature Reviews Genetics*. Nature Publishing Group, pp. 321–334. doi: 10.1038/nrg3686.

Kim, J. E. *et al.* (2019) 'The combined effects of hierarchical scaffolds and mechanical stimuli on ex vivo expansion of haematopoietic stem/progenitor cells', *Artificial Cells, Nanomedicine, and Biotechnology*, 47(1), pp. 586–593. doi: 10.1080/21691401.2019.1573180.

Kim, K. M. *et al.* (2022) 'Taz protects hematopoietic stem cells from an aging-dependent decrease in PU.1 activity', *Nature communications*, 13(1). doi: 10.1038/S41467-022-32970-1.

Kim, Y. G., Cha, J. and Chandrasegaran, S. (1996) 'Hybrid restriction enzymes: Zinc finger fusions to Fok I cleavage domain', *Proceedings of the National Academy of Sciences of the United States of America*, 93(3), pp. 1156–1160. doi: 10.1073/pnas.93.3.1156.

Kitagawa, R. *et al.* (2004) 'Phosphorylation of SMC1 is a critical downstream event in the ATM-NBS1-BRCA1 pathway', *Genes and Development*, 18(12), pp. 1423–1438. doi: 10.1101/gad.1200304.

Klapwijk, J. C. *et al.* (2024) 'Improving the Assessment of Risk Factors Relevant to Potential Carcinogenicity of Gene Therapies: A Consensus Article', *Human gene therapy*, 35(15–16), pp. 527–542. doi: 10.1089/HUM.2024.033.

Kleinstiver, B. P. *et al.* (2016) 'High-fidelity CRISPR-Cas9 nucleases with no detectable genome-wide off-target effects', *Nature*, 529(7587), pp. 490–495. doi: 10.1038/nature16526.

Klompe, S. E. *et al.* (2019) 'Transposon-encoded CRISPR–Cas systems direct RNA-guided DNA integration', *Nature 2019 571:7764*, 571(7764), pp. 219–225. doi: 10.1038/s41586-019-1323-z.

Knight, S. *et al.* (2010) 'Effect of the Internal Promoter on Insertional Gene Activation by Lentiviral Vectors with an Intact HIV Long Terminal Repeat', *Journal of Virology*, 84(9), p. 4856. doi: 10.1128/JVI.02476-09.

Kohn, D. B. *et al.* (2020) *Lentiviral gene therapy for X-linked chronic granulomatous disease*. doi: 10.1038/s41591-019-0735-5.

Kohn, D. B. *et al.* (2021) 'Autologous Ex Vivo Lentiviral Gene Therapy for Adenosine Deaminase Deficiency', *New England Journal of Medicine*, 384(21), pp. 2002–2013. doi: 10.1056/NEJMOA2027675/SUPPL_FILE/NEJMOA2027675_DATA-SHARING.PDF.

Komor, A. C. *et al.* (2016) 'Programmable editing of a target base in genomic DNA without double-stranded DNA cleavage', 533(7603), pp. 420–424. doi: 10.1038/nature17946.

Kosicki, M., Tomberg, K. and Bradley, A. (2018) 'Repair of double-strand breaks induced by CRISPR–Cas9 leads to large deletions and complex rearrangements', *Nature Biotechnology*, 36(8), pp. 765–771. doi: 10.1038/nbt.4192.

Krstevska, S. *et al.* (2011) 'Acute graft versus host disease in hematopoietic stem cell alotransplant recipients.', *Medicinski arhiv*, 65(5), pp. 260–264. doi: 10.5455/medarh.2011.65.260-264.

Kruta, M. *et al.* (2021) 'Hsf1 promotes hematopoietic stem cell fitness and proteostasis in response to ex vivo culture stress and aging', *Cell stem cell*, 28(11), pp. 1950-1965.e6. doi: 10.1016/J.STEM.2021.07.009.

Kurihara, T. *et al.* (2020) 'DNA repair protein RAD51 enhances the CRISPR/Cas9-mediated knock-in efficiency in brain neurons', *Biochemical and Biophysical Research Communications*, 524(3), pp. 621–628. doi: 10.1016/j.bbrc.2020.01.132.

Laird, D. J., von Andrian, U. H. and Wagers, A. J. (2008) 'Stem Cell Trafficking in Tissue Development, Growth, and Disease', *Cell*. Cell, pp. 612–630. doi: 10.1016/j.cell.2008.01.041.

Lapidot, T. *et al.* (1992) 'Cytokine stimulation of multilineage hematopoiesis from immature human cells engrafted in SCID Mice', *Science*, 255(5048), pp. 1137–1141. doi: 10.1126/science.1372131.

Larochelle, A. *et al.* (2012) 'Bone marrow homing and engraftment of human hematopoietic stem and progenitor cells is mediated by a polarized membrane domain', *Blood*, 119(8), p. 1848. doi: 10.1182/BLOOD-2011-08-371583.

Laurenti, E. and Göttgens, B. (2018) 'From haematopoietic stem cells to complex

differentiation landscapes', *Nature*. Nature Publishing Group, pp. 418–426. doi: 10.1038/nature25022.

Lauridsen, F. K. B. *et al.* (2018) 'Differences in Cell Cycle Status Underlie Transcriptional Heterogeneity in the HSC Compartment', *Cell reports*, 24(3), pp. 766–780. doi: 10.1016/J.CELREP.2018.06.057.

Lehnertz, B. *et al.* (2021) 'HLF expression defines the human hematopoietic stem cell state', *Blood*, 138(25), pp. 2642–2654. doi: 10.1182/BLOOD.2021010745.

Leibowitz, M. L. *et al.* (2021) 'Chromothripsis as an on-target consequence of CRISPR–Cas9 genome editing', *Nature Genetics 2021 53:6*, 53(6), pp. 895–905. doi: 10.1038/s41588-021-00838-7.

Lengefeld, J. *et al.* (2021) 'Cell size is a determinant of stem cell potential during aging', *Science Advances*, 7(46), p. 271. doi: 10.1126/SCIADV.ABK0271/SUPPL_FILE/SCIADV.ABK0271_TABLES_S1_TO_S3.ZIP.

Li, G. *et al.* (2018) 'Suppressing Ku70/Ku80 expression elevates homology-directed repair efficiency in primary fibroblasts', *International Journal of Biochemistry and Cell Biology*, 99, pp. 154–160. doi: 10.1016/j.biocel.2018.04.011.

Li, H. *et al.* (2021) 'Biomechanical cues as master regulators of hematopoietic stem cell fate', *Cellular and Molecular Life Sciences 2021 78:16*, 78(16), pp. 5881–5902. doi: 10.1007/S00018-021-03882-Y.

Li, Yinghui *et al.* (2023) 'Expansion of human megakaryocyte-biased hematopoietic stem cells by biomimetic Microniche', *Nature Communications 2023 14:1*, 14(1), pp. 1–16. doi: 10.1038/s41467-023-37954-3.

Liang, R. *et al.* (2020) 'Restraining Lysosomal Activity Preserves Hematopoietic Stem Cell Quiescence and Potency', *Cell stem cell*, 26(3), pp. 359-376.e7. doi: 10.1016/J.STEM.2020.01.013.

Liao, H. K. *et al.* (2017) 'In Vivo Target Gene Activation via CRISPR/Cas9-Mediated Trans-epigenetic Modulation', *Cell*, 171(7), pp. 1495-1507.e15. doi: 10.1016/J.CELL.2017.10.025/ATTACHMENT/2A412C56-7993-4E26-AE3E-6C807DA8073E/MMC1.PDF.

Lieber, M. R. *et al.* (2003) 'Mechanism and regulation of human non-homologous DNA end-joining', *Nature Reviews Molecular Cell Biology*. Nat Rev Mol Cell Biol, pp. 712–720. doi: 10.1038/nrm1202.

Liggett, L. A. and Sankaran, V. G. (2020) 'Unraveling Hematopoiesis through the Lens of Genomics', *Cell*, 182(6), pp. 1384–1400. doi: 10.1016/J.CELL.2020.08.030.

Lin, S. *et al.* (2014) 'Enhanced homology-directed human genome engineering by controlled timing of CRISPR/Cas9 delivery', *eLife*, 3, p. e04766. doi: 10.7554/eLife.04766.

Liu, M. *et al.* (2019) 'Methodologies for improving HDR efficiency', *Frontiers in Genetics*. Frontiers Media S.A., p. 691. doi: 10.3389/fgene.2018.00691.

Liu, S. Y. *et al.* (2012) 'Systematic identification of type I and type II interferon-induced antiviral factors', *Proceedings of the National Academy of Sciences of the United States of America*, 109(11), pp. 4239–4244. doi: 10.1073/pnas.1114981109.

Liu, Z. *et al.* (2019) 'Primary cilia regulate hematopoietic stem and progenitor cell specification through Notch signaling in zebrafish', *Nature Communications 2019 10:1*, 10(1), pp. 1–11. doi: 10.1038/s41467-019-09403-7.

Lombardo, A. *et al.* (2007) 'Gene editing in human stem cells using zinc finger nucleases and integrase-defective lentiviral vector delivery', *Nature Biotechnology*, 25(11), pp. 1298–1306. doi: 10.1038/nbt1353.

Lomova, A. *et al.* (2019) 'Improving Gene Editing Outcomes in Human Hematopoietic Stem and Progenitor Cells by Temporal Control of DNA Repair', *Stem Cells*, 37(2), pp. 284–294. doi: 10.1002/stem.2935.

Longo, G. M. C. *et al.* (2024) 'Linking CRISPR–Cas9 double-strand break profiles to gene editing precision with BreakTag', *Nature Biotechnology 2024*, pp. 1–15. doi: 10.1038/s41587-024-02238-8.

Lundin, V. *et al.* (2020) 'YAP Regulates Hematopoietic Stem Cell Formation in Response to the Biomechanical Forces of Blood Flow', *Developmental cell*, 52(4), pp. 446-460.e5. doi: 10.1016/J.DEVCEL.2020.01.006.

Ma, M. *et al.* (2017) 'Efficient generation of mice carrying homozygous double-floxp alleles using the Cas9-Avidin/Biotin-donor DNA system', *Cell Research*. Nature Publishing Group, pp. 578–581. doi: 10.1038/cr.2017.29.

Magnani, A. *et al.* (2022) 'Long-term safety and efficacy of lentiviral hematopoietic stem/progenitor cell gene therapy for Wiskott–Aldrich syndrome', *Nature Medicine 2022 28:1*, 28(1), pp. 71–80. doi: 10.1038/s41591-021-01641-x.

Maier, P., Von Kalle, C. and Laufs, S. (2010) 'Retroviral vectors for gene therapy', *Future Microbiology*. Future Medicine Ltd London, UK , pp. 1507–1523. doi: 10.2217/fmb.10.100.

Mak, A. N. S. *et al.* (2013) 'TAL effectors: Function, structure, engineering and applications', *Current Opinion in Structural Biology*. NIH Public Access, pp. 93–99. doi: 10.1016/j.sbi.2012.11.001.

Makarova, K. S. *et al.* (2006) 'A putative RNA-interference-based immune system in prokaryotes: computational analysis of the predicted enzymatic machinery, functional analogies with eukaryotic RNAi, and hypothetical mechanisms of action', *Biology direct*, 1. doi: 10.1186/1745-6150-1-7.

Malkova, A. (2018) 'Break-Induced Replication: The Where, The Why, and The

How', *Trends in Genetics*. Elsevier Ltd, pp. 518–531. doi: 10.1016/j.tig.2018.04.002.

Marktel, S. *et al.* (2019) 'Intrabone hematopoietic stem cell gene therapy for adult and pediatric patients affected by transfusion-dependent ß-thalassemia', *Nature Medicine 2019 25:2*, 25(2), pp. 234–241. doi: 10.1038/s41591-018-0301-6.

Maruyama, T. *et al.* (2015) 'Increasing the efficiency of precise genome editing with CRISPR-Cas9 by inhibition of nonhomologous end joining', *Nature Biotechnology*, 33(5), pp. 538–542. doi: 10.1038/nbt.3190.

Marx-Blümel, L. *et al.* (2021) 'Molecular characterization of hematopoietic stem cells after in vitro amplification on biomimetic 3D PDMS cell culture scaffolds', 11(1), pp. 1–14. Available at: https://pubmed.ncbi.nlm.nih.gov/34707135/ (Accessed: 13 April 2023).

Masiuk, K. E. *et al.* (2017) 'Improving Gene Therapy Efficiency through the Enrichment of Human Hematopoietic Stem Cells', *Molecular Therapy*, 25(9), pp. 2163–2175. doi: 10.1016/J.YMTHE.2017.05.023.

Mathew, J., Sankar, P. and Varacallo, M. (2023) 'Physiology, Blood Plasma', *StatPearls*. Available at: https://www.ncbi.nlm.nih.gov/books/NBK531504/ (Accessed: 9 September 2024).

Mátrai, J. *et al.* (2011) 'Hepatocyte-targeted expression by integrase-defective lentiviral vectors induces antigen-specific tolerance in mice with low genotoxic risk', *Hepatology*, 53(5), pp. 1696–1707. doi: 10.1002/hep.24230.

Mazurier, F. *et al.* (2004) 'Lentivector-mediated clonal tracking reveals intrinsic heterogeneity in the human hematopoietic stem cell compartment and culture-induced stem cell impairment', *Blood*, 103(2), pp. 545–552. doi: 10.1182/blood-2003-05-1558.

McCune, J. M. *et al.* (1988) 'The SCID-hu mouse: Murine model for the analysis of human hematolymphoid differentiation and function', *Science*, 241(4873), pp. 1632–1639. doi: 10.1126/science.2971269.

McIntosh, B. E. *et al.* (2015) 'Nonirradiated NOD,B6.SCID Il2rγ-/- kitW41/W41 (NBSGW) mice support multilineage engraftment of human hematopoietic cells', *Stem Cell Reports*, 4(2), pp. 171–180. doi: 10.1016/j.stemcr.2014.12.005.

McVey, M. *et al.* (2016) 'Eukaryotic DNA Polymerases in Homologous Recombination', *Annual Review of Genetics*. Annual Reviews Inc., pp. 393–421. doi: 10.1146/annurev-genet-120215-035243.

Meaker, G. A. and Wilkinson, A. C. (2024) 'Ex vivo hematopoietic stem cell expansion technologies: recent progress, applications, and open questions', *Experimental hematology*, 130. doi: 10.1016/J.EXPHEM.2023.12.001.

Mejia-Ramirez, E. and Florian, M. C. (2020) 'Understanding intrinsic hematopoietic

stem cell aging', *Haematologica*, 105(1), p. 22. doi: 10.3324/HAEMATOL.2018.211342.

Mendelson, A. and Frenette, P. S. (2014) 'Hematopoietic stem cell niche maintenance during homeostasis and regeneration', *Nature Medicine*. Nature Publishing Group, pp. 833–846. doi: 10.1038/nm.3647.

Messa, L. *et al.* (2021) 'Neural Precursor Cells Expanded Inside the 3D Micro-Scaffold Nichoid Present Different Non-Coding RNAs Profiles and Transcript Isoforms Expression: Possible Epigenetic Modulation by 3D Growth', *Biomedicines*, 9(9). doi: 10.3390/BIOMEDICINES9091120.

Miller, C. L. and Lai, B. (2005) 'Human and mouse hematopoietic colony-forming cell assays.', *Methods in molecular biology (Clifton, N.J.)*, 290, pp. 71–89. doi: 10.1385/1-59259-838-2:071.

Miller, J. C. *et al.* (2007) 'An improved zinc-finger nuclease architecture for highly specific genome editing', *Nature Biotechnology*, 25(7), pp. 778–785. doi: 10.1038/nbt1319.

Mingozzi, F. and High, K. A. (2011) 'Therapeutic in vivo gene transfer for genetic disease using AAV: Progress and challenges', *Nature Reviews Genetics*. Nat Rev Genet, pp. 341–355. doi: 10.1038/nrg2988.

Miyamoto, K. *et al.* (2007) 'Foxo3a is essential for maintenance of the hematopoietic stem cell pool', *Cell stem cell*, 1(1), pp. 101–112. doi: 10.1016/J.STEM.2007.02.001.

Morbitzer, R. *et al.* (2011) 'Assembly of custom TALE-type DNA binding domains by modular cloning', *Nucleic Acids Research*, 39(13), pp. 5790–5799. doi: 10.1093/nar/gkr151.

Morgan, R. A. *et al.* (2017) 'Hematopoietic Stem Cell Gene Therapy: Progress and Lessons Learned', *Cell Stem Cell*. Cell Press, pp. 574–590. doi: 10.1016/j.stem.2017.10.010.

Morganti, C. *et al.* (2019) 'Electron transport chain complex II sustains high mitochondrial membrane potential in hematopoietic stem and progenitor cells', *Stem Cell Research*, 40, p. 101573. doi: 10.1016/j.scr.2019.101573.

Morganti, C., Cabezas-Wallscheid, N. and Ito, K. (2022) 'Metabolic Regulation of Hematopoietic Stem Cells', *HemaSphere*, 6(7), p. E740. doi: 10.1097/HS9.0000000000000740.

Morrison, S. J. and Scadden, D. T. (2014) 'The bone marrow niche for haematopoietic stem cells', *Nature*. Nature Publishing Group, pp. 327–334. doi: 10.1038/nature12984.

Morrison, S. J. and Spradling, A. C. (2008) 'Stem Cells and Niches: Mechanisms

That Promote Stem Cell Maintenance throughout Life', *Cell*. Cell, pp. 598–611. doi: 10.1016/j.cell.2008.01.038.

Moscou, M. J. and Bogdanove, A. J. (2009) 'A simple cipher governs DNA recognition by TAL effectors', *Science*, 326(5959), p. 1501. doi: 10.1126/science.1178817.

Mosier, D. E. *et al.* (1988) 'Transfer of a functional human immune system to mice with severe combined immunodeficiency', *Nature*, 335(6187), pp. 256–259. doi: 10.1038/335256a0.

Mu, W. *et al.* (2019) 'In vitro transcribed sgRNA causes cell death by inducing interferon release', *Protein and Cell*. Higher Education Press, pp. 461–465. doi: 10.1007/s13238-018-0605-9.

Murakami, J. L. *et al.* (2016) 'Evidence that β7 Integrin Regulates Hematopoietic Stem Cell Homing and Engraftment Through Interaction with MAdCAM-1', *Stem cells and development*, 25(1), pp. 18–26. doi: 10.1089/SCD.2014.0551.

Murry, C. E. and Keller, G. (2008) 'Differentiation of Embryonic Stem Cells to Clinically Relevant Populations: Lessons from Embryonic Development', *Cell*. Cell, pp. 661–680. doi: 10.1016/j.cell.2008.02.008.

Nakamura-Ishizu, A., Takizawa, H. and Suda, T. (2014) 'The analysis, roles and regulation of quiescence in hematopoietic stem cells', *Development (Cambridge, England)*, 141(24), pp. 4656–4666. doi: 10.1242/DEV.106575.

Naldini, L. *et al.* (1996) 'In vivo gene delivery and stable transduction of nondividing cells by a lentiviral vector', *Science (New York, N.Y.)*, 272(5259), pp. 263–267. doi: 10.1126/SCIENCE.272.5259.263.

Naldini, L. (2015) 'Gene therapy returns to centre stage', *Nature*. Nature Publishing Group, pp. 351–360. doi: 10.1038/nature15818.

Namikawa, R. *et al.* (1988) 'Infection of the SCID-hu mouse by HIV-1', *Science*, 242(4886), pp. 1684–1686. doi: 10.1126/science.3201256.

Nava, M. M. *et al.* (2016) 'Two-photon polymerized "nichoid" substrates maintain function of pluripotent stem cells when expanded under feeder-free conditions', *Stem Cell Research and Therapy*, 7(1), pp. 1–12. doi: 10.1186/S13287-016-0387-Z/FIGURES/6.

Nava, M. M. *et al.* (2017) '3d stem cell niche engineering via two-photon laser polymerization', *Methods in Molecular Biology*, 1612, pp. 253–266. doi: 10.1007/978-1-4939-7021-6_19/FIGURES/7.

Nelson, C. E. *et al.* (2019) 'Long-term evaluation of AAV-CRISPR genome editing for Duchenne muscular dystrophy', *Nature Medicine*, 25(3), pp. 427–432. doi: 10.1038/s41591-019-0344-3.

Ni, F. *et al.* (2019) 'Ptpn21 Controls Hematopoietic Stem Cell Homeostasis and Biomechanics', *Cell stem cell*, 24(4), pp. 608-620.e6. doi: 10.1016/J.STEM.2019.02.009.

Nilsson, S. K. *et al.* (2005) 'Osteopontin, a key component of the hematopoietic stem cell niche and regulator of primitive hematopoietic progenitor cells', *Blood*, 106(4), pp. 1232–1239. doi: 10.1182/BLOOD-2004-11-4422.

Nishimasu, H. *et al.* (2018) 'Engineered CRISPR-Cas9 nuclease with expanded targeting space', *Science*, 361(6408), pp. 1259–1262. doi: 10.1126/science.aas9129.

Notta, F. *et al.* (2011) 'Isolation of single human hematopoietic stem cells capable of long-term multilineage engraftment', *Science*, 333(6039), pp. 218–221. doi: 10.1126/science.1201219.

Notta, F. *et al.* (2016) 'Distinct routes of lineage development reshape the human blood hierarchy across ontogeny', *Science*, 351(6269). doi: 10.1126/science.aab2116.

Notta, F., Doulatov, S. and Dick, J. E. (2010) 'Engraftment of human hematopoietic stem cells is more efficient in female NOD/SCID/IL-2Rgc-null recipients', *Blood*, 115(18), pp. 3704–3707. doi: 10.1182/blood-2009-10-249326.

O'Connor, T. P. and Crystal, R. G. (2006) 'Genetic medicines: Treatment strategies for hereditary disorders', *Nature Reviews Genetics*. Nat Rev Genet, pp. 261–276. doi: 10.1038/nrg1829.

Ogrunc, M. *et al.* (2014) 'Oncogene-induced reactive oxygen species fuel hyperproliferation and DNA damage response activation', *Cell death and differentiation*, 21(6), pp. 998–1012. doi: 10.1038/CDD.2014.16.

Orkin, S. H. and Zon, L. I. (2008) 'Hematopoiesis: an evolving paradigm for stem cell biology', *Cell*, 132(4), pp. 631–644. doi: 10.1016/J.CELL.2008.01.025.

Pajcini, K. V., Speck, N. A. and Pear, W. S. (2011) 'Notch signaling in mammalian hematopoietic stem cells', *Leukemia*, 25(10), p. 1525. doi: 10.1038/LEU.2011.127.

Pang, W. W., Schrier, S. L. and Weissman, I. L. (2017) 'Age-associated changes in human hematopoietic stem cells', *Seminars in hematology*, 54(1), pp. 39–42. doi: 10.1053/J.SEMINHEMATOL.2016.10.004.

Pattabhi, S. *et al.* (2019) 'In Vivo Outcome of Homology-Directed Repair at the HBB Gene in HSC Using Alternative Donor Template Delivery Methods', *Molecular Therapy - Nucleic Acids*, 17, pp. 277–288. doi: 10.1016/j.omtn.2019.05.025.

Petrillo, C. *et al.* (2018) 'Cyclosporine H Overcomes Innate Immune Restrictions to Improve Lentiviral Transduction and Gene Editing In Human Hematopoietic Stem Cells', 23(6), pp. 820-832.e9. Available at: /pmc/articles/PMC6292841/ (Accessed:

28 April 2021).

Pievani, A. *et al.* (2017) 'Human umbilical cord blood-borne fibroblasts contain marrow niche precursors that form a bone/marrow organoid in vivo', *Development (Cambridge, England)*, 144(6), pp. 1035–1044. doi: 10.1242/DEV.142836.

Pike, B. L. and Robinson, W. A. (1970) 'Human bone marrow colony growth in agar-gel', *Journal of Cellular Physiology*, 76(1), pp. 77–84. doi: 10.1002/jcp.1040760111.

Pinder, J., Salsman, J. and Dellaire, G. (2015) 'Nuclear domain "knock-in" screen for the evaluation and identification of small molecule enhancers of CRISPR-based genome editing', *Nucleic Acids Research*, 43(19), pp. 9379–9392. doi: 10.1093/nar/gkv993.

Piras, F. *et al.* (2017) 'Lentiviral vectors escape innate sensing but trigger p53 in human hematopoietic stem and progenitor cells', *EMBO Molecular Medicine*, 9(9), pp. 1198–1211. doi: 10.15252/emmm.201707922.

Piras, F. and Kajaste-Rudnitski, A. (2021) 'Antiviral immunity and nucleic acid sensing in haematopoietic stem cell gene engineering', *Gene Therapy*. Springer Nature, pp. 16–28. doi: 10.1038/s41434-020-0175-3.

Porteus, M. H. (2019) 'A New Class of Medicines through DNA Editing', 380(10), pp. 947–959. Available at: https://www.nejm.org/doi/10.1056/NEJMra1800729 (Accessed: 20 July 2023).

Povirk, L. F. *et al.* (2007) 'Processing of 3'-phosphoglycolate-terminated DNA double strand breaks by artemis nuclease', *Journal of Biological Chemistry*, 282(6), pp. 3547–3558. doi: 10.1074/jbc.M607745200.

Pruett-Miller, S. M. (2013) 'Genome Editing in Somatic Cells Using Zinc Finger Nucleases and Transcription Activator-Like Effector Nucleases', in *Principles of Cloning: Second Edition*. Elsevier Inc., pp. 369–378. doi: 10.1016/B978-0-12-386541-0.00029-1.

Publicover, A. *et al.* (2013) 'Use of a biosimilar granulocyte colony-stimulating factor for peripheral blood stem cell mobilization: an analysis of mobilization and engraftment', *British Journal of Haematology*, 162(1), pp. 107–111. doi: 10.1111/bjh.12345.

Punatar, R. S. *et al.* (2017) 'Resolution of single and double Holliday junction recombination intermediates by GEN 1', *Proceedings of the National Academy of Sciences of the United States of America*, 114(3), pp. 443–450. doi: 10.1073/pnas.1619790114.

Raaijmakers, M. H. G. P. *et al.* (2010) 'Bone progenitor dysfunction induces myelodysplasia and secondary leukaemia', *Nature*, 464(7290), pp. 852–857. doi:

10.1038/NATURE08851.

Rai, R. *et al.* (2023) 'An improved medium formulation for efficient ex vivo gene editing, expansion and engraftment of hematopoietic stem and progenitor cells', *Molecular Therapy - Methods & Clinical Development*, 29, pp. 58–69. doi: 10.1016/J.OMTM.2023.02.014.

De Ravin, S. S. *et al.* (2017) 'CRISPR-Cas9 gene repair of hematopoietic stem cells from patients with X-linked chronic granulomatous disease', *Science Translational Medicine*, 9(372). doi: 10.1126/scitranslmed.aah3480.

Remuzzi, A. *et al.* (2020) 'Effect of the 3D Artificial Nichoid on the Morphology and Mechanobiological Response of Mesenchymal Stem Cells Cultured In Vitro', *Cells*, 9(8). doi: 10.3390/CELLS9081873.

Rey, F. *et al.* (2020) 'Dissecting the Effect of a 3D Microscaffold on the Transcriptome of Neural Stem Cells with Computational Approaches: A Focus on Mechanotransduction', *International Journal of Molecular Sciences 2020, Vol. 21, Page 6775*, 21(18), p. 6775. doi: 10.3390/IJMS21186775.

Reyon, D. *et al.* (2012) 'FLASH assembly of TALENs for high-throughput genome editing', *Nature Biotechnology*, 30(5), pp. 460–465. doi: 10.1038/nbt.2170.

Ricci, D. *et al.* (2017) 'Scaling-Up Techniques for the Nanofabrication of Cell Culture Substrates via Two-Photon Polymerization for Industrial-Scale Expansion of Stem Cells', *Materials (Basel, Switzerland)*, 10(1). doi: 10.3390/MA10010066.

Río, P. *et al.* (2019) 'Successful engraftment of gene-corrected hematopoietic stem cells in non-conditioned patients with Fanconi anemia', *Nature Medicine 2019 25:9*, 25(9), pp. 1396–1401. doi: 10.1038/s41591-019-0550-z.

Robert, F. *et al.* (2015) 'Pharmacological inhibition of DNA-PK stimulates Cas9-mediated genome editing', *Genome Medicine*, 7(1). doi: 10.1186/s13073-015-0215-6.

Romero, Z. *et al.* (2019) 'Editing the Sickle Cell Disease Mutation in Human Hematopoietic Stem Cells: Comparison of Endonucleases and Homologous Donor Templates', *Molecular Therapy*, 27(8), pp. 1389–1406. doi: 10.1016/j.ymthe.2019.05.014.

Rongvaux, A. *et al.* (2011) 'Human thrombopoietin knockin mice efficiently support human hematopoiesis in vivo', *Proceedings of the National Academy of Sciences of the United States of America*, 108(6), pp. 2378–2383. doi: 10.1073/pnas.1019524108.

Rubio-Lara, J. A. *et al.* (2023) 'Expanding hematopoietic stem cell ex vivo: recent advances and technical considerations', *Experimental Hematology*, 125–126, pp. 6–15. doi: 10.1016/J.EXPHEM.2023.07.006.

Russell, S. *et al.* (2017) 'Efficacy and safety of voretigene neparvovec (AAV2-hRPE65v2) in patients with RPE65-mediated inherited retinal dystrophy: a randomised, controlled, open-label, phase 3 trial', *The Lancet*, 390(10097), pp. 849–860. doi: 10.1016/S0140-6736(17)31868-8.

Sadok, A. and Marshall, C. J. (2014) 'Rho GTPases: masters of cell migration', *Small GTPases*, 5(4). doi: 10.4161/SGTP.29710.

Sakurai, M. *et al.* (2023) 'Chemically defined cytokine-free expansion of human haematopoietic stem cells', *Nature*, 615(7950), pp. 127–133. Available at: https://pubmed.ncbi.nlm.nih.gov/36813966/ (Accessed: 20 July 2023).

Satomura, A. *et al.* (2017) 'Precise genome-wide base editing by the CRISPR Nickase system in yeast', *Scientific Reports 2017 7:1*, 7(1), pp. 1–10. doi: 10.1038/s41598-017-02013-7.

Savage, S. A. and Niewisch, M. R. (2023) 'Dyskeratosis Congenita and Related Telomere Biology Disorders', *GeneReviews®*. Available at: https://www.ncbi.nlm.nih.gov/books/NBK22301/ (Accessed: 13 October 2024).

Savic, N. *et al.* (2018) 'Covalent linkage of the DNA repair template to the CRISPR-Cas9 nuclease enhances homology-directed repair', *eLife*, 7. doi: 10.7554/eLife.33761.

Scadden, D. T. (2006) 'The stem-cell niche as an entity of action', *Nature*. Nature Publishing Group, pp. 1075–1079. doi: 10.1038/nature04957.

Scapin, G. *et al.* (2018) 'Piezo1-Sensitive Biomechanical Pulsation Stimulates Long-Term Hematopoietic Stem Cell Formation', *Blood*, 132(Supplement 1), pp. 3826–3826. doi: 10.1182/BLOOD-2018-99-110265.

Schiroli, G. *et al.* (2017) 'Preclinical modeling highlights the therapeutic potential of hematopoietic stem cell gene editing for correction of SCID-X1', *Science Translational Medicine*, 9(411). doi: 10.1126/scitranslmed.aan0820.

Schiroli, G. *et al.* (2019) 'Precise Gene Editing Preserves Hematopoietic Stem Cell Function following Transient p53-Mediated DNA Damage Response', *Cell Stem Cell*, 24(4), pp. 551-565.e8. doi: 10.1016/j.stem.2019.02.019.

Schofield, R. (1978) 'The relationship between the spleen colony-forming cell and the haemopoietic stem cell', *Blood cells*, 4(1–2), pp. 7–25. Available at: https://pubmed.ncbi.nlm.nih.gov/747780/ (Accessed: 16 September 2024).

Scully, R. *et al.* (2019) 'DNA double-strand break repair-pathway choice in somatic mammalian cells', *Nature Reviews Molecular Cell Biology*. Nature Publishing Group, pp. 698–714. doi: 10.1038/s41580-019-0152-0.

Shahbazi, R. *et al.* (2019) 'Targeted homology-directed repair in blood stem and progenitor cells with CRISPR nanoformulations', *Nature materials*, 18(10), pp. 1124–

1132. doi: 10.1038/S41563-019-0385-5.

Sharma, M. *et al.* (2011) 'Stromal-derived factor-1/CXCR4 signaling: Indispensable role in homing and engraftment of hematopoietic stem cells in bone marrow', *Stem Cells and Development*, 20(6), pp. 933–946. doi: 10.1089/SCD.2010.0263/ASSET/IMAGES/LARGE/FIGURE5.JPEG.

Shen, T. N. Y. *et al.* (2017) 'Interleukin-6 stimulates Akt and p38 MAPK phosphorylation and fibroblast migration in non-diabetic but not diabetic mice', *PLOS ONE*, 12(5), p. e0178232. doi: 10.1371/JOURNAL.PONE.0178232.

Sheridan, C. (2024) 'The world's first CRISPR therapy is approved: who will receive it?', *Nature Biotechnology*, 42(1), pp. 3–4. doi: 10.1038/D41587-023-00016-6.

Shiloh, Y. (2006) 'The ATM-mediated DNA-damage response: taking shape', *Trends in Biochemical Sciences*. Elsevier, pp. 402–410. doi: 10.1016/j.tibs.2006.05.004.

Shultz, L. D. *et al.* (1995) 'Multiple defects in innate and adaptive immunologic function in NOD/LtSz-scid mice.', *The Journal of Immunology*, 154(1).

Shultz, L. D. *et al.* (2005) ' Human Lymphoid and Myeloid Cell Development in NOD/LtSz- scid IL2R γ null Mice Engrafted with Mobilized Human Hemopoietic Stem Cells ', *The Journal of Immunology*, 174(10), pp. 6477–6489. doi: 10.4049/jimmunol.174.10.6477.

Siegner, S. M. *et al.* (2022) 'Adenine base editing efficiently restores the function of Fanconi anemia hematopoietic stem and progenitor cells', *Nature communications*, 13(1). doi: 10.1038/S41467-022-34479-Z.

Signer, R. A. J. *et al.* (2014) 'Haematopoietic stem cells require a highly regulated protein synthesis rate', *Nature*, 509(7498), pp. 49–54. doi: 10.1038/NATURE13035.

Simsek, T. *et al.* (2010) 'The distinct metabolic profile of hematopoietic stem cells reflects their location in a hypoxic niche', *Cell Stem Cell*, 7(3), pp. 380–390. doi: 10.1016/j.stem.2010.07.011.

Soutoglou, E. *et al.* (2007) 'Positional stability of single double-strand breaks in mammalian cells', *Nature Cell Biology*, 9(6), pp. 675–682. doi: 10.1038/ncb1591.

Staal, F. J. T., Chhatta, A. and Mikkers, H. (2016) 'Caught in a Wnt storm: Complexities of Wnt signaling in hematopoiesis', *Experimental Hematology*, 44(6), pp. 451–457. doi: 10.1016/J.EXPHEM.2016.03.004.

Stark, J. M. *et al.* (2002) 'ATP hydrolysis by mammalian RAD51 has a key role during homology-directed DNA repair', *Journal of Biological Chemistry*, 277(23), pp. 20185–20194. doi: 10.1074/jbc.M112132200.

Sugiyama, T. *et al.* (2006) 'Maintenance of the hematopoietic stem cell pool by CXCL12-CXCR4 chemokine signaling in bone marrow stromal cell niches', *Immunity*,

25(6), pp. 977–988. doi: 10.1016/J.IMMUNI.2006.10.016.

Sulli, G., Di Micco, R. and Di Fagagna, F. D. A. (2012) 'Crosstalk between chromatin state and DNA damage response in cellular senescence and cancer', *Nature Reviews Cancer*. Nat Rev Cancer, pp. 709–720. doi: 10.1038/nrc3344.

Symington, L. S. (2016) 'Mechanism and regulation of DNA end resection in eukaryotes', *Critical Reviews in Biochemistry and Molecular Biology*. Taylor and Francis Ltd, pp. 195–212. doi: 10.3109/10409238.2016.1172552.

Takata, M. *et al.* (1998) 'Homologous recombination and non-homologous end-joining pathways of DNA double-strand break repair have overlapping roles in the maintenance of chromosomal integrity in vertebrate cells', *EMBO Journal*, 17(18), pp. 5497–5508. doi: 10.1093/emboj/17.18.5497.

Takihara, Y. J. *et al.* (2019) 'High mitochondrial mass is associated with reconstitution capacity and quiescence of hematopoietic stem cells', *Blood Advances*, 3(15), pp. 2323–2327. doi: 10.1182/bloodadvances.2019032169.

Takubo, K. *et al.* (2013) 'Regulation of glycolysis by Pdk functions as a metabolic checkpoint for cell cycle quiescence in hematopoietic stem cells', *Cell Stem Cell*, 12(1), pp. 49–61. doi: 10.1016/j.stem.2012.10.011.

Tebas, P. *et al.* (2014) 'Gene Editing of *CCR5* in Autologous CD4 T Cells of Persons Infected with HIV', *New England Journal of Medicine*, 370(10), pp. 901–910. doi: 10.1056/NEJMoa1300662.

Tesio, M. *et al.* (2015) 'Hematopoietic stem cell quiescence and function are controlled by the CYLD-TRAF2-p38MAPK pathway', *Journal of Experimental Medicine*, 212(4), pp. 525–538. doi: 10.1084/jem.20141438.

Testa, C. *et al.* (2023) 'Whole transcriptomic analysis of mesenchymal stem cells cultured in Nichoid micro-scaffolds', *Frontiers in Bioengineering and Biotechnology*, 10, p. 945474. doi: 10.3389/FBIOE.2022.945474/BIBTEX.

Thompson, A. A. *et al.* (2018) 'Gene Therapy in Patients with Transfusion-Dependent β-Thalassemia', 378(16), pp. 1479–1493. Available at: https://pubmed.ncbi.nlm.nih.gov/29669226/ (Accessed: 13 March 2021).

Tomellini, E. *et al.* (2019) 'Integrin-α3 Is a Functional Marker of Ex Vivo Expanded Human Long-Term Hematopoietic Stem Cells', *Cell reports*, 28(4), pp. 1063-1073.e5. doi: 10.1016/J.CELREP.2019.06.084.

Torisawa, Y. S. *et al.* (2014) 'Bone marrow-on-a-chip replicates hematopoietic niche physiology in vitro', *Nature methods*, 11(6), pp. 663–669. doi: 10.1038/NMETH.2938.

Tornabene, P. *et al.* (2022) 'Therapeutic homology-independent targeted integration in retina and liver', *Nature Communications 2022 13:1*, 13(1), pp. 1–14.

doi: 10.1038/s41467-022-29550-8.

Tothova, Z. *et al.* (2007) 'FoxOs are critical mediators of hematopoietic stem cell resistance to physiologic oxidative stress', *Cell*, 128(2), pp. 325–339. doi: 10.1016/J.CELL.2007.01.003.

Tran, N.-T. *et al.* (2019) 'Enhancement of Precise Gene Editing by the Association of Cas9 With Homologous Recombination Factors', *Frontiers in Genetics*, 10(APR), p. 365. doi: 10.3389/fgene.2019.00365.

Tsai, S. Q. *et al.* (2015) 'GUIDE-seq enables genome-wide profiling of off-target cleavage by CRISPR-Cas nucleases', *Nature Biotechnology*, 33(2), pp. 187–198. doi: 10.1038/nbt.3117.

Tsai, S. Q. *et al.* (2017) 'CIRCLE-seq: A highly sensitive in vitro screen for genome-wide CRISPR-Cas9 nuclease off-targets', *Nature Methods*, 14(6), pp. 607–614. doi: 10.1038/nmeth.4278.

Tucci, F. *et al.* (2021) 'Update on Clinical Ex Vivo Hematopoietic Stem Cell Gene Therapy for Inherited Monogenic Diseases', *Molecular therapy : the journal of the American Society of Gene Therapy*, 29(2), pp. 489–504. doi: 10.1016/J.YMTHE.2020.11.020.

Turchiano, G. *et al.* (2021) 'Quantitative evaluation of chromosomal rearrangements in gene-edited human stem cells by CAST-Seq', *Cell Stem Cell*, pp. 1136-1147.e5. Available at: http://www.cell.com/article/S1934590921000527/fulltext (Accessed: 27 April 2021).

Turnell, A. S. and Grand, R. J. (2012) 'DNA viruses and the cellular DNA-damage response', *Journal of General Virology*. J Gen Virol, pp. 2076–2097. doi: 10.1099/vir.0.044412-0.

Uziel, T. *et al.* (2003) 'Requirement of the MRN complex for ATM activation by DNA damage', *EMBO Journal*, 22(20), pp. 5612–5621. doi: 10.1093/emboj/cdg541.

Valeri, E. *et al.* (2024) 'Removal of innate immune barriers allows efficient transduction of quiescent human hematopoietic stem cells', *Molecular therapy : the journal of the American Society of Gene Therapy*, 32(1), pp. 124–139. doi: 10.1016/J.YMTHE.2023.11.020.

Vanamee, É. S., Santagata, S. and Aggarwal, A. K. (2001) 'FokI requires two specific DNA sites for cleavage', *Journal of Molecular Biology*, 309(1), pp. 69–78. doi: 10.1006/jmbi.2001.4635.

Vavassori, V. *et al.* (2023) 'Lipid nanoparticles allow efficient and harmless ex vivo gene editing of human hematopoietic cells', *Blood*, 142(9), pp. 812–826. doi: 10.1182/BLOOD.2022019333.

Verma, I. M. and Weitzman, M. D. (2005) 'Gene therapy: Twenty-first century medicine', *Annual Review of Biochemistry*. Annu Rev Biochem, pp. 711–738. doi: 10.1146/annurev.biochem.74.050304.091637.

Walter, D. *et al.* (2015) 'Exit from dormancy provokes DNA-damage-induced attrition in haematopoietic stem cells', *Nature*, 520(7548), pp. 549–552. doi: 10.1038/nature14131.

Walton, R. T. *et al.* (2020) 'Unconstrained genome targeting with near-PAMless engineered CRISPR-Cas9 variants', *Science*, 368(6488), pp. 290–296. doi: 10.1126/science.aba8853.

Wang, H. and Xu, X. (2017) 'Microhomology-mediated end joining: New players join the team', *Cell and Bioscience*. BioMed Central Ltd., pp. 1–6. doi: 10.1186/s13578-017-0136-8.

Wang, L. *et al.* (2015) 'Comparative Study of Liver Gene Transfer with AAV Vectors Based on Natural and Engineered AAV Capsids', *Molecular Therapy*, 23(12), pp. 1877–1887. doi: 10.1038/mt.2015.179.

Wang, L. *et al.* (2017) 'Enhanced base editing by co-expression of free uracil DNA glycosylase inhibitor', *Cell Research 2017 27:10*, 27(10), pp. 1289–1292. doi: 10.1038/cr.2017.111.

Weissman, I. L. and Shizuru, J. A. (2008) 'The origins of the identification and isolation of hematopoietic stem cells, and their capability to induce donor-specific transplantation tolerance and treat autoimmune diseases', *Blood*, 112(9), pp. 3543–3553. doi: 10.1182/blood-2008-08-078220.

Weston, A. and Poirier, M. C. (2014) 'Carcinogen-DNA Adduct Formation and DNA Repair', in *Encyclopedia of Toxicology: Third Edition*. Elsevier, pp. 705–712. doi: 10.1016/B978-0-12-386454-3.00593-5.

Wienert, B. *et al.* (2019) 'Unbiased detection of CRISPR off-targets in vivo using DISCOVER-Seq', *Science*, 364(6437), pp. 286–289. doi: 10.1126/science.aav9023.

Wienert, B. *et al.* (2020) 'Timed inhibition of CDC7 increases CRISPR-Cas9 mediated templated repair', *Nature Communications*, 11(1), pp. 1–15. doi: 10.1038/s41467-020-15845-1.

Willinger, T. *et al.* (2011) 'Improving human hemato-lymphoid-system mice by cytokine knock-in gene replacement', *Trends in Immunology*. Elsevier, pp. 321–327. doi: 10.1016/j.it.2011.04.005.

Wilson, A. *et al.* (2008) 'Hematopoietic Stem Cells Reversibly Switch from Dormancy to Self-Renewal during Homeostasis and Repair', *Cell*, 135(6), pp. 1118–1129. doi: 10.1016/j.cell.2008.10.048.

Woods, N. B. *et al.* (2006) 'Gene therapy: Therapeutic gene causing lymphoma',

Nature, 440(7088), p. 1123. doi: 10.1038/4401123a.

Xu, X. *et al.* (2019) 'Delivery of CRISPR/Cas9 for therapeutic genome editing', *The Journal of Gene Medicine*, 21(7), p. e3107. doi: 10.1002/jgm.3107.

Yang, D. *et al.* (2016) 'Enrichment of G2/M cell cycle phase in human pluripotent stem cells enhances HDR-mediated gene repair with customizable endonucleases', *Scientific Reports*, 6. doi: 10.1038/srep21264.

Yang, H. *et al.* (2020) 'Methods favoring homology-directed repair choice in response to crispr/cas9 induced-double strand breaks', *International Journal of Molecular Sciences*. MDPI AG, pp. 1–20. doi: 10.3390/ijms21186461.

Yokomizo, T. *et al.* (2022) 'Independent origins of fetal liver haematopoietic stem and progenitor cells', *Nature 2022 609:7928*, 609(7928), pp. 779–784. doi: 10.1038/s41586-022-05203-0.

Young, J. L. and Dean, D. A. (2015) 'Electroporation-mediated gene delivery', *Advances in genetics*, 89, pp. 49–88. doi: 10.1016/BS.ADGEN.2014.10.003.

Yu, C. *et al.* (2015) 'Small molecules enhance crispr genome editing in pluripotent stem cells', *Cell Stem Cell*, 16(2), pp. 142–147. doi: 10.1016/j.stem.2015.01.003.

Zandrini, T. *et al.* (2023) 'Breaking the resolution limits of 3D bioprinting: future opportunities and present challenges', *Trends in Biotechnology*, 41(5), pp. 604–614. doi: 10.1016/j.tibtech.2022.10.009.

Zeng, J. *et al.* (2020) 'Therapeutic base editing of human hematopoietic stem cells', *Nature medicine*, 26(4). doi: 10.1038/S41591-020-0790-Y.

Zhang, P. *et al.* (2019) 'The physical microenvironment of hematopoietic stem cells and its emerging roles in engineering applications', *Stem Cell Research & Therapy 2019 10:1*, 10(1), pp. 1–13. doi: 10.1186/S13287-019-1422-7.

Zhang, Y., Zhang, Z. and Ge, W. (2018) 'An efficient platform for generating somatic point mutations with germline transmission in the zebrafish by CRISPR/Cas9-mediated gene editing', *Journal of Biological Chemistry*, 293(17), pp. 6611–6622. doi: 10.1074/jbc.RA117.001080.

Zhao, C., Deng, W. and Gage, F. H. (2008) 'Mechanisms and Functional Implications of Adult Neurogenesis', *Cell*. Cell, pp. 645–660. doi: 10.1016/j.cell.2008.01.033.

Zhao, J. *et al.* (2024) 'Inherited blood cancer predisposition through altered transcription elongation', *Cell*, 187(3), pp. 642-658.e19. Available at: http://www.cell.com/article/S009286742301348X/fulltext (Accessed: 9 July 2024).

Zhao, M. *et al.* (2014) 'Megakaryocytes maintain homeostatic quiescence and promote post-injury regeneration of hematopoietic stem cells', *Nature medicine*, 20(11), pp. 1321–1326. doi: 10.1038/NM.3706.

Zhao, X. *et al.* (2017) 'Cell cycle-dependent control of homologous recombination', *Acta Biochimica et Biophysica Sinica*. Oxford University Press, pp. 655–668. doi: 10.1093/abbs/gmx055.

Zhou, D. *et al.* (2020) 'A 3D engineered scaffold for hematopoietic progenitor/stem cell co-culture in vitro', *Scientific Reports 2020 10:1*, 10(1), pp. 1–11. doi: 10.1038/s41598-020-68250-5.

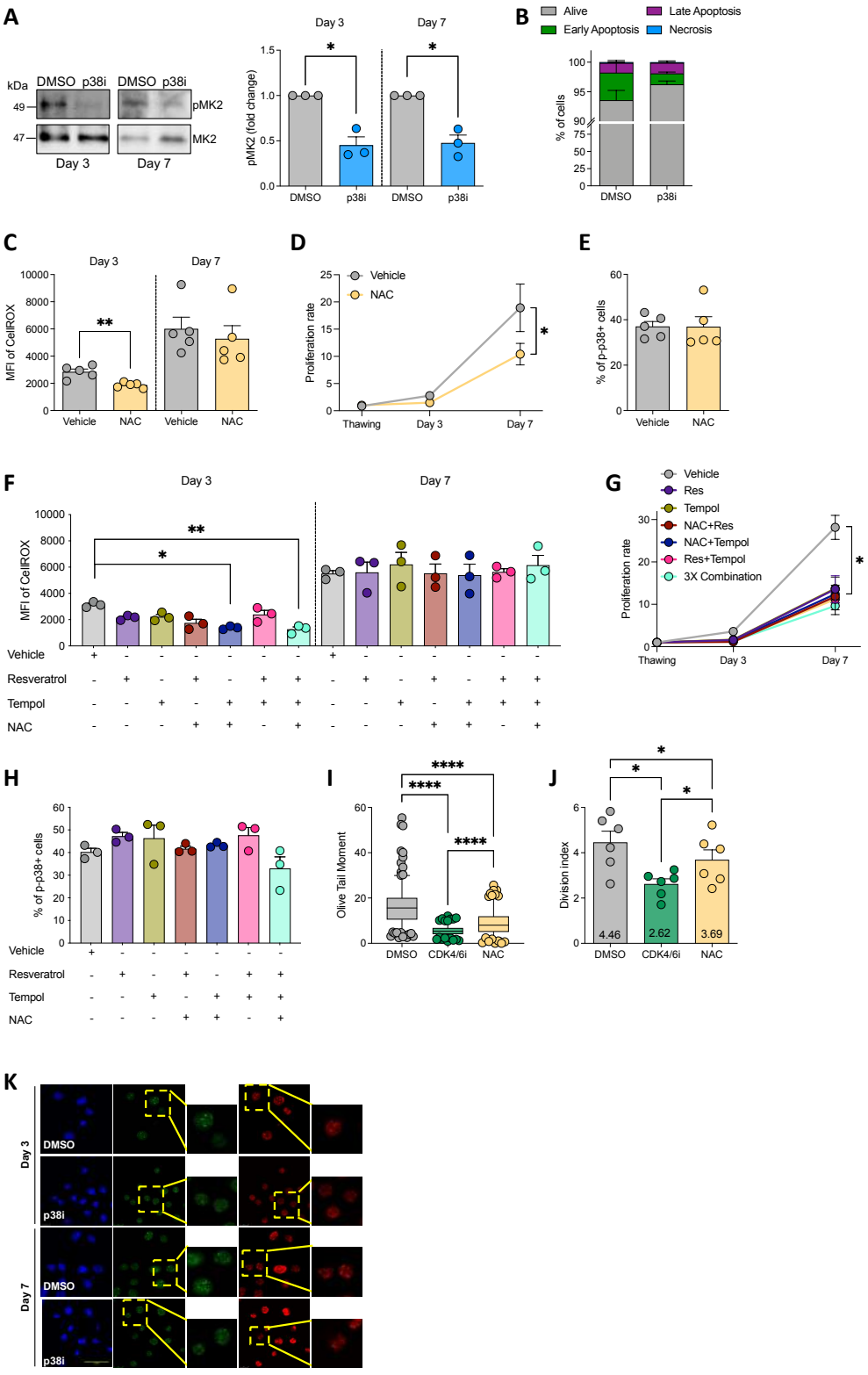
Zonari, E. *et al.* (2017) 'Efficient Ex Vivo Engineering and Expansion of Highly Purified Human Hematopoietic Stem and Progenitor Cell Populations for Gene Therapy', *Stem Cell Reports*, 8(4), pp. 977–990. doi: 10.1016/j.stemcr.2017.02.010.

Zou, L. and Elledge, S. J. (2003) 'Sensing DNA damage through ATRIP recognition of RPA-ssDNA complexes', *Science*, 300(5625), pp. 1542–1548. doi: 10.1126/science.1083430.

Zufferey, R. *et al.* (1998) 'Self-inactivating lentivirus vector for safe and efficient in vivo gene delivery', *Journal of virology*, 72(12), pp. 9873–9880. doi: 10.1128/JVI.72.12.9873-9880.1998.



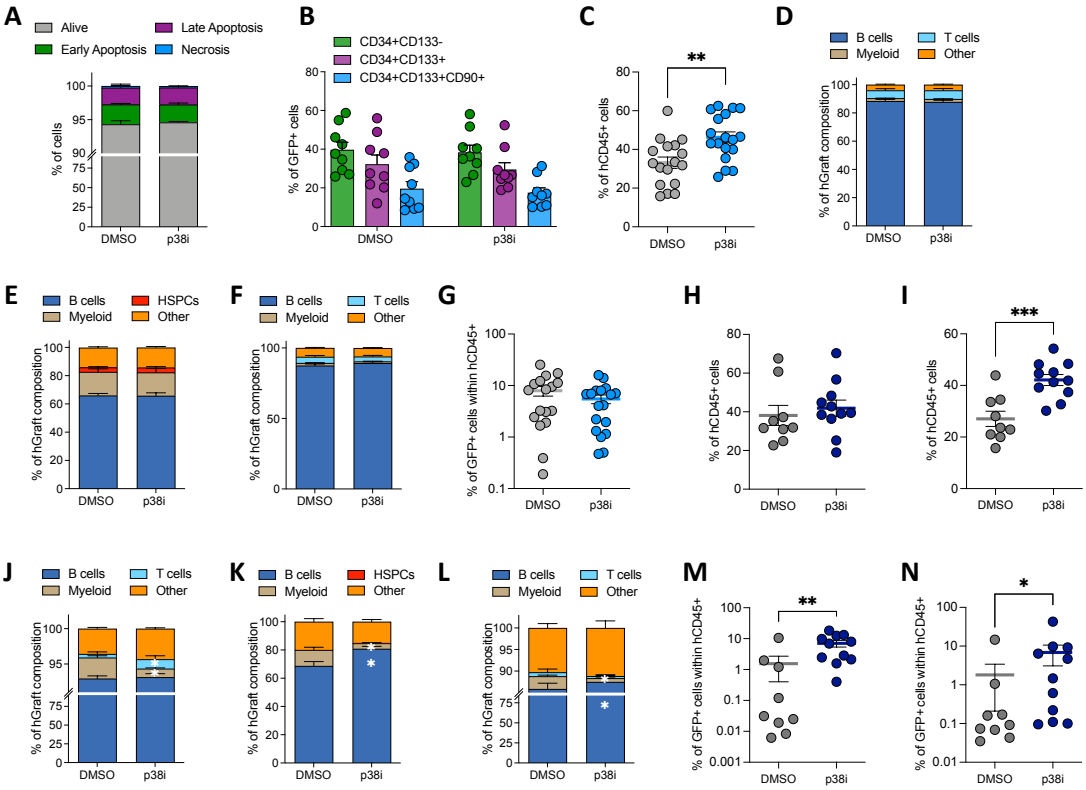
Appendix 1



Appendix 1. Mitogenic ROS promotes HSPC proliferation leading to DNA damage. *(**A**) Western Blot analysis of the p38 target pMK2 (n=3). MK2 was used as loading control and fold*

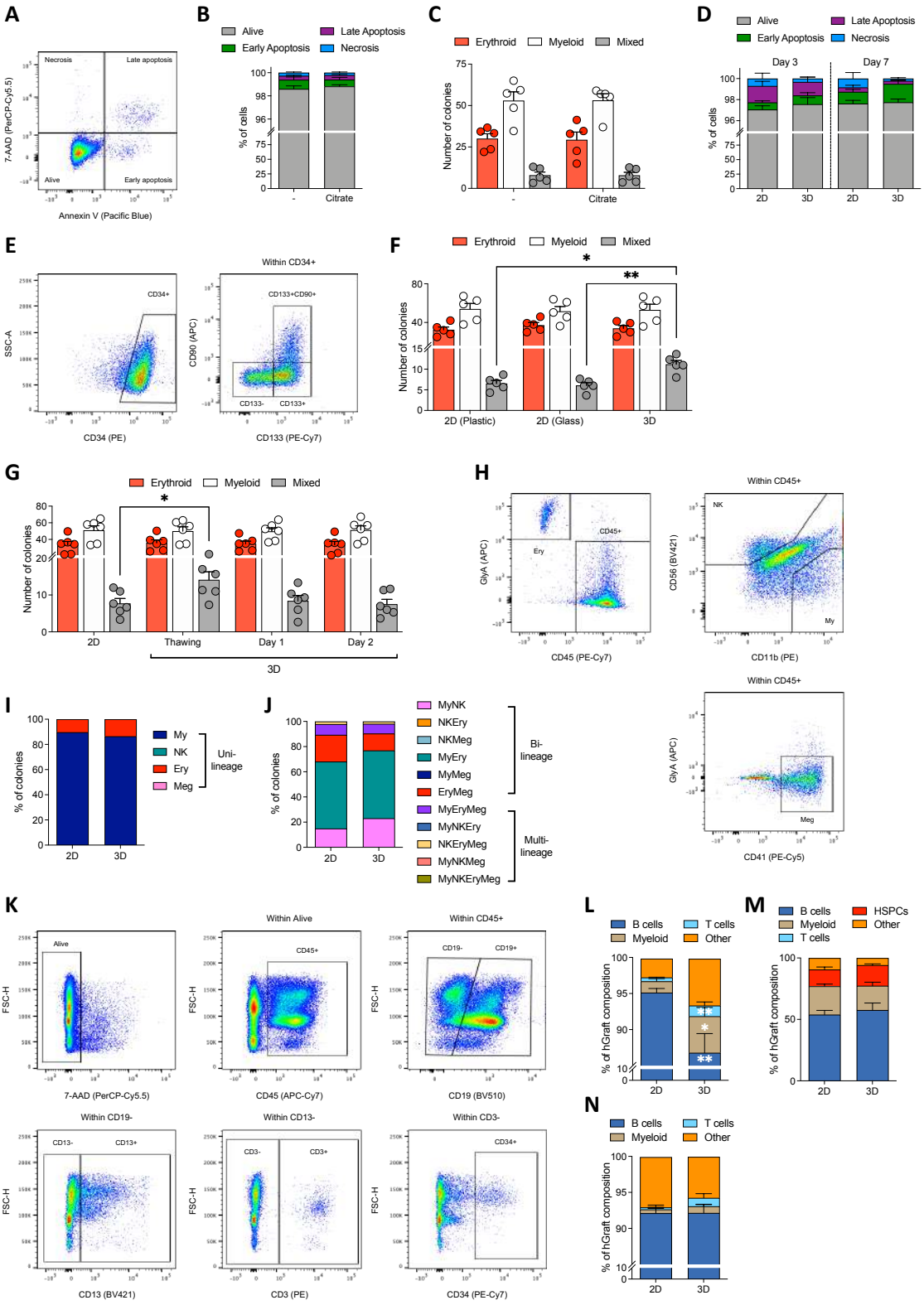
*changes relative to DMSO are reported. One-sample T-test. (**B**) Apoptosis analysis performed within CD34+ cells (n=4). (**C**) MFI of CellROX (n=5). Mann-Whitney test. (**D**) Proliferation rate of HSPC over time (n=6). Wilcoxon test. (**E**) Percentage of p-p38+ cells on day 7 (n=5). (**F**) MFI of CellROX (n=3). Kruskal-Wallis test. (**G**) Proliferation rate of HSPC over time (n=5). Mann-Whitney test (each treatment vs. vehicle). (**H**) Percentage of p-p38+ cells on day 7 (n=3). (**I**) Quantification of SSBs and DSBs by alkaline comet assay on day 7; each dot represents a single cell (more than 200 cells were analyzed for each condition). Median ± 95% CI. Mann-Whitney test. (**J**) Division index measured from CellTrace dye dilution on day 7 (n=6). Wilcoxon test. (**K**) Representative immunofluorescence staining of DAPI (blue), γH2AX (green), and pRPA (red). Yellow boxes indicate zoomed-in images. Unless otherwise specified, Mean ± SEM. *p < 0.05; **p < 0.01; ****p < 0.0001.*

Appendix 2



Appendix 2. p38i increases the long-term engraftment of HDR-edited HSPCs. *(**A**) Apoptosis analysis performed within CD34+ cells on day 4 (n=6). (**B**) Percentage of GFP+ cells within HSPC subsets on day 7 (n=9). (**C**) Percentage of hCD45+ cells measured in the SP at the endpoint of transplanted mice (n=16,18). Mann-Whitney test. (**D-F**) Percentage of human graft composition in the PB (**D**), BM (**E**), and SP (**F**) at the endpoint of transplanted mice (n=16,18). (**G**) Percentage of GFP+ cells (within hCD45+ cells) in the SP at the endpoint of mice in (**C**) (n=16,18). (**H,I**) Percentage of hCD45+ cells measured in the BM (**H**) and SP (**I**) at the endpoint of transplanted secondary recipients (n=9,11). (**J-L**) Percentage of human graft composition in the PB (**J**), BM (**K**), and SP (**L**) at the endpoint of transplanted secondary recipients (n=9,11). Mann-Whitney test. (**M,N**) Percentage of GFP+ cells (within hCD45+ cells) measured in the BM (**M**) and SP (**N**) at the endpoint of mice in (**H,I**) (n=9,11). Mann-Whitney test. Mean ± SEM. *p < 0.05; **p < 0.01.*

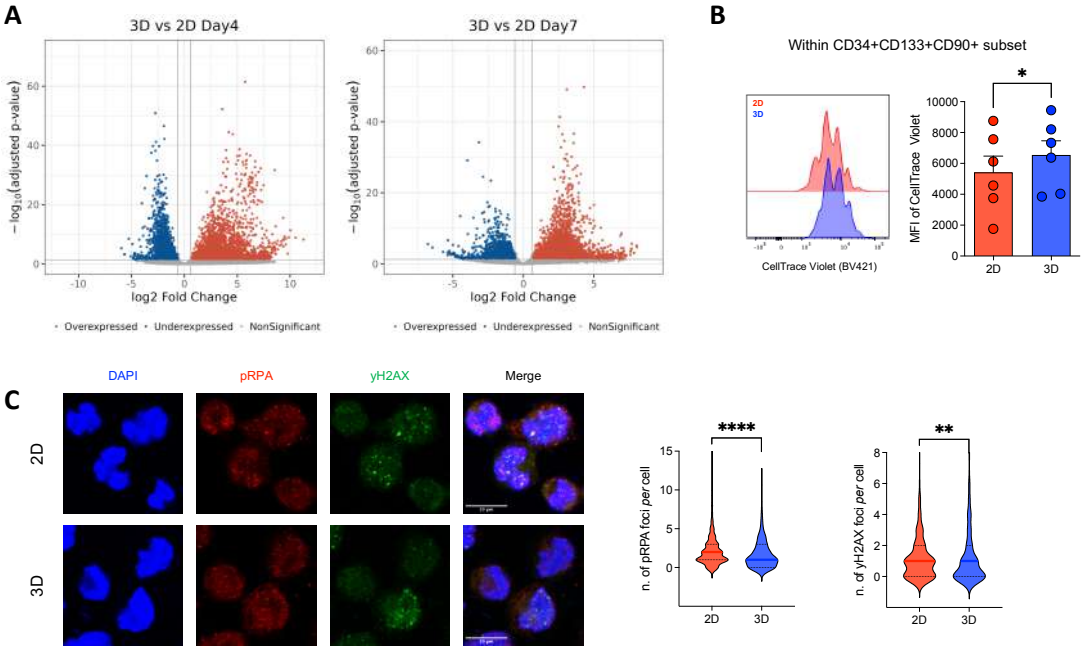
Appendix 3



Appendix 3. Nichoids increase the functionality of ex vivo cultured HSPCs. *(**A**) Representative gating strategy for apoptosis analysis. Cells are distinguished as alive (7-AAD-*

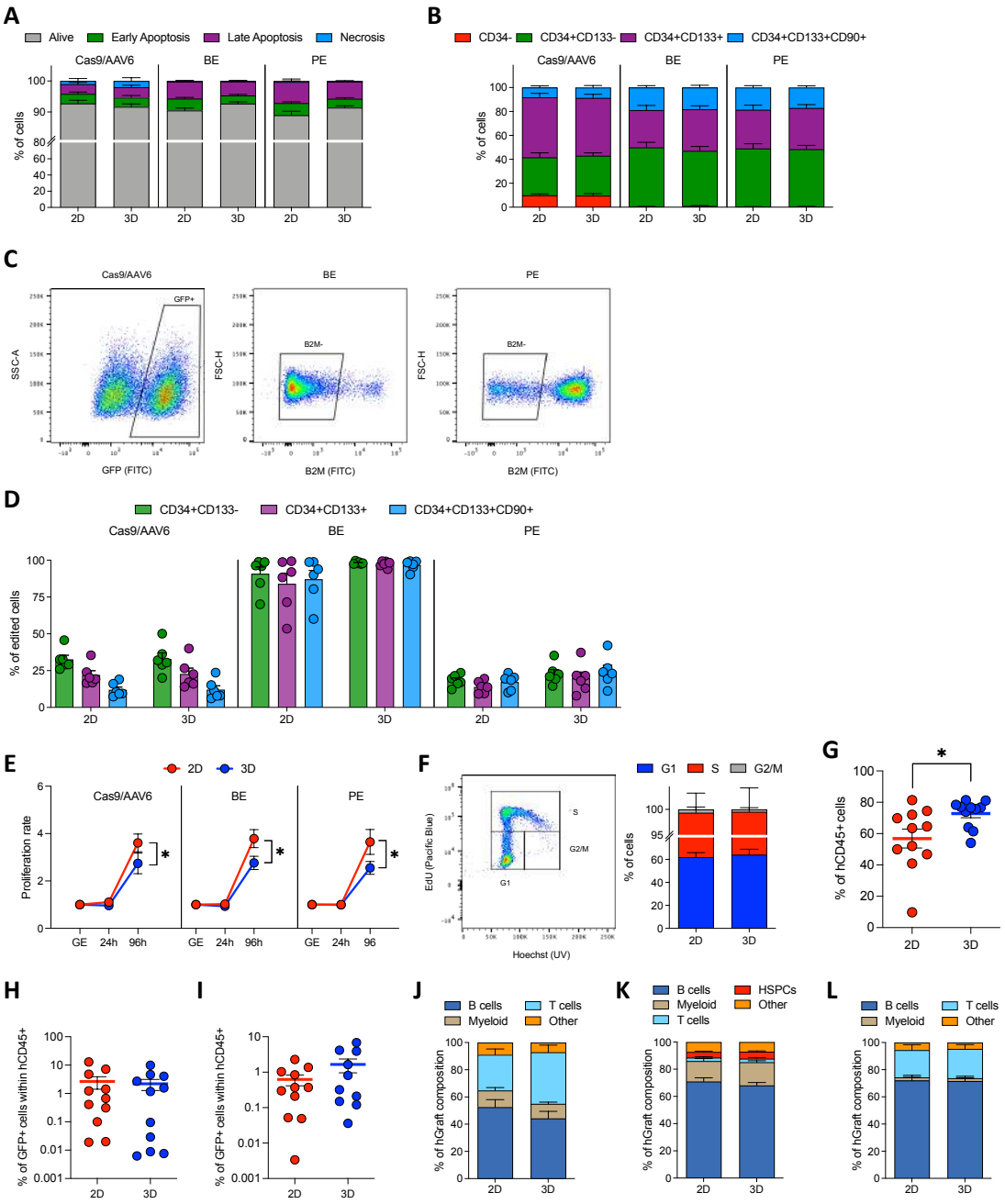
*Annexin V-), early apoptotic (7-AAD-Annexin V+), late apoptotic (7-AAD+Annexin V+), and necrotic (7-AAD+Annexin V-). (**B**) Apoptosis analysis performed within CD34+ cells treated or not with a citrate solution (n=5). (**C**) Number of erythroid, myeloid, and mixed colonies generated in CFU-C assay from HSPCs treated or not with a citrate solution seeded on day 3 (n=5). (**D**) Apoptosis analysis performed within CD34+ cells (n=6,6,5,5). (**E**) Representative gating strategy for phenotypically defined HSPC subsets analysis. CD34+ cells were identified within alive cells from (a). HSPC subpopulations were discriminated as CD34+CD133-CD90-, CD34+CD133+CD90-, and primitive fraction CD34+CD133+CD90+. (**F**) Number of erythroid, myeloid, and mixed colonies generated in CFU-C assay from HSPCs seeded on day 3 upon culture in different settings (n=5). Mann-Whitney test. (**G**) Number of erythroid, myeloid, and mixed colonies generated in CFU-C assay from HSPCs seeded on 2D or 3D immediately after thawing or upon one or two days after initial 2D culture (n=6). Wilcoxon test. (**H**) Representative gating strategy for HSC-enriched single-cell differentiation assay. Colonies were considered in the analysis only if >30 cells were present in the following gates: Erythroid, Ery (CD45-GlyA+); Myeloid, My (CD45+CD11b+); Natural Killer, NK (CD45+CD56+CD11b-); Megakaryocyte, Meg (CD45+CD41+GlyA-). (**I,J**) Percentage of different lineages within uni-lineage (i) or bi/multi-lineage (j) colonies generated in single-cell differentiation assay. (**K**) Representative gating strategy for PB, BM, and SP analyses. hCD45+ cells were identified within alive cells (7-AAD-). Within the human graft, cells were discriminated as B cells (CD45+CD19+), myeloid cells (CD45+CD19-CD13+), T cells (CD45+CD19-CD13-CD3+), HSPCs (CD45+CD19-CD13-CD3-CD34+) or other (CD45+CD19-CD13-CD3-CD34-). (**L-N**) Percentage of human graft composition in the PB (**L**), BM (**M**), and SP (**N**) at the endpoint of transplanted mice (n=5). Mann-Whitney test. Mean ± SEM. *p < 0.05; **p < 0.01.*

Appendix 4



Appendix 4. 3D culture remodels HSPC transcriptional profile, reducing cell proliferation and DNA damage accumulation. *(**A**) Differentially expressed genes (FDR < 0.05) in 3D- vs. 2D-cultured HSPCs. (**B**) Representative plot (left) and MFI (right) of CellTrace dye dilution on day 7 (n=6) in the HSC-enriched subset. Mean ± SEM. Wilcoxon test. (**C**) Representative immunofluorescence staining (left) of DAPI (blue), pRPA (red), and yH2AX (green) and number of DDR foci (right) per cell (more than 800 cells were analyzed for each condition). Median. Mann-Whitney test. *p < 0.05; **p < 0.01; ****p < 0.0001.*

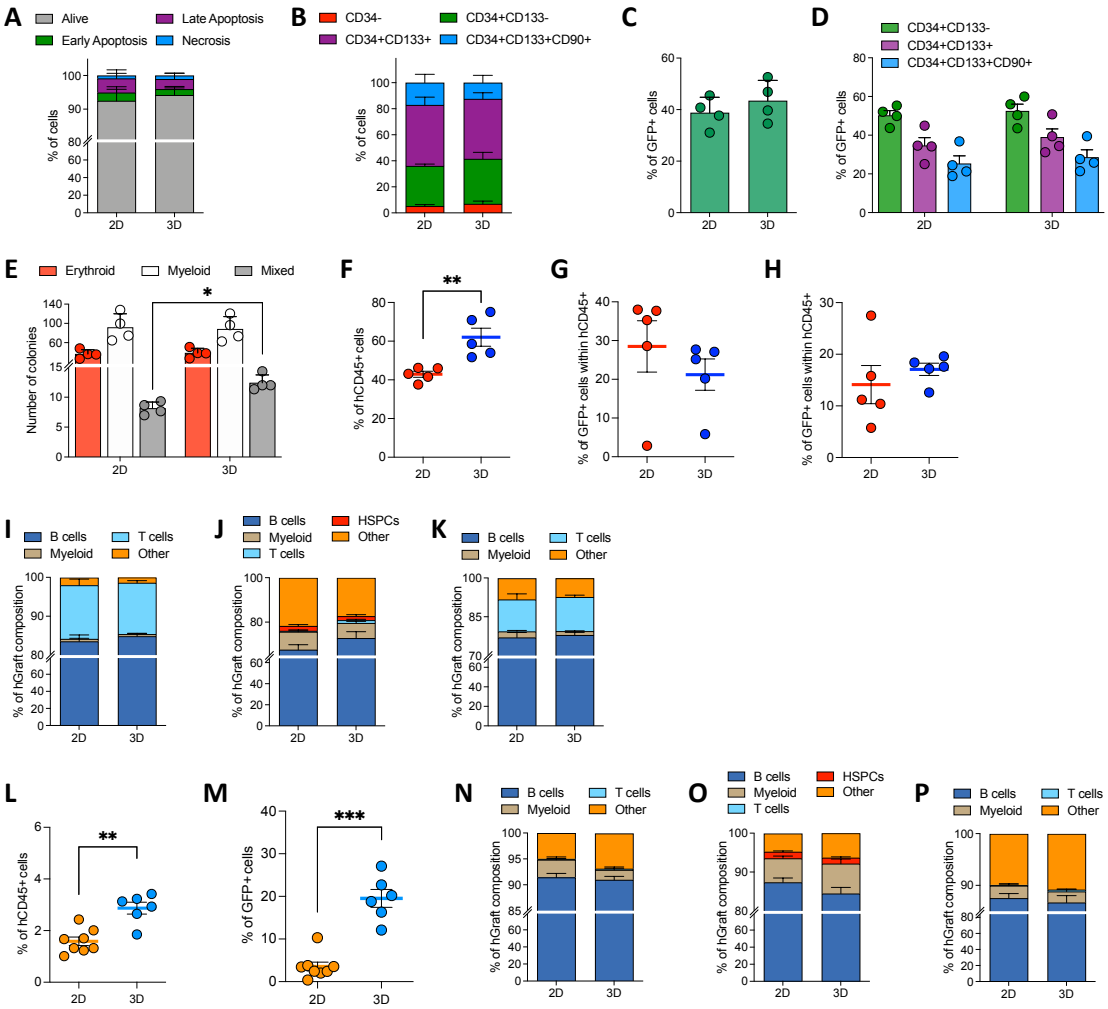
Appendix 5



Appendix 5. Nichoids allow efficient GE by Cas9/AAV6, BE, and PE. *(**A**) Apoptosis analysis performed within CD34+ cells on day 4 (n=6). (**B**) Percentage of phenotypically defined HSPC subsets on day 4 (n=6). (**C**) Representative gating strategy for editing efficiency analysis. GFP+ or B2M- cells were identified within CD34+ cells (gated within alive cells). (**D**) Percentage of edited cells within HSPC subsets on day 7 (n=6). (**E**) Proliferation rate of HSPC upon GE (GE=day 3, 24h=day 4, 96h=day 7). (n=6). Wilcoxon test. (**F**) Representative plot (left) and percentage of HSPCs in indicated cell cycle phases (right) on day 3 (before GE). (**G**) Percentage of hCD45+ cells measured in the SP at the endpoint of transplanted mice (n=11). Mann-Whitney test. (**H,I**) Percentage of GFP+ cells (within hCD45+ cells) in the BM (**H**) and SP (**I**) at the endpoint of transplanted mice (n=11). (**J-L**) Percentage of human graft*

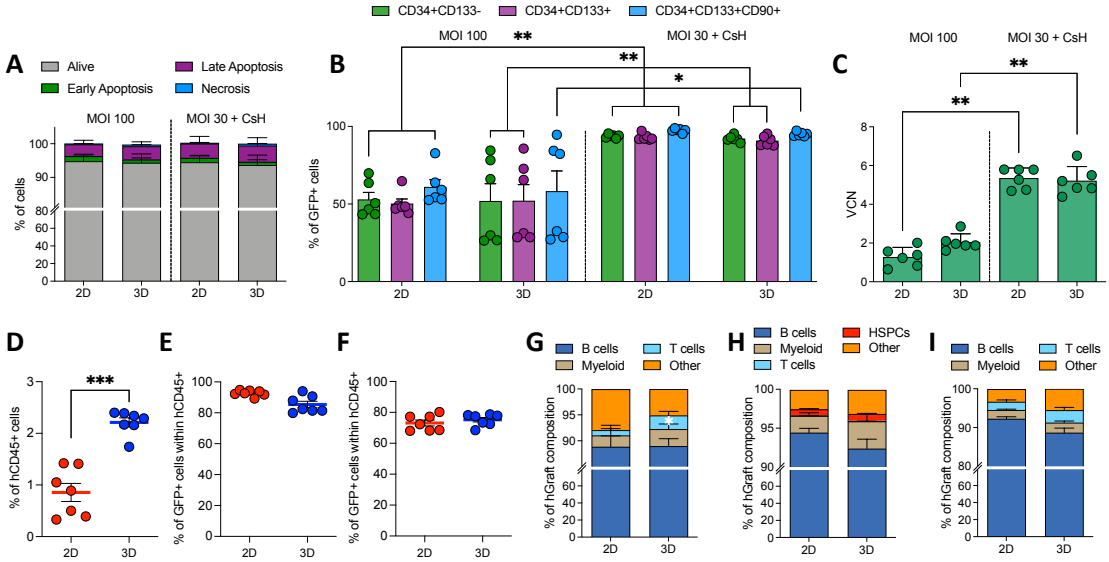
*composition in the PB (**J**), BM (**K**), and SP (**L**) at the endpoint of transplanted mice (n=11). Mean ± SEM. *p < 0.05.*

Appendix 6



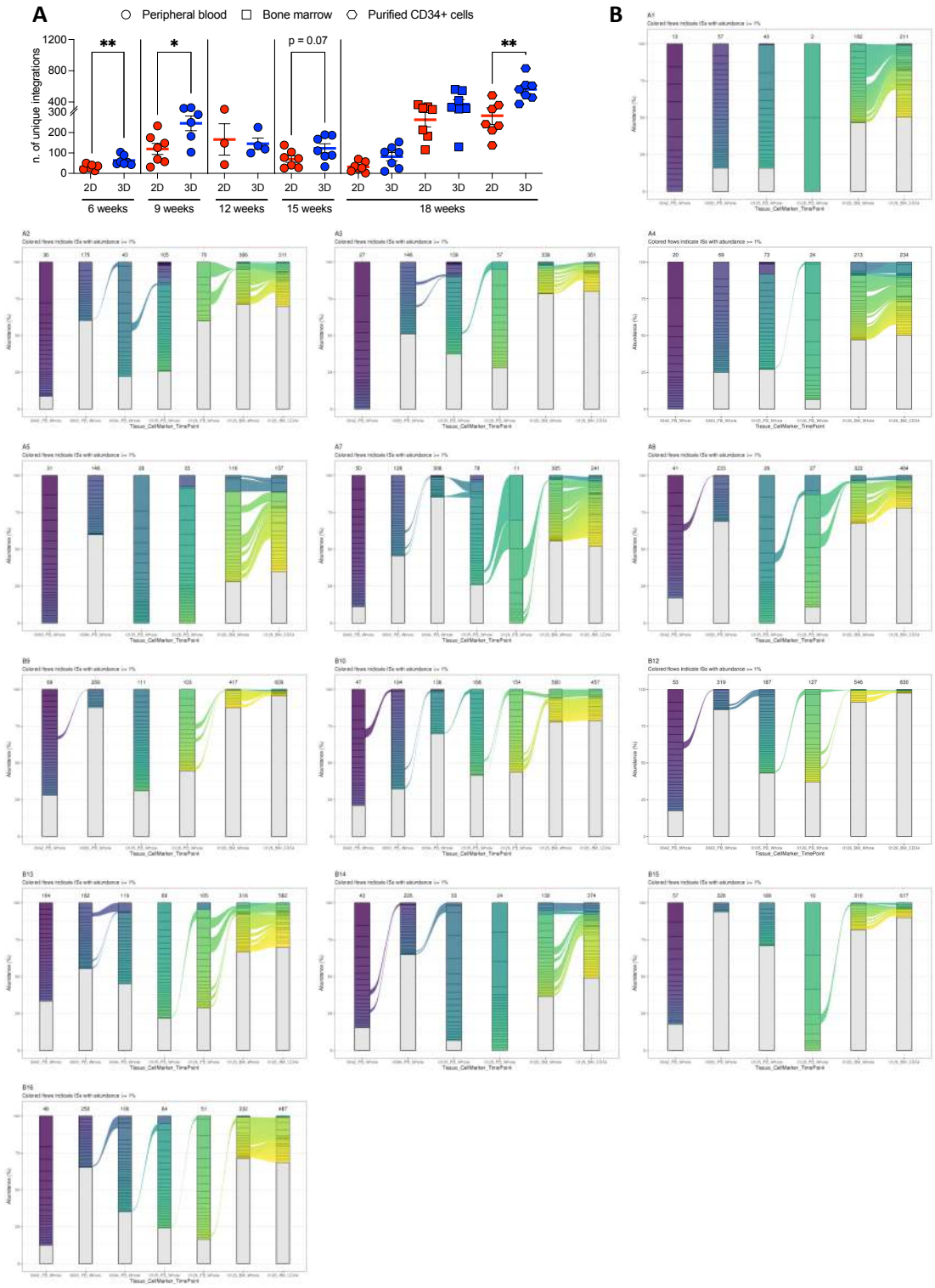
Appendix 6. 3D culture improves HDR-edited HSPC repopulating capacity in long-term experiments. *(**A**) Apoptosis analysis performed within CD34+ cells on day 4 (n=4). (**B**) Percentage of phenotypically defined HSPC subsets on day 4 (n=4). (**C,D**) Percentage of GFP+ cells within CD34+ cells (c) and HSPC subsets (d) on day 7 (n=4). (**E**) Number of erythroid, myeloid, and mixed colonies generated in CFU-C assay from edited HSPCs seeded on day 4 (n=4). Mann-Whitney test. (**F**) Percentage of hCD45+ cells measured in the SP at the endpoint of transplanted mice (n=5). Mann-Whitney test. (**G,H**) Percentage of GFP+ cells (within hCD45+ cells) in the BM (g) and SP (h) at the endpoint of transplanted mice (n=5). (**I-K**) Percentage of human graft composition in the PB (i), BM (j), and SP (k) at the endpoint of transplanted mice (n=5). (**L,M**) Percentage of hCD45+ cells (**L**) and GFP+ cells (within hCD45+ cells) (**M**) measured in the SP at the endpoint of transplanted secondary recipients (n=8,6). Mann-Whitney test. (**N-P**) Percentage of human graft composition in the PB (**N**), BM (**O**), and SP (**P**) at the endpoint of transplanted secondary recipients (n=8,6). Mean ± SEM. *p < 0.05; **p < 0.01; ***p < 0.001.*

Appendix 7



Appendix 7. 3D culture enables efficient LV-mediated gene addition. *(**A**) Apoptosis analysis performed within CD34+ cells on day 2 (n=3). (**B**) Percentage of GFP+ cells within HSPC subsets on day 10 (n=6). Mann-Whitney test. (**C**) VCN of transduced HSPC on day 10 (n=6). Mann-Whitney test. (**D**) Percentage of hCD45+ cells measured in the SP at the endpoint of transplanted mice (n=7). Mann-Whitney test. (**E,F**) Percentage of GFP+ cells (within hCD45+ cells) in the BM (**E**) and SP (**F**) at the endpoint of transplanted mice (n=7). (**G-I**) Percentage of human graft composition in the PB (**G**), BM (**H**), and SP (**I**) at the endpoint of transplanted mice (n=7). Mann-Whitney test. Mean ± SEM. *p < 0.05; **p < 0.01; ***p < 0.001.*

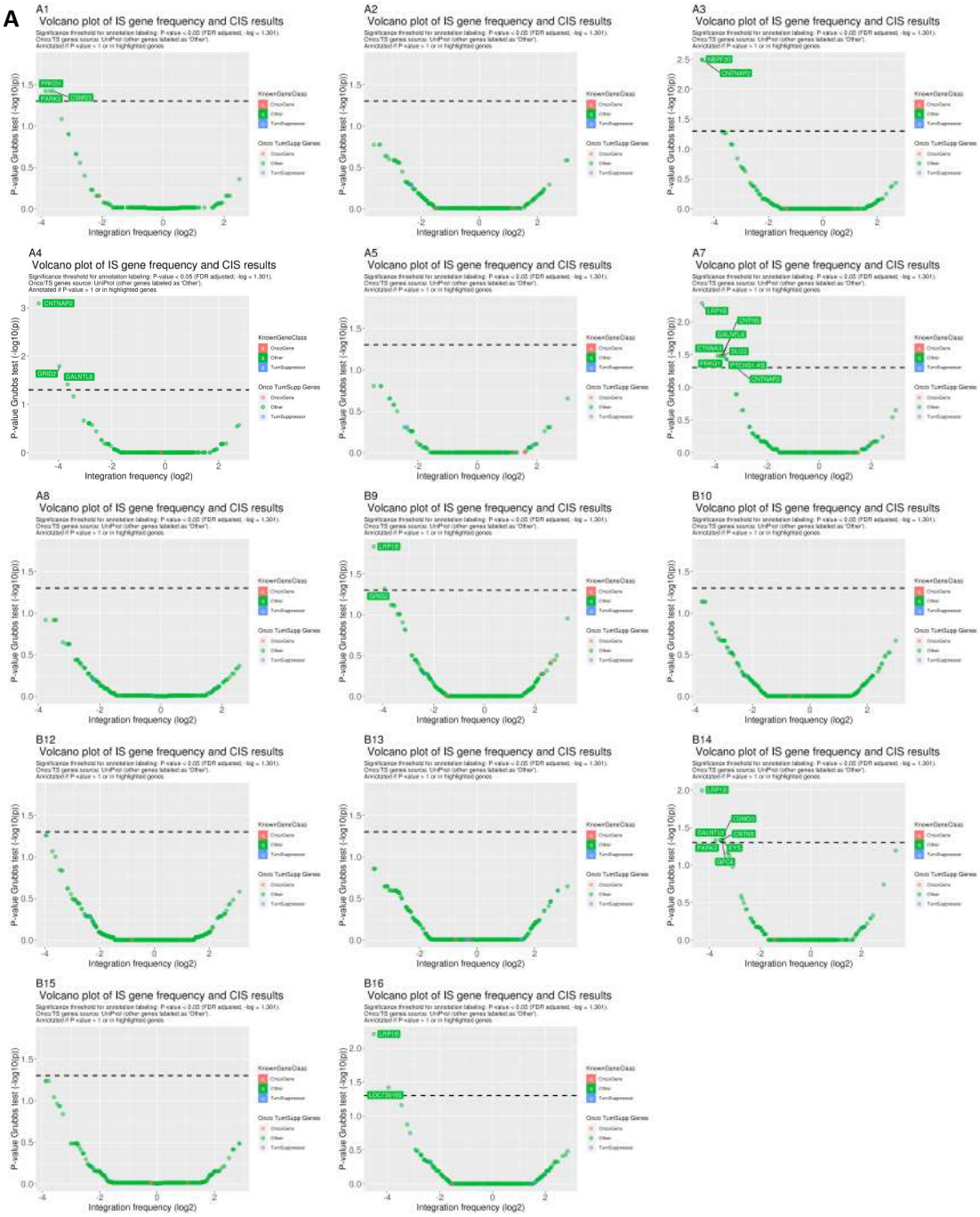
Appendix 8



Appendix 8. IS analyses in the human graft of LV-transduced HSPCs. *(**A**) Number of unique integrations from IS analyses. Mean ± SEM. Mann-Whitney test. (**B**) Tracking and relative abundance of ISs reported over time in transplanted mice (A=2D, B=3D). Each colored bar univocally identifies an IS with ≥1% representation in at least one time point, with its*

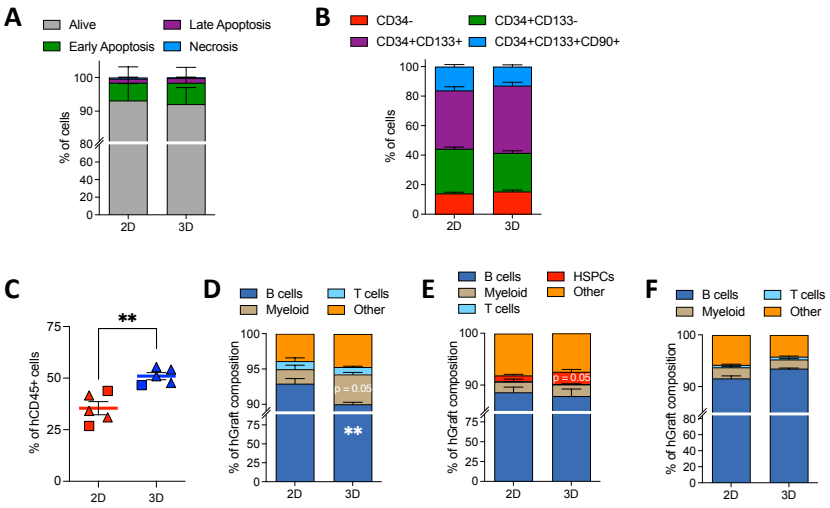
*abundance proportional to the height of the bar; a colored ribbon connects two neighboring time points for each recaptured clone. The total number of unique ISs is reported on top of each bar. *p < 0.05; **p < 0.01.*

Appendix 9



Appendix 9. Integration profile from IS analyses. *(**A**) IS gene frequency and CIS analysis in transplanted mice (A=2D, B=3D). Each dot represents a gene, which is labeled with the corresponding color if observed as significant. The dashed line is the alpha value 0.05. Grubbs test.*

Appendix 10



Appendix 10. Nichoids for gene addition in WAS patient-derived HSPCs. *(**A**) Apoptosis analysis performed within CD34+ cells on day 3 (n=6). (**B**) Percentage of phenotypically defined HSPC subsets on day 3 (n=6). (**C**) Percentage of hCD45+ cells measured in the SP at the endpoint of transplanted mice (n=5). Different symbols identify the two patients. Mann-Whitney test. (**D-F**) Percentage of human graft composition in the PB (**D**), BM (**E**), and SP (**F**) at the endpoint of transplanted mice (n=7). Mann-Whitney test. Mean ± SEM. **p < 0.01.*